The design and technical evaluation of ERiKA:

An Energy Recovering Knee-Ankle prosthesis that provides support during standing up and sitting down

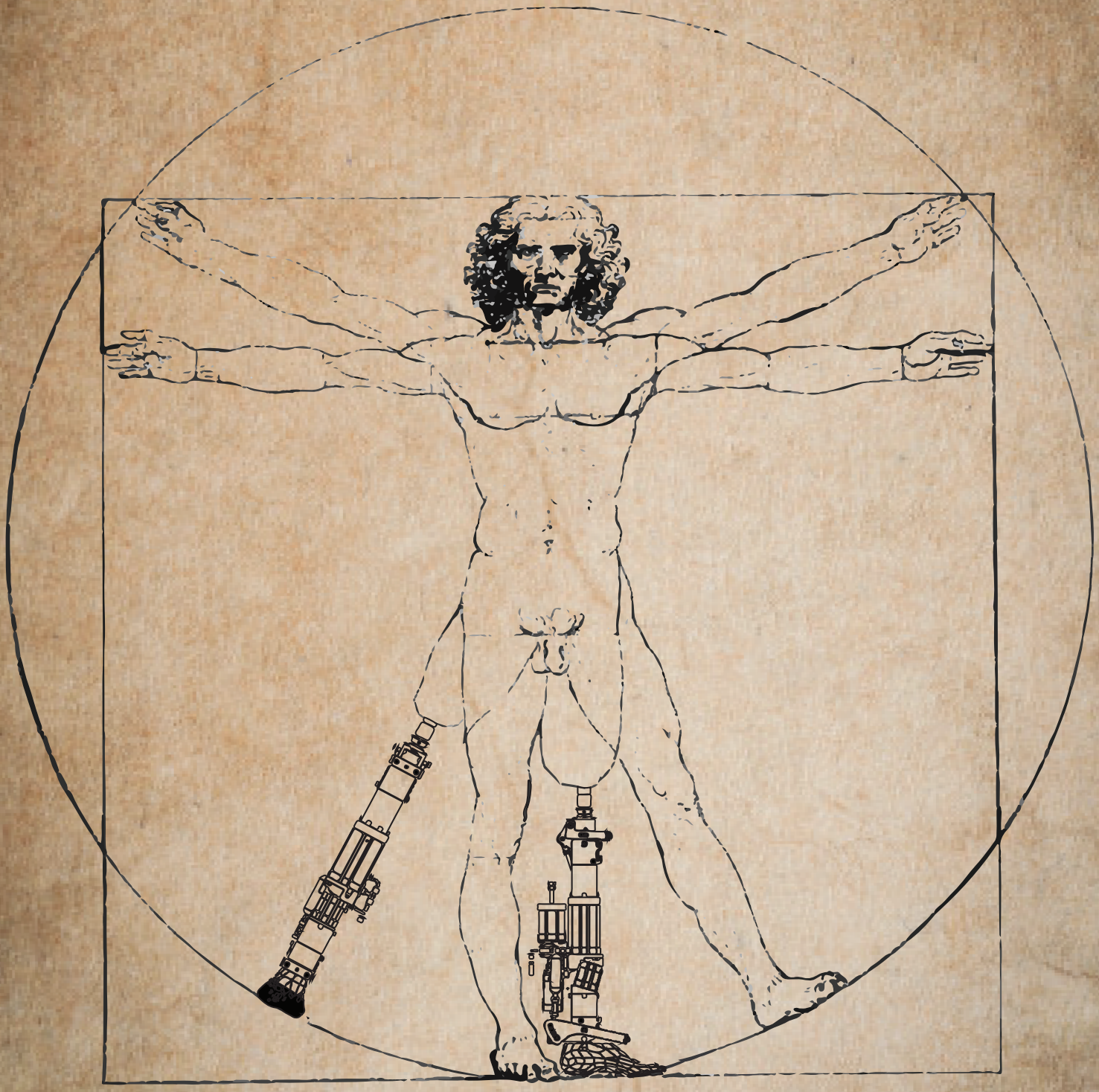

Simon van der Helm

The design and technical evaluation of ERiKA: An Energy Recovering Knee-Ankle prosthesis that provides support during standing up and sitting down

by

Simon van der Helm

to obtain the degree of **Master of Science**

at the Delft University of Technology

to be defended publicly on Monday April 20, 2020 at 14:30 AM

Student number:	4231783	
Project duration:	March 13, 2019 - April 20, 2020	
Thesis committee:	Prof. Dr. Ir. H. Vallery	TU Delft, Supervisor
	Dr. Ir. G. Smit	TU Delft, Supervisor
	Prof. Dr. Ir. J. Harlaar	TU Delft, External Committee Member

TU Delft

PREFACE

Graduating is by far the most challenging thing that I've done in my life. It is rivalled only by the literature review that came before it. But as Roosevelt said: "Nothing in the world is worth having or worth doing unless it means effort, pain, difficulty...". The effort it takes to become an engineer can therefore only mean that the title of engineer is worth having.

I would like to begin by thanking Heike and Gerwin for their guidance and supervision during the two years I have been working on this project. I know I probably have not been a model student for the entire period, but I hope the results make up for that. I was often nervous for our meetings, but I always came out with new energy and ideas.

Next, I would like to thank the Squad for their enormous mental support during this process. The initial coffee-deal, which turned into cookies and of course the Fellowship of the Pas have carried me through and helped me get out of bed in the mornings. Special thanks go out to Peterke and Johan for proofreading my paper. Of course, I have to thank my parents for sticking with me no matter what, and for doing anything that needed to be done. Susan, special thanks to you for being there for me, for putting up with my (lack of) planning and stupid notion that I should postpone going on a summer holiday until I have graduated. And of course for the editing of the figures in my paper. And finally, a very special thanks to my sister, Nina, for helping me through the tough process of writing a paper, for talking about structure and for long nights of commenting on my work. It could not have been done without you.

Simon

CONTENTS

The design and technical evaluation of ERiKA: An Energy Recovering Knee-Ankle prosthesis that provides support during standing up and sitting down

Simon G. van der Helm, Dr. Ir. Gerwin Smit and Prof. Dr. Ir. Heike Vallery

***Abstract*—The Sit-to-Stand (SitTS) and Stand-to-Sit (StandTS) transitions are among the most demanding activities of daily living in terms of required muscle strength. Many elderly struggle with the transitions, which become even harder after a transfemoral amputation. The current state of the art in knee prostheses does not supply any support to reduce the required muscle strength.**

A new, energy-recovering ankle-knee prosthesis was designed to provide support during SitTS and StandTS, with a natural torque profile. The prosthesis uses pneumatic cylinders to store energy during StandTS, and recover it during SitTS. To make the use of the prosthesis as intuitive as possible, the design was optimized to mimic natural torque profiles during the transition. The addition of an ankle joint enables a more posterior placement of the prosthetic limb, which should reduce the required knee torque. The prototype provides a peak extending knee torque of 21.7 Nm and a peak plantarflexing ankle torque of 10.8 Nm during SitTS, which can be further increased by increasing the pre-pressure in the system. It is concluded that the current prototype has the potential to provide support during the SitTS and StandTS transitions, but that alterations are required to improve the available joint torques. The next phase will be user tests with transfemoral amputees.

I. Introduction

In 2005 an estimate of 600.000 people were living in the United States with a major lower limb amputation (transfemoral, transtibial or foot amputation), and that amount is projected to increase [1]. Most of these amputations are caused by vascular problems, which are most prevalent in elderly individuals. In 1996, the incidence rates of limb loss in the United States due to vascular disease rose from 147.2 per 100.000 in males aged 55-64 to 495.6 per 100.000 in males aged over 85 [2]. A quarter of these amputations were transfemoral. In the Netherlands, 600 to 700 individuals undergo transfemoral amputation every year [3].

Sit-to-Stand (SitTS) and Stand-to-Sit (StandTS) transitions are crucial for an individual's mobility. They are performed an average of 60 times a day [4]. The transitions require high muscle forces, especially in the knee [5,6], and a proper balance control [7]. Both muscle force and balance control tend to decrease with age [8–10], and therefore SitTS and StandTS can pose a problem for the elderly [6]. After the loss of a leg, and specifically a knee, these transitions become very hard to impossible, since the required knee torque must be exerted with just one leg. The inability to exert the required knee torque can shift the problem to the hips by a change in strategy. Therefore it would be beneficial if also the knee prosthesis would be able to contribute to the required torque.

The current state of the art in prostheses does not cover these problems. Burger et al. found that passive prostheses do not provide a support moment in the knee, and that amputees only load their prosthesis after the SitTS transition [11]. The Power Knee (Össur) is the only available prosthesis with an active stand-assist. However, in a comparison study between the Power Knee and two damping assisted prosthesis, the C-Leg (Otto Bock) and the Mauch SNS (Össur), none of the prosthesis were found to provide any significant support moment in the knee [12]. On average, the tested prostheses even counteracted the knee extension during SitTS. The active stand-assist in the Power Knee was found to engage after the peak torque requirement in the SitTS transition, and thus did not help [12]. A custom active knee-ankle prosthesis [13], in which both joints behave as non-linear springs, was found to provide more support torque, and a similar ground reaction force asymmetry as the Power Knee . One downside of prostheses with active stand-assist is that they tend to be heavy, and weight is reported to be a common reason to stop using a prosthesis [14].

To help elderly amputees regain their mobility, there is need for a lightweight, passive prosthesis that provides support during SitTS and StandTS. To fit this need, the ERiK prosthesis was developed at the TU Delft [15]. This prosthesis uses a pneumatic circuit with a cylinder and a pressure tank to store energy during StandTS and release it during SitTS to contribute to the necessary joint torque. The torque provided by this prosthesis however, is insufficient and the peak torque does not occur at the right time during the transition. Additionally the prosthesis does not have the required range of motion at both the knee and the ankle.

The goal of this study is to design a new type of passive knee-ankle prosthesis, that provides support during SitTS and StandTS in an intuitive manner. The performance of the Energy Recovering Knee-Ankle prothesis (ERiKA) will be tested in a technical evaluation.

In the first section the design requirements of the prosthesis are deduced from literature and the evaluation of the previous prototype. These requirements are then applied in a concept design, and further elaborated in a prototype design. In the third section the test methods are described, and the results are published. Finally, the results and design are discussed, and some recommendations for improvement are made.

II. Design requirements

This section contains the design requirements for the ERiKA prosthesis. First, the basic requirements for an energy

recovering knee-ankle prosthesis are presented. Then, the results of the user tests of the previous prototype, designed with similar requirements are summarized. Finally, the areas of improvement of the previous prototype are used to find a desired behavior for the ERiKA prosthesis.

A. Basic design requirements

The goal of the energy recovering prosthesis is to help elderly amputees regain their mobility. In order to do so, it must reduce the required joint torques in the healthy limb during SitTS and StandTS transitions. To quantify the target reduction of the healthy joint torques, the available muscle strength in elderly was compared with the required joint torques during SitTS found in literature [16]. Based on the relationship between age and available muscle strength, the average elderly individual loses the ability to produce the required joint torques around the mean age of 60. To extend this age by about 15 years to an age of 75 years, the required peak healthy hip torque must be reduced by 30 % and the required peak healthy knee torque must be reduced by 40 %. In addition the prosthesis should support the body weight of the user during gait, and not be too heavy for a comfortable swing phase. Chamlian found that one of the main reasons for amputees to stop using their prosthesis is the weight of the prosthesis [14]. To compete with the current state of the art in leg prostheses, the total mass of the device should be less than 3 kg. The prosthesis should at least be able to support an individual weighing 80 kg.

One of the issues prosthetic users face, is trusting their prosthesis to support their weight. To ensure amputees are comfortable to place their full weight on the prosthesis, both knee and ankle should not flex unintended during gait. Additionally, when the user is seated, it is undesirable for the knee to extend unintended and unexpectedly.

B. Evaluation of the previous prototype

The performance of the ERiK prosthesis was tested in experiments conducted prior to this investigation. The raw data processing and analysis was conducted within the scope of this investigation, to identify the areas of improvement of the previous design. Seven participants with a transfemoral amputation took part in the test. SitTS and StandTS transitions were tested with knee torque support enabled and with the support disabled. The order was randomized within each participant to negate learning effects. The conditions were tested in trials of 1, 3 or 5 repetitions, with the aim of completing the transition as fast as possible.

Markers were placed over bony landmarks in the legs and torso [17], which were captured by a motion capture system consisting of 4 cameras. The 3D positions of the markers were used to calculate the joint angles. Force plates were used to measure the ground reaction forces (GRFs) under both feet and the chair.

The joint moments in the knee and hip were calculated for both the healthy and the prosthetic leg by taking the cross product of the position vector of the joint with respect to the center of pressure (CoP) under the foot and the GRF vector. A symmetry measure was calculated for each trial by taking the median over time of the vertical GRF ratio between the healthy and prosthetic side. Here, a value of 1 represents full symmetry and a value of 0 means all weight is placed on the healthy leg. Paired *t*-tests were used to show significant differences between conditions.

Four of the seven participants had no difficulties performing SitTS and StandTS, both with and without support. Two participants had difficulties during StandTS trials with support enabled, one of whom also showed difficulties during SitTS trials with support enabled. The last participant could only perform consistent SitTS transitions with support enabled.

During SitTS, the participants positioned the prosthetic foot on its toe and in front of the healthy foot in both conditions. With support enabled, the prosthetic knee was often fully extended before the healthy knee, and before trunk extension started. During StandTS the prosthetic foot was also placed in front of the healthy foot. Both with and without support, participants showed difficulties initiating knee flexion, often caused by insufficient weight being placed on the prosthesis. In most trials, knee flexion was finally initiated by placing the prosthesis on its toe and pressing the residual limb forward. After initial flexion, most subjects collapsed onto the chair. In some trials, unwanted knee extension occurred after seat-on.

The results showed a significant decrease in sound-side knee torque during SitTS for the condition with support enabled (1.02 Nm/kg vs. 1.09 Nm/kg, $p = 0.015$). Other joint torques did not show significant differences. The weight distribution was significantly more symmetric in trials with support in both SitTS and StandTS ($p = 0.048$ and $p = 0.008$). All but one of the subjects had a decrease in sound-side knee torque for the StandTS trials with support, but this did not reach significance. A more detailed overview of the test methods and results can be found in Appendix A. The results of the user tests show that the ERiK prosthesis has the potential to help transfemoral amputees perform SitTS and StandTS transitions. Both the small reduction in sound-side knee torque and the increase in GRF symmetry show promise that the energy recovering concept might work. There is room for improvement however, to reach the target reductions presented in subsection II-A.

C. Desired dynamic performance

As shown in the previous section, the previous prototype does not provide sufficient support to reach the new target reductions. The resulting sound side knee and hip torques are similar to the ones measured by Burger [11] and Highsmith [12], in studies which concluded that the used prostheses gave little to no support during the transitions. Therefore, the ERiKA prosthesis should have a larger potential support torque, to reach the joint torque reduction goals set in subsection II-A.

Furthermore, the knee torque in the ERiK prototype was not similar to the natural knee torque profile during SitTS. The residual forces during quiet standing and sitting resulted in unintended knee extension and difficulty initiating knee flexion, as described in subsection II-B. Therefore, the ERiKA prosthesis should have a knee torque profile that resembles a

natural knee torque profile, with a peak extension torque right after seat-off and negligible torque at the start and finish of the transition.

To achieve this, reference data for the torque and angle during the transition is required. The torque provided by the prosthesis can then be optimized to match this reference data. As reference data, the torque and angle profile provided in a paper by Doorenbosch was selected [18]. The first reason for the selection is that it is a complete dataset of both torque and angle data for the hip, knee and ankle joints. Furthermore, a literature review has shown that the results are close to the median values from the scattered data measured in literature [16]. The reference data was multiplied with the desired bodyweight (80 kg), and scaled to match the peak torques of the presented hypothetical prosthetic SitTS transition in the literature review [16]. The reference torque profiles are shown in Fig. 1.

Finally, the placement of the prosthesis on the toe during both SitTS and StandTS showed that the ERiK prosthesis lacked a degree of freedom (DoF) in the ankle. Ankle dorsiflexion is crucial during the SitTS and StandTS transition to position the center of mass (CoM) over the base of support (BoS) [19]. Studies have shown that a more forward placement of the feet increases the required joint torque in the hips [20]. Therefore, the ERiKA prosthesis should have a DoF in the ankle, with a range of motion (RoM) of least $15°$ of dorsiflexion. To allow a flat foot placement in a seated position, the RoM of the knee flexion should be increased by the same angle.

An overview of the requirements is shown in Table I.

TABLE I: An overview of the design requirements and desirements of the ERiKA prosthesis.

Requirements	**Value**
Mass	< 3 kg
Supported Bodyweight	80 kg
Peak Healthy Hip Torque Reduction	30 %
Peak Healthy Knee Torque Reduction	40 %
Knee Range of Motion	$0° - \geq 105°$
Ankle Range of Motion	$0° - \geq 15°$
No Unwanted Flexion during Gait	-
No Unwanted Extension while Seated	-
Desirements	
Natural Joint Torque Profile, like [18]	

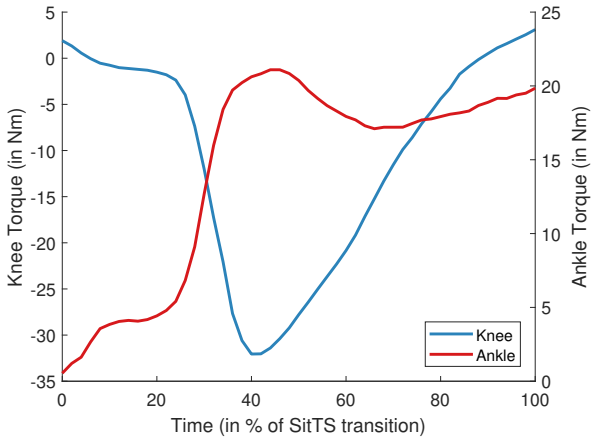

(a) The torque trajectory over time

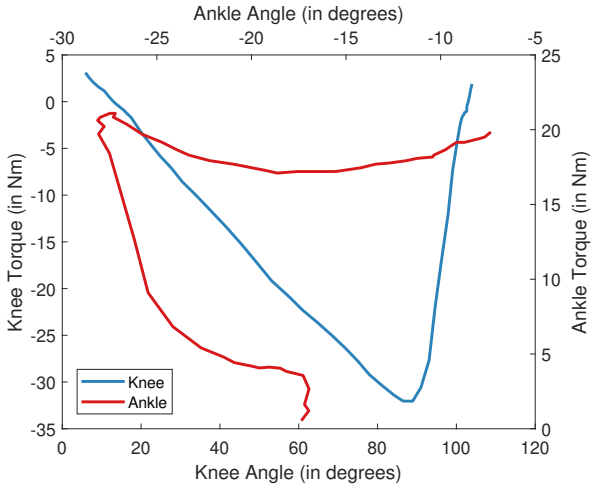

(b) The torque trajectory over the joint angle

Fig. 1: The reference profiles for the ERiKA prosthesis design from Doorenbosch [18]. The average profile of 9 subjects is shown, synchronized at seat-off. The blue line represents the knee torque profile (left axis) and the red line represents the ankle torque profile (right axis). Knee flexion and ankle plantarflexion are defined as positive.

III. Prototype Design

The goal of this section is to describe the design of an knee-ankle prosthesis that can store and release energy during the StandTS and SitTS transitions. First the design concept is introduced and the process of optimizing it is explained. Then an integrated design is proposed. Next, a proof-of-concept prototype is introduced and its mechanical realization is explained. Finally, the pneumatic circuit of the prototype is described.

A. Concept design

For energy storage and release, pneumatic actuators are selected, because of the high energy density. As the reference data in Fig. 1b shows, in the reference movement the ankle dorsiflexes and then plantarflexes, with a different torque each way. To make this possible in a design featuring pneumatic cylinders with spring-like behavior, the ankle cylinder has to be connected to the knee cylinder. However, when comparing the lines in Fig. 1a, high ankle torque values do not coincide with high knee torque values. Since the pressure in the shared system is the same in both cylinders, high actuator force, and thus high joint torques, will coincide in the prosthesis. A second ankle actuator is added to counter this. The second actuator supplies the high ankle plantarflexion torque at the end of the cycle. The primary ankle actuator supplies a dorsiflexion torque to counter this extra actuator torque at the start of the transition.

To reduce the weight of the prosthesis, two of the cylinders are placed rigidly in the shank to act as structure members. Since they can no longer rotate, an extra transmission is required

in the form of a transmission rod. The global concept of the prosthesis is therefore one with a single push cylinder at the knee, integrated in the shank and with a transmission rod. The cylinder shares a pressure tank with the main ankle cylinder, also integrated in the shank and also a push cylinder. A secondary ankle cylinder, with a separate pressure tank, counteracts the main ankle cylinder by pulling. A schematic drawing of the concept is shown in Fig. 2a.

The intended behavior of the prosthesis is supposed to mimic the reference torque in Fig. 1 as close as possible during the entire transition. To attain this, the joint torques applied in the prosthesis were optimized in a static optimization. The reference data was discretized to 51 datapoints, containing reference angles and torques for the ankle and the knee. The angle data was then used to calculate the pressure in the pistons, and the predicted joint torques in both the knee and the ankle. The calculations are explained in more detail in Appendix B. The difference between the predicted knee and ankle torque and the reference torques were summed, and the sum of squares was calculated, as is shown in equation (1).

$$S = \sum_{i=1}^{N} \left(W_K \cdot (K_{r,i} - K_{c,i}) + W_A \cdot (A_{r,i} - A_{c,i})\right)^2 \quad (1)$$

Here S is the sum of squares, i is the datapoint and N is the total number of datapoints. W_K and W_A are the weights of the knee and ankle error, respectively. $K_{r,i}$ is the reference knee torque at instance i and $K_{c,i}$ is the calculated knee torque at instance i. $A_{r,i}$ and $A_{c,i}$ are the reference and calculated ankle torques. The calculated torques $K_{c,i}$ and $A_{c,i}$ depend on the parameter values.

This sum of squares was used as the cost function in a gradient search optimization. Because of the influence of the starting point, and the high risk of local minima, this optimization was run multiple times with randomized starting points within the constraints. The optimization was repeated until a total number of 1 million function evaluations was reached. A further elaboration of the calculation of the torques and the optimization is given in appendix B. The constraints of the optimization are also presented there.

The optimization parameters were the positions of the attachment points of the cylinders, the diameter of the cylinders, the length of the transmission rods, the angle of the cylinders, the pre-pressure of the pressure systems and the maximum pressure of the pressure systems. The parameters are visualized in Fig. 2. In the next subsection a result of the optimization of the concept was used to design an integrated prototype of the prosthesis.

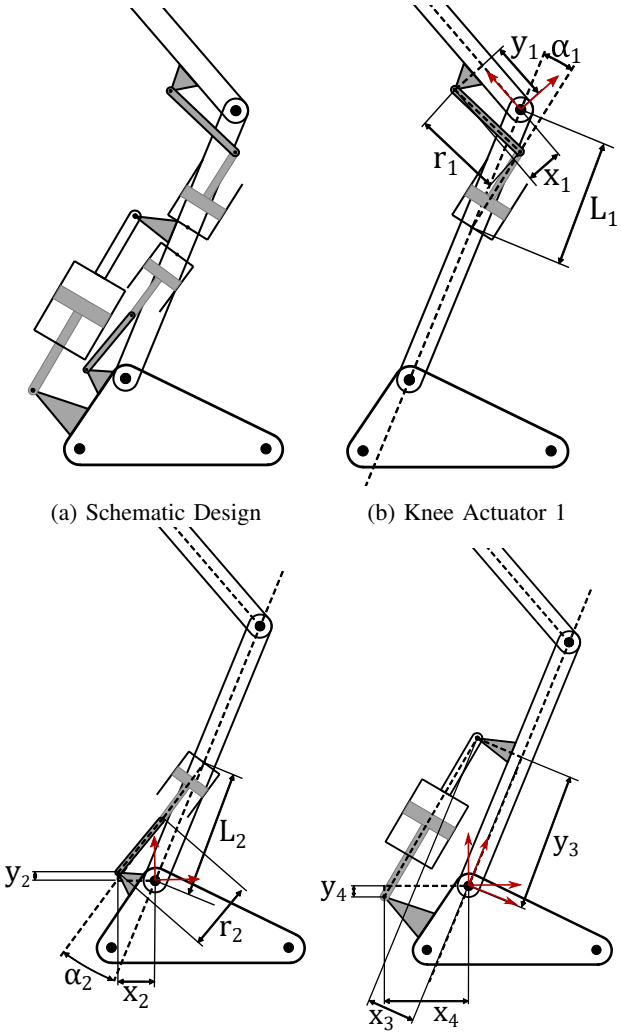

(a) Schematic Design (b) Knee Actuator 1

(c) Main Ankle Actuator 2 (d) Sec. Ankle Actuator 3

Fig. 2: The schematic design of the prosthesis. The cylinders in the shank are push actuators, and the posterior cylinder is a pull actuator. The position of the attachment points of the actuators are given by an x- and y-coordinate in the segment-joint coordinate system. The y-axis of the segment-joint coordinate system points from the joint to the proximal segment along the primary axis of the segment. The x-axis points anterior and perpendicular. Connecting rod lengths r are defined in terms of the minimum length, which is the maximum distance from the cylinder main axis to the attachment point.

B. Integrated design

In Fig. 3 a concept for an integrated design is shown. A single piece of aluminium precision tube was used to house the main knee and ankle pistons, and thus their diameters are equal. They were both set at 0.063 m, which is a standard dimension for precision tube. Additionally, both pistons have to be in line with the primary axis of the shank. The secondary ankle cylinder was placed inside the foot. It is attached to the foot and an extended piece of shank. The upper and lower bounds for the attachment points of this cylinder were set to be within the profile of the foot. The diameter of the piston was fixed at 0.032 m, also a standard dimension for precision tube, and small enough to fit in a foot. The benefits of this configuration are that the cylinder is hidden from view in the foot, and it does not interfere with the main ankle cylinder. The downside is that its weight is placed more distal in the leg, and therefore walking is more energy demanding.

The pressure tank of the main pneumatic circuit is located

in the tube, integrated as dead volume in the ankle chamber. The knee chamber is separated from the ankle chamber by a pneumatic circuit, containing a solenoid valve and a check valve, that prevents unwanted extension while seated. The volume of the pressure tank/ankle chamber is altered by adjusting the length r of the piston rod of the ankle piston. The pressure tank of the secondary pneumatic circuit was also integrated as dead volume in the secondary ankle cylinder. Integrating these components in a single tube enables the prosthesis to be smaller and lighter, and more pleasant to look at. Additionally, it reduces the dead volume introduced by connection tubes that would otherwise be required. The design shows the possibilities of the concept to make a small, clean and light prosthesis that can apply the required joint torques.

However, the design is complicated and expensive, while the underlying principle has not yet been tested. Furthermore, the integration of the pneumatic components make them inaccessible during testing, for adjustments and alterations. Therefore the decision was made to switch from the integrated design to a different, less integrated proof-of-concept prototype, which is more suitable for testing the performance of the torque profiles during StandTS and SitTS. This proof-of-concept was constructed with off-the-shelf components and simple connection pieces, to reduce cost. Weight and size were of secondary importance in the prototype, as it will not be tested for walking. The use of off-the-shelf components had some practical implications on the design space, and thus a new optimization had to be performed. The optimization and design of the proof-of-concept will be further elaborated in the next section.

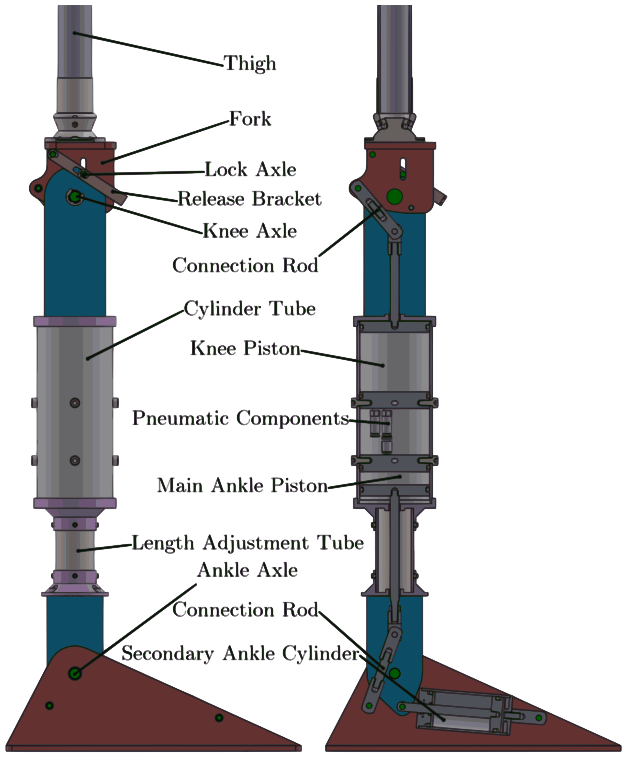

Fig. 3: Outside and sectional view of the integrated design

C. Proof-of-concept prototype

In this subsection the proof-of-concept prototype and its workings will be discussed. In Fig. 6 the design of the prototype is shown. The prosthesis consists of three sub-assemblies, representing the thigh, shank and foot segments. The shank sub-assembly contains three pneumatic cylinders, two of which are connected to the foot segment and one of which is connected to the thigh segment.

In Fig. 4 the positions of the joints and pistons are shown at four events during the SitTS cycle: start, seat-off, maximum ankle dorsiflexion and the end of the cycle. The knee starts in full flexion, with the ankle dorsiflexed slightly to place the foot flat on the ground. The knee piston is fully compressed, and both ankle pistons are compressed a little. Due to the short moment arm at the knee, the resulting knee torque is still small, while the ankle cylinders counteract each other to have a small resulting ankle torque as well. The instances of seat-off and maximum ankle dorsiflexion follow each other shortly, with the ankle at maximum dorsiflexion, and the knee still at a considerable flexion. This still results in a small torque at the knee, due to the short arm, while the torque at the ankle has risen close to its maximum and final value. Thereafter, both joints extend to a fully extended position, releasing pressure in the knee cylinder and secondary ankle cylinder, but building it in the main ankle cylinder. This effect is negligible however, due to the small volume of the main ankle cylinder. The knee torque peaks between maximum dorsiflexion and full stance, when the combination of pressure and moment arm is optimal. The ankle torque remains more or less constant during this part of the cycle.

For the proof-of-concept prototype, a new optimization was performed, taking the limits of off-the-shelf products into consideration. The secondary ankle cylinder was moved to a position posterior to the shank, by changing the parameter constraints of the attachment points. After initial optimization the diameters of the pneumatic cylinders were rounded to available sizes and locked. Furthermore, the height of the foot attachment points of the ankle cylinders was set to the height of the main axle. Finally, the foot attachment points were moved posterior to make space for the cylinder bodies. After further optimization, the main ankle cylinder was rotated to reduce friction caused by radial loads in the piston, incurred by the angle of the connection rod. For the same reason, the connection rod of the main knee cylinder was elongated. Then a final optimization was performed. The constraints and values of the parameters after the final optimization are shown in tables II and III. The modeled performance of the prosthesis is shown in Fig. 5.

The most important difference between the modeled data and the reference data is in the timing and magnitude of the peak knee torque. The peak knee extension torque in the reference data for a user with a bodyweight of 80 kg is 32.1 Nm, which occurs at $88.9°$ or at 40 % completion of the SitTS transition. In the modeled data the peak knee extension torque

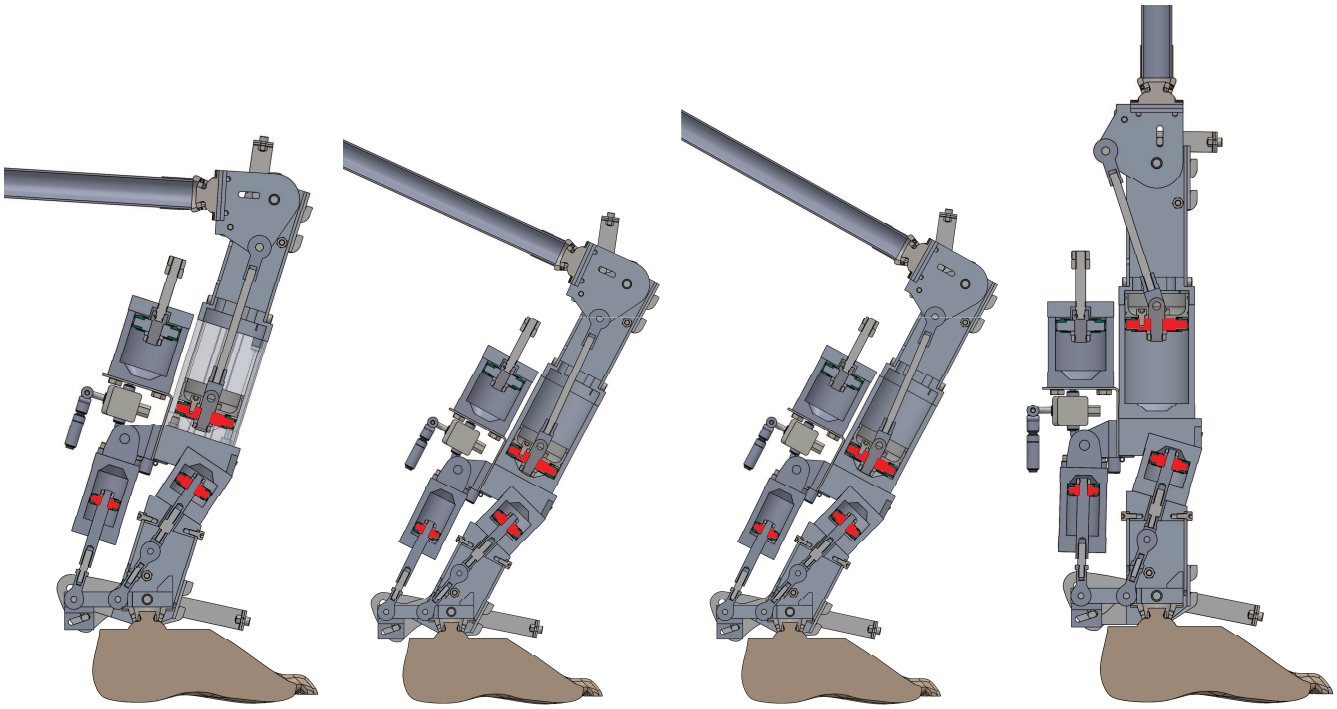

(a) Start of movement (b) Seat-off (c) Maximum dorsiflexion (d) End of movement

Fig. 4: The positions of the joints and the pistons of the prosthesis at the four landmarks during the Sit-to-Stand transition.

is 29.8 Nm, which occurs at 77.9° or at 48 % completion of the SitTS transition. The shape of the ankle torque profile is different when comparing the model with the reference as shown in Fig. 5d. The torque increase during the initial dorsiflexion is more linear and the curve during plantarflexion is flipped. The magnitude of the peak ankle torque is similar between reference and model.

To make the prosthesis applicable for a range of users with different bodyweights, the pre-pressure in both pressure systems can be adjusted. In addition, the volume of the pressure tank in the main pressure system can be adjusted. In Fig. 5 the performance of the prosthesis for a user with a bodyweight of 60 kg, 80 kg and 100 kg is plotted. The relative difference in peak knee extension torque between reference and model is larger in the heavy configuration, while the timing of the peak knee torque is delayed further in the light configuration.

D. Mechanical Realization

In this subsection the mechanical realization of the major components of the prototype is described. The components are grouped according to function.

Shank The shank is the main structure of the prosthesis. It was built from two standardized compact cylinders (ADN-63 and ADN-40, Festo, Esslingen, Germany) of 63 mm and 40 mm. The cylinders are connected to each other and two sections of aluminium square tube (Aluminium 5050) by custom aluminium connection pieces (Aluminium 7075-T6). These connection pieces also allow the ankle cylinder to be rotated 16°. In the location where the aluminium square tubes interact with the main axles, the endstops and the joint locks, the aluminium is reinforced using stainless steel plates.

Knee Piston The knee piston can move in the upper cylinder of the shank. The piston consists of the standard piston head of the ADN-63 piston, with a shortened piston rod. Shortening the piston rod allows the use of a longer connection rod, without elongating the shank length of the prosthesis. The connection rod consist of a piece of M8 thread, connected with a clevis to the piston rod, and by a rod-eye to the thigh segment. To prevent radial movement of the piston head in the cylinder, a POM piston skirt was added.

Main Ankle Piston The main ankle piston can move in the lower cylinder of the shank. The cylinder was rotated to reduce friction due to radial forces. The radial forces were further reduced by a guidance bushing, placed in the lower connection piece. A clevis and rod-eye joint connects the connection rod to the piston rod. The other end of the connection rod is connected to the foot segment using another rod-eye.

Secondary Ankle Piston The second ankle piston can move in an extra cylinder (ADN-32, Festo, Esslingen, Germany) placed anterior to the shank. The cylinder is connected to the shank using a standard hinging connection (SNCS/LBG-32, Festo, Esslingen, Germany), to allow rotation between the cylinder and the shank. The piston is connected to the foot segment using a rod-eye.

Thigh The thigh segment consists of a fork, two custom aluminium parts (Aluminium 7075-T6) held together by a male pyramid adapter (2R54, Otto Bock). The fork is

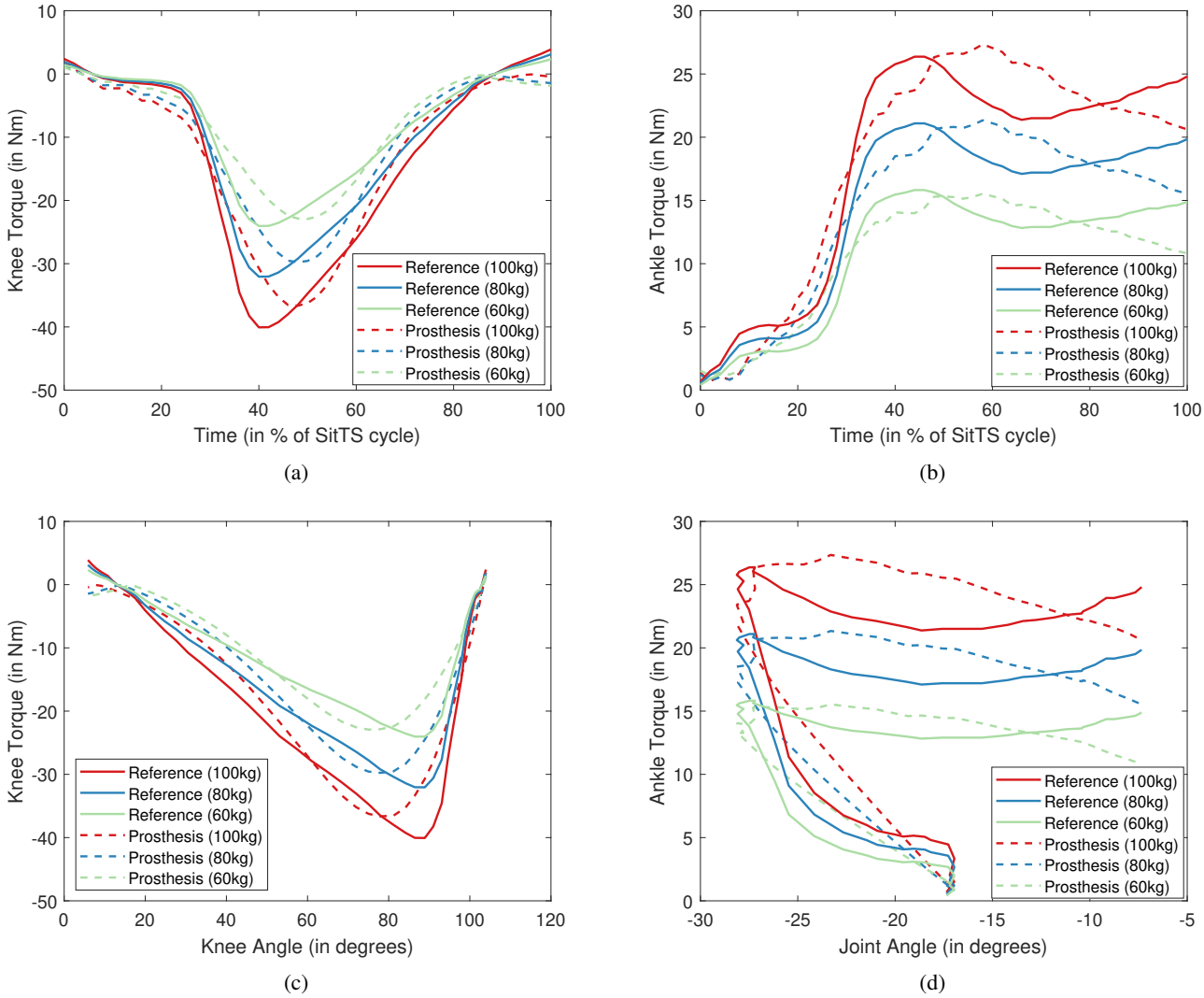

Fig. 5: The modeled performance of the prosthesis compared to the reference profiles. The three solid lines represent the reference torque profile from Doorenbosch et al. [18], multiplied by one of three different bodyweights, 60, 80 and 100 kg. The three dashed lines represent the calculated performance of the prosthesis at the configuration best suited for the bodyweight.

TABLE II: The upper and lower limits of the optimized parameters for the proof-of-concept prototype. The description of the geometric parameters is shown in Fig. 2. D_1, D_2 parameters and D_3 represent the diameters of the cylinders. p_0 and p_1 are the pre-pressure and compressed pressure.

Main Knee Actuator			**Main Ankle Actuator**			**Main Pressure System**			**Secondary Ankle Actuator**			**Secondary Pressure System**		
	LL	**UL**		**LL**	**UL**		**LL**	**UL**		**LL**	**UL**		**LL**	**UL**
x_1	-60 mm	50 mm	x_2	-50 mm	-30 mm	$p_{0,1}$	0 bar	4 bar	x_3	-61 mm	-61 mm	$p_{0,2}$	0 bar	9 bar
y_1	-50 mm	50 mm	y_2	0 mm	0 mm	$p_{1,1}$	2 bar	10 bar	y_3	150 mm	200 mm	$p_{1,2}$	2 bar	10 bar
r_1	160 mm	165 mm	r_2	48 mm	60 mm				x_4	-75 mm	-75 mm			
L_1	25 mm	250 mm	L_2	90 mm	110 mm				y_4	0 mm	0 mm			
D_1	63 mm	63 mm	D_2	40 mm	40 mm				D_3	32 mm	32 mm			
α_1	$0°$	$0°$	α_2	$-16°$	$-16°$									

connected to the shank segment by the stainless steel knee axle. Bronze bushings were used to prevent friction in the joint. The connection rod of the knee piston is connected by another stainless steel axle. The pyramid adapter is used to connect the prosthesis to a user's prescribed socket.

Foot The foot segment is formed by a low-profile prosthetic foot (1G6 Pedilan, Otto Bock). It is connected to a custom aluminium foot plate (Aluminium 7075-T6) by a female pyramid adapter. The custom foot plate houses the main ankle axle, and two connection rod axles. All axles are stainless steel. Again, bronze bushings were used to prevent friction.

Knee Lock To ensure the prototype can support the user

TABLE III: The final values of the optimized parameters for the proof of concept prototype.

Main Knee Actuator		Main Ankle Actuator		Main Pressure System		Secondary Ankle Actuator		Secondary Pressure System	
x_1	-48 mm	x_2	-30 mm	$p_{0,1}$	0.00 bar	x_3	-61 mm	$p_{0,2}$	3.71 bar
y_1	11 mm	y_2	0 mm	$p_{1,1}$	10.00 bar	y_3	150 mm	$p_{1,2}$	8.48 bar
r_1	160 mm	r_2	60 mm			x_4	-75 mm		
L_1	229 mm	L_2	90 mm			y_4	0 mm		
D_1	63 mm	D_2	40 mm			D_3	32 mm		
α_1	$0°$	α_2	$-16°$						

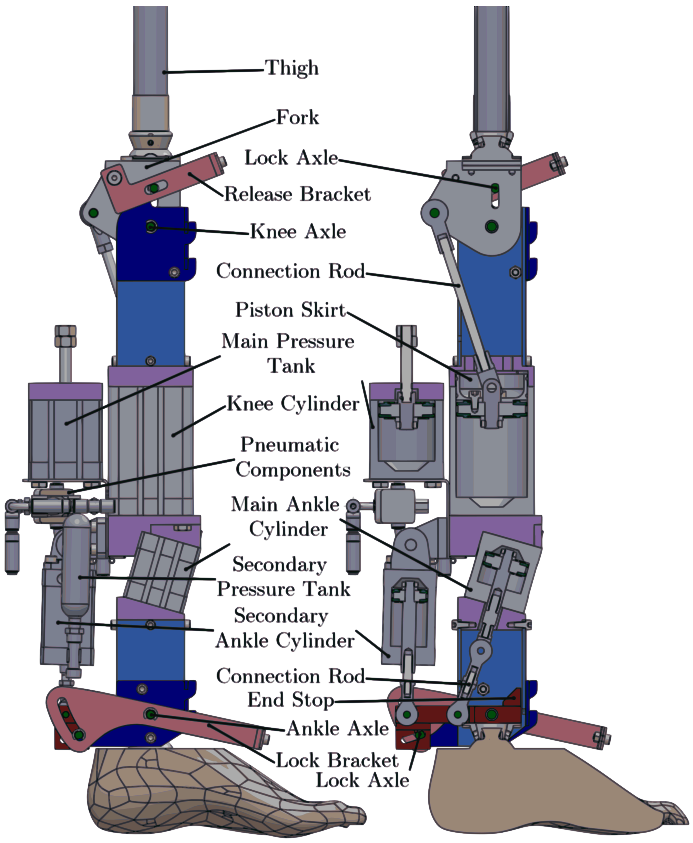

Fig. 6: Outside and sectional view of the prototype design

while moving around, a lock was incorporated at the ankle and the knee joint. A slot in the fork houses the stainless steel knee lock axle. The lock axle was flattened on two sides to reduce surface pressure. When locked and loaded, the axle is pressed against a protruding part of the stainless steel reinforcement plate by a flexing moment, preventing rotation. The lock is released by pulling the stainless steel release bracket, thus moving the lock axle over the edge of the reinforcement plate. An elastic element pulls the axle back towards the main knee axle, to automatically engage the lock when the knee is fully extended.

Ankle Lock The ankle lock was designed similar to the knee lock. A flattened lock axle was placed in a slot beneath the foot plate. A protruding part of the reinforcement plate presses against the axle when loaded by an ankle dorsiflexing moment. The lock is released by pulling the release bracket and moving the lock axle over the edge of the reinforcement plate. The release bracket was designed with a curved slot to produce an optimal release force on the axle along the slot, with a minimal release torque.

Endstops Over-rotation of the ankle and the knee is prevented by mechanical endstops. The knee is limited from overextending by the design of the fork, which hits the inside of the aluminium square tube. A small layer of rubber was used to reduce the impact. In a similar manner, an aluminium block was placed on the foot plate, to prevent ankle plantarflexion further than the neutral position. Knee flexion is limited by the bolts of the release bracket hitting the reinforcement plate. Finally, ankle dorsiflexion is limited by the end position of the ankle pistons inside the cylinders.

E. Pneumatic components

The pneumatic circuit is shown in Fig. 7. It is an adaptation of the circuit in the ERiK prototype [15]. The main pneumatic circuit consists of two cylinders, a pressure tank, two check valves and a solenoid valve. During StandTS the air volume in the knee cylinder will decrease, which will increase the pressure in the entire system through the check valve. After the StandTS transition is completed, the air cannot flow back, preventing unwanted knee extension while the user is seated. Opening the solenoid valve allows the air to flow back to the knee cylinder, to provide an extension torque in the knee during SitTS. The ankle cylinder is connected directly to the pressure tank. Because the ankle cylinder has a smaller diameter and a smaller stroke than the knee cylinder, the movement of this cylinder does not influence the pressure in the system as much. The ankle cylinder is not disconnected from the pressure tank because the counteracting ankle cylinders ensure an equilibrium point that is close to the seated ankle position. The second ankle cylinder is connected directly to a separate pressure tank.

The pre-pressure in both systems, as well as the volume of the pressure tank in the main pneumatic circuit can be adjusted to account for the body weight and required torque of the user. The pre-pressure in both circuits is set by supplying pressured air to the inlet check valves attached to the pressure tanks. The main pressure tank consists of an adjusted compact cylinder (ADN series, Festo, Esslingen, Germany) where the piston rod was replaced by thread, to lock the piston in place and allow it to be screwed in and out, which alters the internal volume.

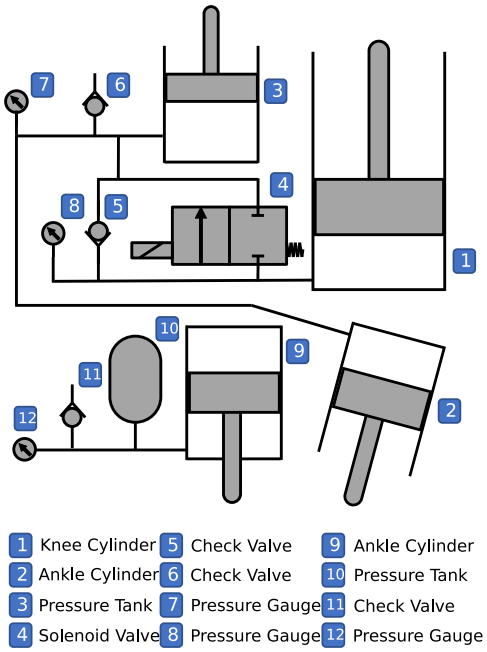

Fig. 7: The pneumatic system of the prosthesis, consisting of two separate circuits.

IV. Prototype Evaluation

The goal of this section is to evaluate the prosthesis to see whether it fulfills the requirements set in section II. The section is split in four parts. In the first part, the test setup used to evaluate the properties of the prosthesis is described. In the second part, the test protocol and the configuration of the prosthesis are explained. The third part explains the analysis of the data. Finally, the results of the tests are presented in the fourth part.

A. Test Setup

The length, weight and range of motion were measured using measuring tape, a load cell and an angle meter. The joint torque in the knee and ankle however, were not as trivial to measure. Their magnitude depends on the angle of both the knee and the ankle. In order to accurately determine the behavior of the prosthesis, the influence of friction has to be taken into account. The friction causes the joint torque to depend on the direction of travel. This behavior can only be measured when the joint is moving. Therefore, one joint was fixed in several positions, while the other joint was forced through its RoM. This was repeated with the other joint fixed. In Fig. 8 a photograph and schematic of the test setup are shown. The prosthetic foot and pyramid adapter were removed from the prosthesis. They were replaced by aluminium square tubes, to create a convenient moment arm to generate torque. A long prosthetic tube was attached to the pyramid adapter on the thigh part of the prosthesis for the same reason. The shank of the prosthesis was placed on a construction of aluminium square tubes and pipe clamps. It was held in place by two leveling feet that can be extended to push the prosthesis against two corner profiles. The construction supporting the shank piece was fixed to a wooden plate. Also fixed to the wooden plate were two guide rails, one for the thigh segment and one for the foot segment. On each rail, a pipe clamp was placed that could move along the rail. The pipe clamp was fixed to either the thigh or the foot segment by means of a 3D printed part. By sliding the clamp along the guide rail, the joint angle was altered. Each trial, one of the clamps was clamped down, keeping one of the joint angles constant.

A rope was attached to the segment that was not fixed in place, to pull it through the RoM. Between the rope and the segment a loadcell was placed to measure the pull force in the rope. The rope was pulled around a pulley, which was also attached to the wooden plate. From the position of the pulley, the direction of the pulling force can be deducted, which is important to calculate the magnitude of the joint torque. To calculate the direction of the force, the position of the attachment point of the rope to the prosthesis is required, which can be calculated using the angle of the joint.

To measure the angle of the joint, a linear encoder was used in combination with a piece of wire and a position wheel. The position wheel was fixed rigidly to the shank. The wire was placed along one side of the position wheel and the end was fixed to the wheel. The other end of the wire was fixed to the linear encoder, which is spring loaded to keep tension in the wire. When the joint is flexed, more wire is required along the circumference of the position wheel, which pulls the linear encoder out. By measuring the position of the linear encoder, the angular position of the joint was determined.

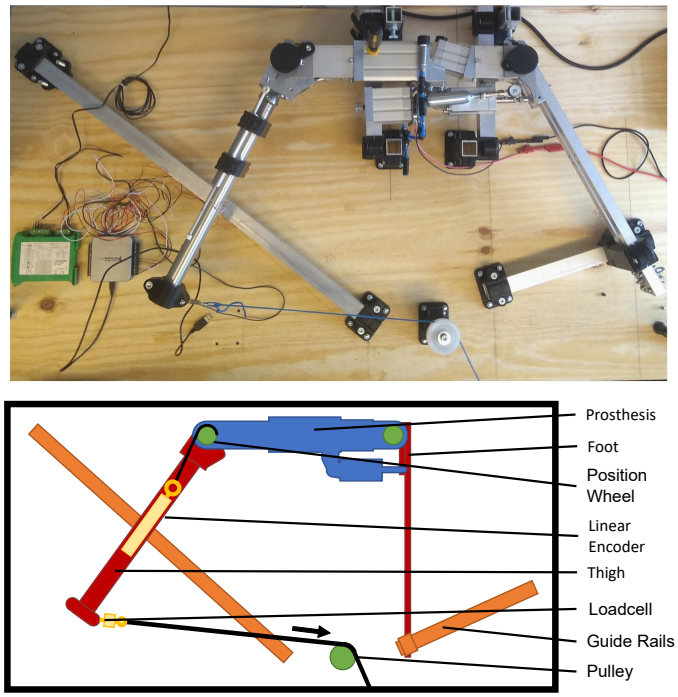

Fig. 8: The top view and schematic of the test setup used to evaluate the joint torques in the prototype. One of the joints is fixed using the guide rails. The angle of the other joint is measured using a linear encoder. A loadcell is used to measure the joint torque.

B. Test Protocol

Both joints were measured while moving through their entire RoM, with the other joint fixed in a number of angles. For the knee joint the fixation angles ranged from 0° to 104° with increments of 15°. The final value represents the limit of the test setup. For the ankle joint the fixation angles ranged from 0° to 27.5° with increments of 5°, where again the final value represents the limit of the test setup. For each fixation angle, the other joint was pulled and released through its RoM in both directions 5 times, to remove the effects of stick-slip behavior and human error. To negate the effects of inertia and damping, the trials were performed at a low velocity, that was kept constant manually.

For some knee positions, the ankle has an equilibrium position in which the joint torque is zero. To measure the behavior of the prosthesis on both sides of the equilibrium position, the attachment point and pulley were moved to the opposite side of the foot segment. This switched the direction of the pull force. The knee joint has an equilibrium point for all ankle positions. However, the joint does not stick in this position, as the equilibrium point is meta-stable. To measure the behavior on both sides of this equilibrium point, a push force was exerted on the loadcell in the direction of the rope. Since the loadcell can measure both tension and compression forces, the torque of the push force can be calculated as well.

For the base configuration, the pressure tank was set to its smallest volume, and the pre-pressure was set equal to the atmospheric pressure. The pre-pressure in the secondary ankle cylinder was set such that the ankle had an equilibrium point of 17.5° when the knee was fully flexed. This led to a pre-pressure of 2 bar. This configuration is supposed to be close to the heaviest calculated configuration, as described in subsection III-C.

To evaluate the influence of pressure tank volume and pre-pressure, the prosthesis was also tested in a configuration with the pressure tank cylinder extended by 5 mm and a configuration with a pre-pressure of 1 bar. The influence of ankle pre-pressure was tested by altering it to 3 bar.

C. Data Analysis

For each repetition the start of the movement was defined as the first five consecutive samples with movement in the same direction. The end of the movement was defined as the last five consecutive samples with movement in the same direction. Since it is impossible to recreate an exact SitTS or StandTS transition on a workbench, a characterization of the prosthesis on all angles is required. To find this characterization of the prosthesis, polynomials were fitted to the data of each individual fixation. Separate polynomials were fitted to both directions of movement, to quantify the hysteresis. Multiple trials of the same fixation angle with opposite force directions were combined, to characterize the behavior on both sides of the equilibrium point. Two approaches were used to calculate the joint torque for a given set of joint angles and movement direction. The first method fitted 2D polynomials to the individual trials, and used the parameters to calculate the joint torque for the given moving angle at all fixed angles. Then cubic interpolation was used to find the corresponding joint torque for intermediate angles. The polynomials were first order for the ankle, since the behavior of the ankle joint is linear through the range of motion used in the SitTS transition. To remove any bias caused by the area beyond the range of motion used in the transition. these datapoints were ignored. The polynomials were fifth order for the knee, because lower orders do not fit the behavior accurately near full flexion and full extension. These areas are crucial for the behavior of the prosthesis.

The second method fitted a 3D surface polynomial to the data of all trials for both joints, and used the parameters to calculate the joint torque directly. The order of the 3D polynomials was first for the ankle and fifth for the knee. An example of the 3D polynomial is given in equation (2).

$$\begin{aligned} T = {} & p_1\alpha^1\beta^4 + p_2\alpha^1\beta^3 + p_3\alpha^1\beta^2 + p_4\alpha^1\beta^1 \\ & + p_5\alpha^1\beta^0 + p_6\alpha^0\beta^5 + p_7\alpha^0\beta^4 + p_8\alpha^0\beta^3 \\ & + p_9\alpha^0\beta^2 + p_10\alpha^0\beta^1 + p_11\alpha^0\beta^0 \end{aligned} \tag{2}$$

Here T is either the ankle or the knee joint torque, and p_i are the coefficients of the polynomial. Finally, α and β are the ankle and knee angle respectively.

D. Test Results

In Fig. 9 an example of a single trial of five repetitions is shown. The measured joint torque is shown for the knee and the ankle, with the other joint fixed in the neutral position. These example trials will be used to show the fitting of the polynomials in the first part of this subsection. In the data of both joints hysteresis is clearly visible, which will be shown in more detail in the second part of the subsection. Then the polynomials are used to calculate trajectories for both the SitTS and StandTS transitions. Finally the results from the adjustments will be compared to the base configuration.

Fitting of polynomials: In Fig. 9 fitted 2D and 3D polynomials are shown, as well as measured data of the movement. In Table IV the fitness of the polynomials is expressed in the RMSE value. The RMSE value shows the errors between the calculated values and the measured values. A lower RMSE value indicates a better fit. In Table IV the average RMSE value indicates the 2D fit of the polynomials, averaged over all trials. The overall RMSE value indicates the 3D fit of the polynomials, calculated for all data points. The 2D polynomial method scores a little better for all polynomials. However, it is not possible test the fit of either method at intermediate angles, which causes a slight bias towards the 2D polynomial method. The 3D polynomial method is faster and uses less coefficients. Therefore, despite its worse RMSE, the 3D polynomial method was selected to calculate the joint torques in the SitTS and StandTS transitions.

Effect of hysteresis: In Fig. 9 the hysteresis in the system is visible in the form of a torque difference between the flexion and extension of the joint. In Fig. 10 this hysteresis is shown. It is compared to an additional trial in which the cylinders are connected directly to the atmosphere, to measure the friction

TABLE IV: The RMSE values of the two fitting methods. For the average RMSE value, the RMSE is calculated for individual trials and averaged. The overall RMSE value is calculated for all datapoints.

	2D Polynomial		3D Polynomial	
Joint	**Average RMSE**	**Overall RMSE**	**Average RMSE**	**Overall RMSE**
Knee Flexion	0.6187 Nm	0.6206 Nm	0.7021 Nm	0.7271 Nm
Knee Extension	1.2210 Nm	0.8635 Nm	1.4162 Nm	1.5290 Nm
Ankle Dorsiflexion	0.1880 Nm	0.2005 Nm	0.2074 Nm	0.2155 Nm
Ankle Plantarflexion	0.2835 Nm	0.2784 Nm	0.2973 Nm	0.2984 Nm

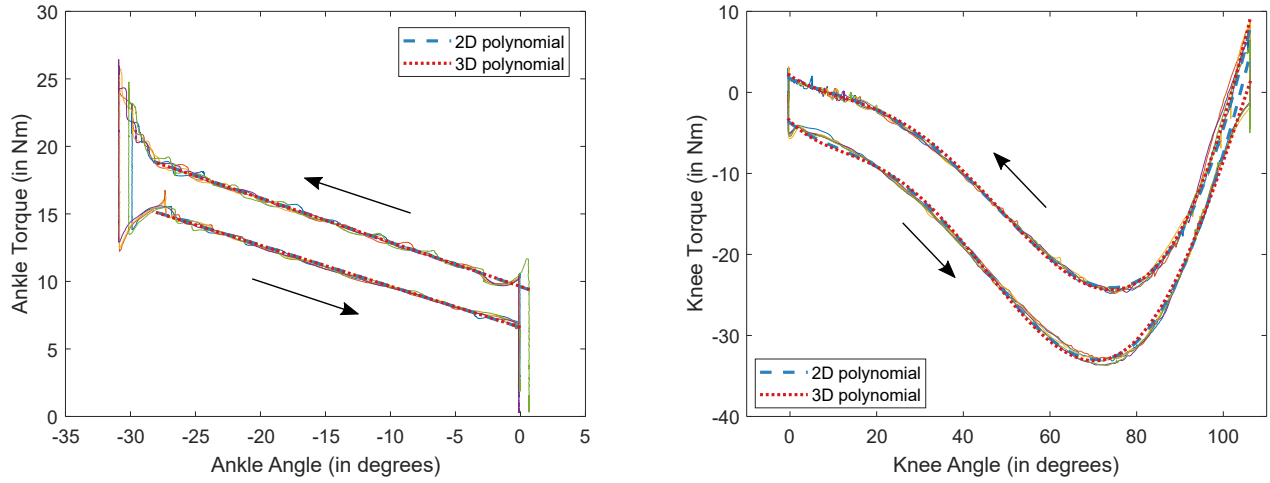

(a) Ankle (b) Knee

Fig. 9: Raw data of the ankle torque (9a) and the knee torque (9a), for five repetitions of one trial. For the depicted trials, the joint angle of the other joint was fixed at 0°. On top of the raw data, polynomials are fitted. The 2D polynomials are fitted to the raw data of this trial, while the 3D polynomials are fitted to the raw data of all trials. The polynomials are 1st order for the ankle, and 5th order for the knee. A clear hysteresis is visible between the two direction of travel.

without pressure. In both the knee and ankle the measured friction without pressure is smaller than the hysteresis when the system is pressured.

The knee hysteresis shows a peak at an angle of about 60°. This peak is not visible in the measurements without pressure. This peak hysteresis is caused by the friction due to the radial load on the piston skirt. The radial load peaks at this angle due to a combination of the actuator force and the angle between the connection rod an the piston rod. The knee angle at which it occurs is similar to the expected angle of 61° in the model. The friction force increases near full flexion to about 4 Nm. This force occurs due to the elastic properties of the piston head being compressed in the chamber at the equilibrium point.

The ankle hysteresis shows a peak near full dorsiflexion in both the measurements with pressure and the ones without pressure. This peak is likely caused by the elastic properties of the piston head again.

SitTS and StandTS trajectories: In Fig. 11 the calculated SitTS and StandTS trajectories, and the measured trajectories are shown. The measured torque in the ankle is smaller than the torque of all three configurations as calculated in III-C during the design phase. This was expected as the base pre-pressure is smaller than the calculated pre-pressure in the optimization. The SitTS and StandTS trajectories for the ankle switch twice, as the direction of travel of the ankle switches twice during the movement. A change in the direction of travel flips the direction of the friction torque, altering the hysteresis. These switches between curves cause the individual trajectories to match the calculated trajectories a little less. Without the unmodeled hysteresis, the shape of the trajectory in Fig. 11a would have been similar to the expected shape. The peak of the measured knee torque during SitTS is smaller than the peak of the calculated trajectories during SitTS. The measured peak knee torque is 18.3 Nm, while the calculated peak knee torque for the heavy configuration is 36.6 Nm. The calculated peak knee torque for the light configuration is 22.9 Nm. Additionally, the peak knee torque occurs at a smaller knee flexion angle than the calculated trajectories. The peak knee torque in the calculated trajectories occurs between 75° and 78°. The peak knee torque in the measured trajectory occurs at 68.5°. The hysteresis between the SitTS and StandTS trajectory is larger than the calculated hysteresis, especially near the start and end of the SitTS movement.

In Fig. 12 the measured knee and ankle trajectories are shown again, this time compared to the reference trajectories for a user with a bodyweight of 60, 80 and 100 kg. It is clear that the measured knee extension torque is further from the reference than the calculated torques. The peak knee extension torque in the reference data occurs at an angle of 88.9°. In the measured data it occurs at 68.5°. The magnitude of the peak

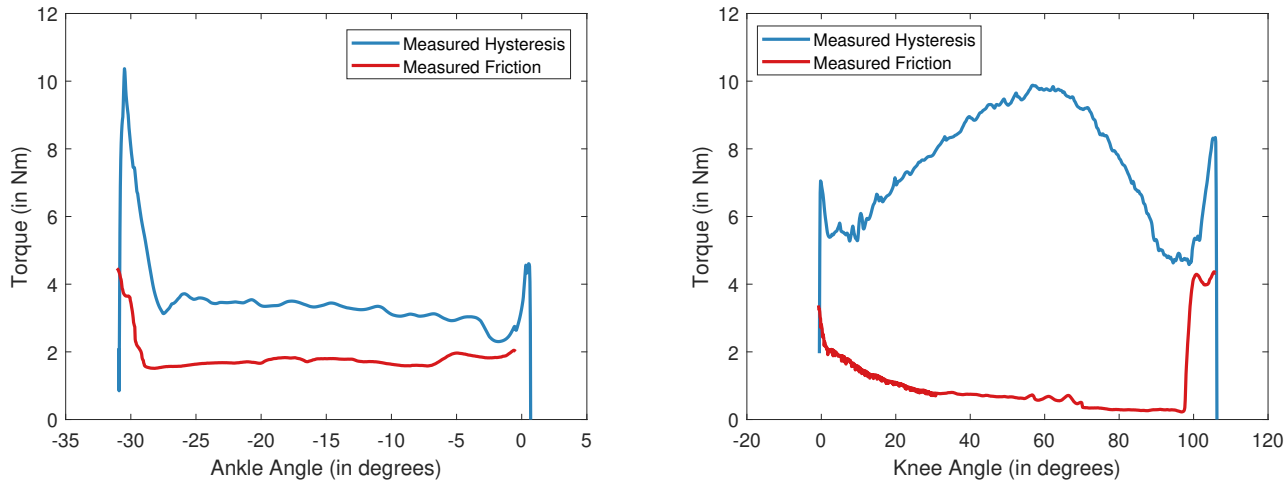

(a) The ankle hysteresis

(b) The knee hysteresis

Fig. 10: The hysteresis between the flexing and extending moment is shown for the knee and ankle, both in the base configuration and a configuration in which the cylinders are connected to the the atmosphere. The difference between the configurations represents the extra losses caused by the pressure in the system.

knee extension torque is smaller as well, with a peak torque of 18.5 Nm. The peak knee extension torque in the reference data is 40.1 Nm for a user weighing 100 kg, and 24.0 Nm for a user weighing 60 kg.

Effect of pre-pressure and tank volume: In Fig. 13 the influence of several adjustments on the performance of the device is shown. In Fig. 13b the measured trajectory of the base configuration is compared to the measured trajectory of the configuration with a larger pressure tank volume and the configuration with a higher pre-pressure in the main system. As expected, a larger pressure tank volume results in a lower peak knee torque, as less pressure amounts in the system. A higher pre-pressure results in a higher peak knee extension torque, as more air is compressed in the system. Additionally the pre-pressure results in a higher knee torque near the end of the SitTS transition. The larger pressure tank volume results in a lower knee torque near the end of the SitTS transition.
In the ankle, a larger pressure tank volume in the main circuit also leads to a lower start, and peak torque, as is visible in Fig. 13a. This is caused by the fact that the pre-pressure in the secondary system is dropped to set the equilibrium angle to 17.5°. The pre-pressure configuration is Fig. 13a corresponds to a configuration with 3 bar of pre-pressure in the secondary pressure circuit. As expected, that leads to higher ankle torque during the entire cycle.

V. Discussion

In this section the results from Section IV will be compared to the requirements from Section II and the predictions from Section III. Furthermore, the strengths and weaknesses of the prosthesis will be compared to the previous prototype, and other prostheses described in several studies. Finally an assessment is made of the viability for the prosthesis for use in everyday life.

A. Evaluation of the prototype

In this section the proof-of-concept prototype is evaluated. In the first part, its key characteristics will be compared to the design requirements. Then the performance of the ERiKA prosthesis will be compared to the desired torque profiles and finally, the modeled torque profiles.

Design requirements: In Table V the design requirements are compared to the actual values of the prosthesis. The prosthesis does fulfill the requirements for RoM and supported bodyweight. The achieved ankle RoM is even twice as large as the required RoM. This extra range of motion is necessary to follow the used reference trajectory [18]. The supported bodyweight is an estimation based on the finite element analysis of the design, and not a measured value. The weight of the bare prosthesis, ending at the pyramid adapter at the knee, is more than the maximum weight in the requirements. The reason for this however can be found in the use of off-the-shelf pressure cylinders. These cylinders have an industrial build quality, and are considerably longer than the stroke, which introduces more weight to the system than strictly necessary. On the other side, components like circuit boards and batteries to control the solenoid valve are not included in the weight. The weight issue is resolved in the integrated design.
The reductions in peak healthy hip and knee torque are unknown, since user tests have not been conducted yet with the new prototype. In subsection V-B the measured support torques are compared with the support torque in other prosthesis to make a prediction of the effect of the prosthesis.
Not included in the requirements was the shank length of the prosthesis, and the location of the ankle joint. The extra length of the cylinders increases the minimum shank length of the prosthesis. The prosthesis has a non-adjustable shank length, from ankle to knee, of 430 mm, which corresponds to a user height of about 1.75 m [21]. The shank length is not adjustable,

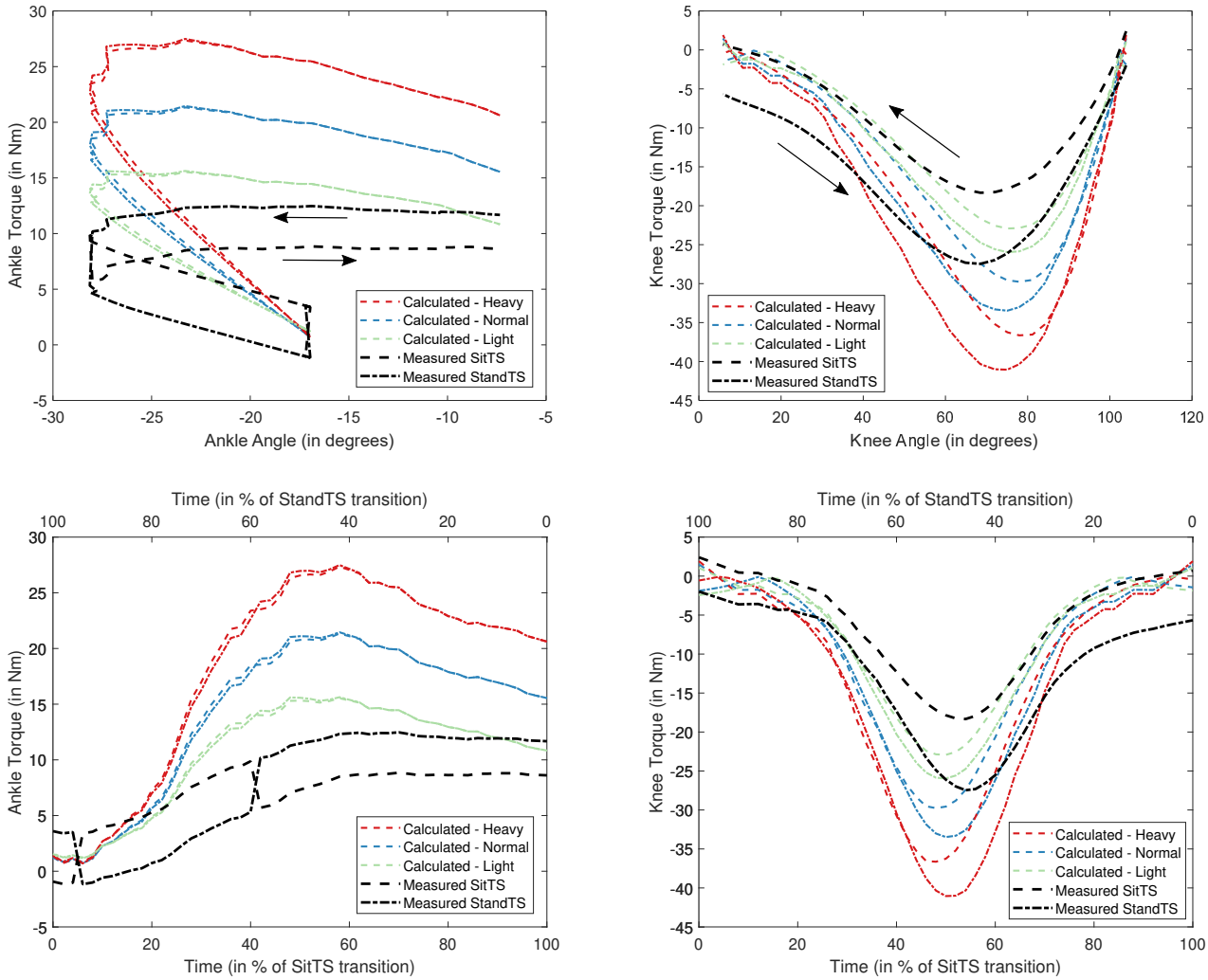

(a) The ankle trajectory

(b) The knee trajectory

Fig. 11: The calculated and measured performance of the prosthesis during SitTS and StandTS. The calculated trajectories of the knee and ankle are shown for a bodyweight of 60, 80 and 100 kg. The calculated trajectories are based on static calculations of the pressure and actuator force in the cylinders. The measured performance is based on a 3D polynomial fitted to test data of the prototype. Angle data from [18] is used to calculate all trajectories. The direction of travel in the ankle switches twice, which causes a switch in hysteresis visible in the figures.

which is not convenient for user testing. This can be negated by placing support blocks under one of the feet. The height of the ankle joint from the ground is 104.5 mm, which is higher than the ankle joint in a healthy individual of 1.75 m [21]. The build height of the standard prosthetic foot and pyramid adapter combination does not allow a lower ankle joint. During user tests, this can also be negated by support blocks under the feet. As with the weight, the shank length issue is also resolved in the integrated design.

TABLE V: The comparison between the requirements and the actual values of the technical evaluation.

Requirements	**Required Value**	**Actual Value**
Mass	< 3 kg	6.1 kg
Supported Bodyweight	80 kg	100 kg (modeled)
Peak Healthy Hip Torque Reduction	30 %	Unknown
Peak Healthy Knee Torque Reduction	40 %	Unknown
Knee Range of Motion	$0° - \geq 105°$	$0° - 106°$
Ankle Range of Motion	$0° - \geq 15°$	$0° - 30.5°$

Reference and modeled trajectory comparison: The desired torque profiles of the ERiKA prosthesis were approached. The overall shape of both the knee and the ankle torque trajectory is very similar to the reference trajectories. The reduced knee torque at full extension should reduce the difficulty initiating knee flexion. Additionally, unwanted knee extension while seated should be prevented by the reduced knee torque at full flexion. Furthermore, the ankle torque profile is shaped to allow dorsiflexion in the early phases of the SitTS transition, as well as provide plantarflexion support during the latter phases.

The most important difference between the reference and the

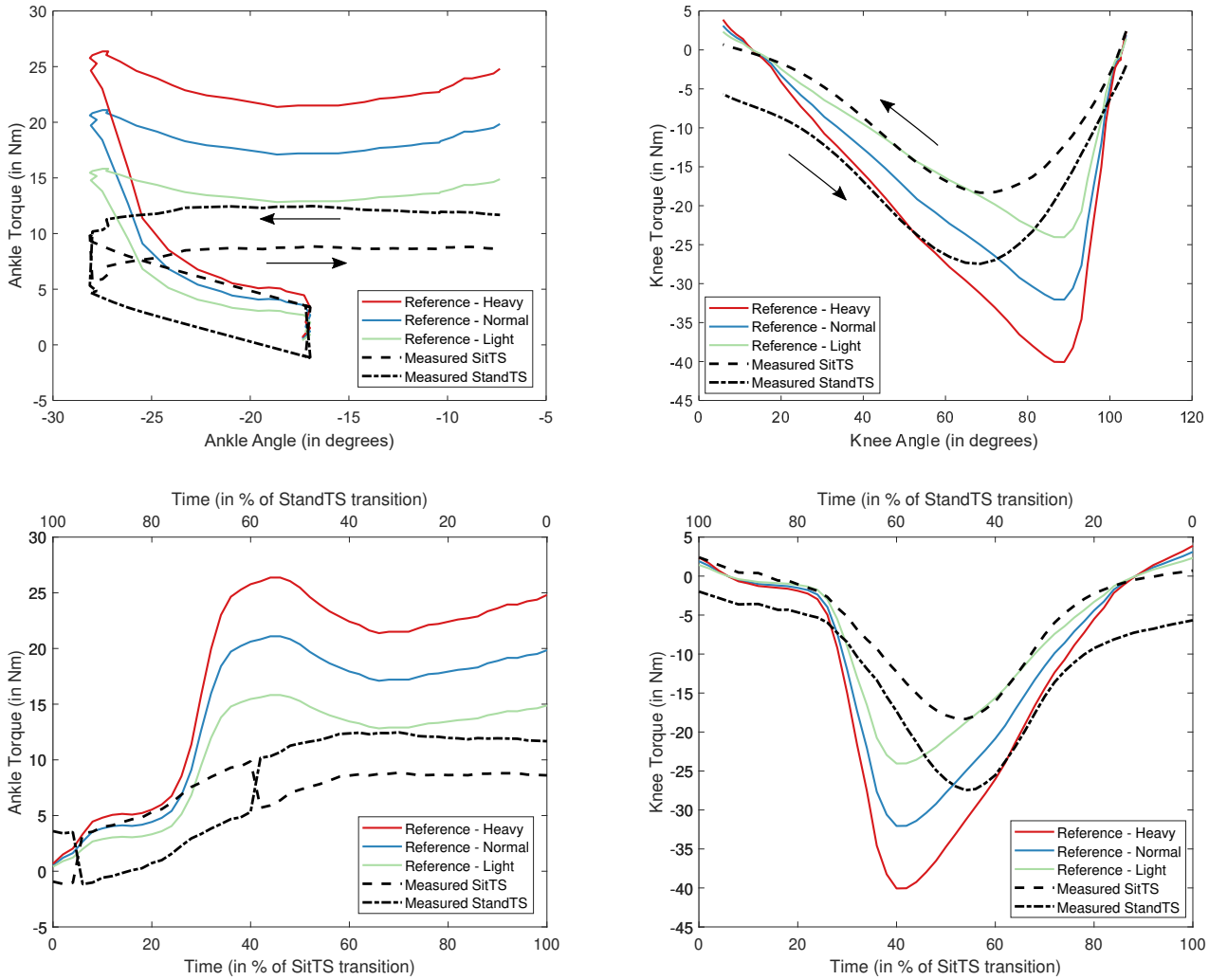

(a) The ankle trajectory

(b) The knee trajectory

Fig. 12: The reference trajectories of the knee and ankle are shown for a bodyweight of 60, 80 and 100 kg. Also the measured performance of the prosthesis is plotted, both for SitTS and StandTS. The reference trajectories are from [18]. The measured performance is based on a 3D polynomial fitted to test data of the prototype. The angle data from [18] is used to calculate the trajectory.

measured trajectories is the delay of the peak knee extension torque from the reference to the prototype. This difference is caused by the moment arm of the actuator force. The attachment points are designed in such a way that the moment arm is near zero in seated position. This causes the small initial knee torque during SitTS present in the reference torque. The moment arm however, can only increase through knee extension, and thus delays the maximum knee torque. By eliminating the initial part of the reference profile for the knee torque optimization, the reference peak knee torque angle could be approached. The reduced knee torque while seated could be realized by the closing and opening of the solenoid valve. This comes at the cost of a sudden increase in knee torque when the valve is opened, which might surprise the user.

A second difference is the magnitude of the peak knee torque. The ERiKA prosthesis in its base configuration supplies a peak knee extension torque that is similar to the reference torque for a users' bodyweight of 60 kg, while the goal was 80 kg. This torque can be increased through an increase in pre-pressure in the main pneumatic circuit, as is shown in Fig. 13b. This comes at the cost of increasing the initial knee torque during StandTS, is disadvantageous when initiating knee flexion during StandTS. This effect can be negated by pressuring both sides of the piston. The pressure on the opposite side of the piston reduces the torque when the knee is extended. When the knee is flexed, the pressure decreases, and its effect is diminished. This option however, does not work with the piston skirt, because the cylinder can not be sealed on the connection rod side.

In the model of the prosthesis the magnitude of the peak knee torque was met. When comparing the base configuration to the model, the main cylinder does not build enough pressure to match the torque calculated in the model. This

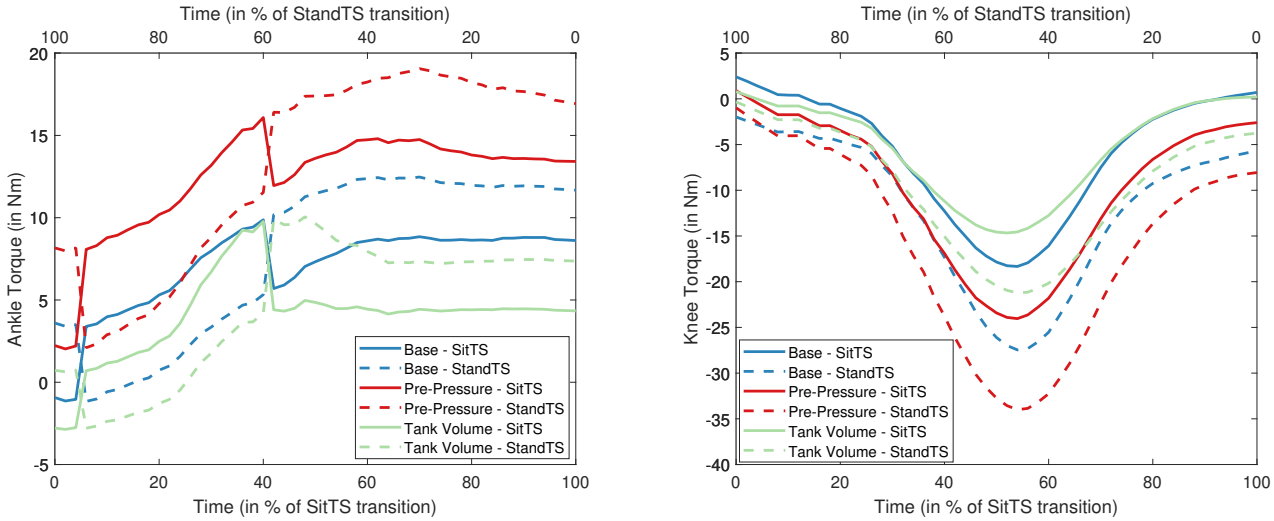

(a) The ankle trajectory

(b) The knee trajectory

Fig. 13: The resulting torque trajectories of the adjustments for bodyweight. The adjustments consist of an increase in the pressure tank volume of 9818 mm^3 and an increase in pre-pressure. For the ankle, this is an increase in pre-pressure in the secondary pneumatic circuit from 2 to 3 bar. For the knee, this is an increase in pre-pressure in the main pneumatic circuit from 0 to 1 bar.

could have a number of explanations. The first explanation is leakage in the system, specifically during the movement of the cylinders. This explanation is unlikely though, since the repeated measurements show the same results, while there is no moment for air to leak back into the system. Additionally, leakage tests showed a pressure drop of less than 0.25 bar in 1.5 hours, with the main pressure system at full pressure.

A second explanation is a dead volume in the system, that is not included in the model. This explanation is more likely, as only the volume of the cylinders and that of the pressure tank are included. The volume of the solenoid valve, check valves and tubing are neglected. Also the shape of the cylinders and pistons is modeled as a perfect cylinder, while the actual shape is more irregular, with a recess in the bottom of the cylinder to fit a nut protruding from the bottom of the piston. To evaluate the likelihood of this explanation, the model was fitted on the measured data, with the pre-pressure and pressure tank volume as only parameters. The missing dead volume is estimated to be about $8.6 \cdot 10^4$ mm^3, which is equal to about a third of the main cylinder or 6.9 m of the used tubing. It is unlikely that such a big dead volume is present somewhere in the system.

Since both these explanations are unlikely, the source of the pressure reduction is unknown. All the assumptions and calculations in the model should be evaluated, and additional tests are required to verify the model calculations.

The discrepancy between the model and the prototype also causes a difference in magnitude between the reference ankle torque and the realized ankle torque. The reduced pressure in the knee piston, combined with the desired equilibrium point of 17.5°, lead to a lower pre-pressure in the secondary ankle cylinder. This reduces the ankle plantarflexion torque in the last phase of the SitTS transition. Increasing the pre-pressure in the secondary cylinder increases the plantarflexion torque during the entire transition. Increased plantarflexion torque in the first phase of the transition decreases the maximum dorsiflexion angle, and makes shifting the CoM over the BoS harder. An increased pressure in the main pneumatic circuit when the knee is fully flexed reduces the plantarflexion torque in the first phase of the SitTS transition, and thus allows a higher pre-pressure.

The reference trajectories are an assumption of an ideal torque profile. An exact replication of the reference trajectory does not necessarily mean that the prosthesis works perfect for all users. People can change their SitTS and StandTS strategy based on the available joint torque and range of motion [22]. A deviation from the reference trajectory might lead to another strategy, that works just as well. The only way the performance of the ERiKA prosthesis during SitTS can be accurately determined is by user tests.

B. Comparison to existing prosthesis

In Table VI the measured joint torques in the ankle and the knee of the ERiKA prosthesis are compared to the joint torques in the previous prosthesis and the joint torques measured in literature. In this subsection the values will be compared to see how they stack up.

ERiKA vs. ERiK: The magnitude of the peak knee extension torques are comparable between ERiKA and ERiK. The peak knee extension torque in the ERiK prototype could be further increased to 29.5 Nm, by increasing the pre-pressure [15]. A similar approach could be taken with the ERiKA prosthesis, as is shown in Fig. 13b. A small increase

in pre-pressure of 1 bar, results in a peak knee extension torque increase of 5.5 Nm to 24 Nm.
The angle at which the peak knee torque occurs has changed between the ERiK and ERiKA prostheses, shifting to a more extended angle. In the reference data the peak knee torque occurs at an angle of 88.9° [18], which is closer to the ERiK prosthesis. An important difference is that the knee torque in the ERiK prosthesis has an almost linear relation to the knee angle. The knee torque of the ERiKA prosthesis has a peak knee extension torque, and a reduced knee torque at full flexion and full extension, which is more similar to the natural knee torque during SitTS and StandTS.

ERiKA vs. Literature: Table VI further shows that the measured torque in the ERiKA prosthesis is higher than the measured torque in existing passive prostheses [11] and in commercially available powered prostheses [12] during SitTS and StandTS. The increased torque should lead to a better performance. Burger et al. found in five passive prosthesis users that the prostheses do not provide supporting knee torque during the transition, and that the users placed little to no weight on the prosthetic limb until the end of the transition [11]. Highsmith et al. measured the Power Knee (Össur), the C-Leg (Otto Bock) and the Mauch SNS (Össur) during both SitTS and StandTS. He found that these prostheses produced small counterproductive flexing joint torques during SitTS at the instance of maximum vertical acceleration. Especially for the Power Knee this was unexpected, since it is supposed to provide assisting torque during SitTS. Highsmith reports that the assistance activates too late during the transition to provide any support [12]. The angle of the peak knee torque in Highsmith was not reported, and thus can not be compared to the ERiKA prosthesis. The notion that the support occurs too late in the cycle however, indicates that the delay of the peak knee torque in the ERiKA prosthesis might reduce the effect of the torque.
In Table VI a custom powered ankle-knee prosthesis by Vanderbilt University [23] is shown to have a comparable, but higher peak knee extension torque during SitTS compared to the ERiKA prosthesis. In addition, Varol reports that the measured torque during SitTS is smaller than the maximum available knee extension torque in the prosthesis, but it was tuned down for the comfort of the user. It is unclear what the effect is of the custom prosthesis on the healthy side joint torques, since they were not measured in the experiment. The user stated that performing SitTS with the Vanderbilt prosthesis was easier than with his prescribed passive prosthesis. This indicates that the support torque in the ERiKA prosthesis might be sufficient to help prosthetic users perform SitTS and StandTS.
However, the findings of Varol and Highsmith on the difference between available knee extension torque and measured peak knee extension torque during SitTS make it hard to predict whether the maximum available knee torque in the ERiKA prosthesis is sufficient to provide support and reduce the healthy side joint torques. It seems to depend both on the timing and the magnitude of the peak knee extension torque whether the users find a prosthesis beneficial or not.
Furthermore, in Table VI the ankle torque of passive prostheses [11] and the Vanderbilt prosthesis [23] is reported to be higher than the torque measured in the ERiKA prosthesis. The passive prostheses in the study by Burger contain single axis, multi axis or energy storing feet. The multi axis foot was found to provide more plantarflexing torque (27.0 Nm) than both the single axis and energy storing foot (14.8 Nm and 16.4 Nm). The torque provided by the active ankle joint in the Vanderbilt prosthesis was similar to the single axis and energy storing foot. The joint torque profile did not show a peak, but was generally highest at the end of the transition.
The ERiKA prosthesis has an unprecedented ankle RoM during SitTS, which allows the feet to be placed further back and the bodyweight to be moved over the BoS more easily. Although the Vanderbilt prosthesis is reported to have a range of motion of 20° of dorsiflexion, only 5° of dorsiflexion is used in the transition. This means the joint is probably in a stiff state during the transition. In the ERiKA prosthesis the ankle torque profile should ensure that the ankle can be dorsiflexed during the first part of the transition. This should make it easier to place the center of mass over the base of support, and should reduce the healthy hip and knee torque. The ankle torque can be adjusted to find a balance between initial dorsiflexion and support later in the transition. Adjustments can be made using the pre-pressure in the secondary ankle cylinder, as is shown in Fig. 13a.

C. Limitations of the design

In Fig. 10 the measured hysteresis during a pressured test is shown, as well as the measured hysteresis during an test without pressure. The difference between the two lines is the hysteresis caused by the pressure in the system. The hysteresis in the test without pressure is mostly due to friction between the piston seals and cylinder walls.
Some of the extra hysteresis was modeled, as it is caused by friction due to the radial load on the pistons and the piston skirt. This friction is most prevalent when both the angle between the connection rod and the piston rod, and the actuator force are large. In Fig. 10b this is shown by a peak around 60°, which is similar to the modeled hysteresis. In the ankle this friction is small, since the connection rod and piston rod are never at a large angle.
A second part of the hysteresis is introduced by friction between the inside of the cylinders and the seals. This friction is inherent to an airtight seal, and it is increased by the pressure difference between both sides of the piston. Low friction seals are available for the current cylinders, which reduce the friction caused by the seals due to the use of a different material and lubricant.
A third source of hysteresis is the pressure drop in the pneumatic components and tubing between the cylinders and the tank. In Appendix C-D the pressure drop was calculated for the used components. It was found to be not significant compared to other sources of hysteresis.
Hysteresis in the knee causes the peak knee torque during SitTS to be about 10 Nm smaller than the peak knee torque during StandTS. The required peak knee torque during

TABLE VI: A comparison of the peak joint torque measured in the ERiKA prosthesis, the ERiK prosthesis and several prostheses found in literature.

	ERiKA	**ERiK [15]**	**Passive Prosthesis [11]**	**Power Knee [12]**	**C-Leg [12]**	**Mauch SNS [12]**	**Vanderbilt Custom Prosthesis [23]**
Peak knee extension torque	18.5 Nm	22 Nm	3.6 Nm	-9.4 Nm	-2.9 Nm	-5.8 Nm	23.3 Nm
Knee angle at peak torque	68.5°	90°	N/A	N/A	N/A	N/A	62.1°
Peak ankle plantarflexion torque	11.3 Nm	N/A	19.4 Nm	N/A	N/A	N/A	17.8 Nm
Ankle angle at peak torque	28.1°	N/A	N/A	N/A	N/A	N/A	-1.0°

StandTS is smaller than the required peak knee torque during SitTS, due to the direction of gravity. Therefore the difference has to be compensated by the user by placing more weight on the prosthetic limb during StandTS than during SitTS.
The hysteresis in the ankle is more complicated, as the ankle has a reciprocating motion during both transitions. During SitTS this means that the plantarflexing torque counteracting the dorsiflexing motion until maximum dorsiflexion is higher than the plantarflexing torque that helps the plantarflexing motion until full stance. Similar, during StandTS the plantarflexing torque that supports until maximum dorsiflexion is larger than the plantarflexing torque that pushes the shank until a seated position is reached. The former is the biggest problem, as the extension part of the transition is the part that requires the most plantarflexing torque. A solution would be to increase the pre-pressure in the secondary ankle cylinder. This will increase the plantarflexing torque during the extension phase, but it will also increase the plantarflexing torque during all other phases. The result will probably be that the maximum dorsiflexion angle will be smaller, which will make it harder for subjects to get their CoM over their BoS.
A second limitation of any pneumatic system is leakage. Although the leakage is limited to about 0.25 bar in the compressed state in the main circuit in 1.5 hours, it might cause problems during daily living. The uncompressed state of the main system has a small pressure difference to the atmosphere, and therefore the leakage is small. In the compressed state the leakage is larger. If the peak knee torque is increased by increasing the pre-pressure, this will lead to more leakage. As this will also increase the friction of the seals, in a future design it is important to minimize the pressure. This means that the piston diameter should be maximized.
The leakage in the system might be further reduced by eliminating number of connection components in the pneumatic circuit, and by selecting different valves. By making an integrated design for all essential pneumatic components, the tubing can be replaced. This will both decrease the dead volume and the chance of leakages.
Any residual leakage left in the system has to be dealt with by a user on a daily basis, as it has a large influence on the working of the prosthesis. Pre-pressure can be restored by an integrated hand pump or a valve for a hand pump. Another option is using pressurized air cartridges and a pressure valve to automatically keep the pressure in the system stable.

D. Future Work

To take the next step from this prototype to a potential product that could help thousands of people, first the prototype has to be evaluated in user tests. The reduction in the healthy side joint torques can only be determined by attaching the device to an amputee, and measuring the torques. The results of the user tests can then be used to improve the performance of the prosthesis.
Additionally, the ERiKA prosthesis can be improved by reducing the weight and size. The integrated design in subsection III-B is lighter and less bulky than the current prototype. Additionally the need for a secondary ankle actuator might be removed, to further reduce weight. By pressurizing both sides of the main ankle piston, the single actuator provides the function of both ankle actuators in the current design. The influence of this approach on the torque profiles should be investigated.
Finally the behavior of the prosthesis during walking can be improved. In the current prosthesis, both the ankle and the knee are fixed during gait. This means walking with the prosthesis is like walking with a wooden leg. That is fine for walking inside the house, but might be improved to improve the mobility of the users. This could be accomplished by introducing a different knee joint in the prosthesis, like a polycentric knee. It is unclear what the effect of a moving rotation point would be on the working of the prosthesis during SitTS and StandTS. In a similar matter, the knee actuator might change the effect of a polycentric knee during gait.
The walking behavior of the prosthesis can be further improved by using the ankle cylinders to provide an ankle push off force. The ankle push off force is important during gait, both for the acceleration of the CoM and for the leg swing [24]. In the current configuration, the ankle is not stiff enough for the high ankle joint torques during gait. This might be improved by reducing the secondary pressure tank volume during gait, by means of another solenoid valve. A smaller pressure tank volume makes the ankle stiffer during gait, while opening the valve restores the compliance of the joint during SitTS and StandTS.

VI. Conclusion

In conclusion the new ERiKA prototype is an innovative prosthesis, that provides a natural torque profile during Sit-to-Stand and Stand-to-Sit transitions, by storing energy during StandTS and releasing it during SitTS. The prosthesis has an unprecedented ankle range of motion during the transition that can make moving the center of mass to the base of support easier, and can subsequently reduce the required joint torques in the healthy limb.

However, the current prototype is heavy and hard to use, and does not yet produce sufficient joint torques. More research is required in the form of user tests to improve the design. Further improvements can be made by reducing the weight and by increasing the actuator forces. An integrated design has been made, but not yet manufactured, that should be able to reduce the weight and size of the prosthesis.

With these improvements and alterations, the ERiKA prosthesis has the potential to become a prosthesis that can help thousands of elderly transfemoral amputees to perform Sit-to-Stand and Stand-to-Sit transitions, and thus regain their mobility after amputation.

VII. Acknowledgements

The authors would like to thank: Rahul Ramesh and John Landers for the interesting discussions during the meetings. Jan van Frankenhuyzen for the advice during the design and realization of the prototype. Wim Velt en Nisse Linskens for the help and advice with the production of the prototype.

References

[1] K. Ziegler-Graham, E. J. MacKenzie, P. L. Ephraim, T. G. Travison, and R. Brookmeyer, "Estimating the Prevalence of Limb Loss in the United States: 2005 to 2050," *Archives of Physical Medicine and Rehabilitation*, vol. 89, no. 3, pp. 422–429, 2008.

[2] T. R. Dillingham, L. E. Pezzin, and E. J. MacKenzie, "Limb Amputation and Limb Deficiency: Epidemiology and Recent Trends in the United States," *Southern Medical Journal*, vol. 95, no. 8, pp. 875–883, 2002.

[3] H. Rietman, *Vallen en Opstaan [Oration]*, Enschede, 2007. [Online]. Available: https://www.utwente.nl/en/academic-ceremonies/inaugural-lectures/booklets-inaugural-lectures/2007-2014/rietman.pdf

[4] P. M. Dall and A. Kerr, "Frequency of the sit to stand task: An observational study of free-living adults," *Applied Ergonomics*, vol. 41, no. 1, pp. 58–61, 2010.

[5] L. L. Ploutz-Snyder, T. Manini, R. J. Ploutz-Snyder, and D. A. Wolf, "Functionally Relevant Thresholds of Quadriceps Femoris Strength," *Journal of Gerontology*, vol. 57, no. 4, pp. 144–152, 2002. [Online]. Available: https://academic.oup.com/biomedgerontology/article-abstract/57/4/B144/600122

[6] M. A. Hughes, B. S. Myers, and M. L. Schenkman, "The role of strength in rising from a chair in the functionally impaired elderly," *Journal of Biomechanics*, 1996.

[7] P. O. Riley, M. L. Schenkman, R. W. Mann, and W. A. Hodge, "Mechanics of a constrained chair rise," *Journal of Biomechanics*, 1991.

[8] T. Harbo, J. Brincks, and H. Andersen, "Maximal isokinetic and isometric muscle strength of major muscle groups related to age, body mass, height, and sex in 178 healthy subjects," *European Journal of Applied Physiology*, 2012.

[9] A. B. Newman, C. L. Haggerty, B. Goodpaster, T. Harris, S. Kritchevsky, M. Nevitt, T. P. Miles, and M. Visser, "Strength and muscle quality in a well-functioning cohort of older adults: The Health, Aging and Body Composition Study," *Journal of the American Geriatrics Society*, 2003.

[10] J. Sheldon, "The Effect of Age on the Control of Sway," *Gerontologia Clinica*, vol. 5, no. 3, pp. 129–138, 1963.

[11] H. Burger, J. Kuželički, and Č. Marinek, "Transition from sitting to standing after trans-femoral amputation," *Prosthetics and Orthotics International*, 2005.

[12] M. J. Highsmith, J. T. Kahle, S. L. Carey, D. J. Lura, R. V. Dubey, K. R. Csavina, and W. S. Quillen, "Kinetic asymmetry in transfemoral amputees while performing sit to stand and stand to sit movements," *Gait and Posture*, 2011.

[13] A. M. Simon, N. P. Fey, K. A. Ingraham, S. B. Finucane, E. G. Halsne, and L. J. Hargrove, "Improved Weight-Bearing Symmetry for Transfemoral Amputees During Standing Up and Sitting Down With a Powered Knee-Ankle Prosthesis," *Archives of Physical Medicine and Rehabilitation*, vol. 97, no. 7, pp. 1100–1106, 2016.

[14] T. R. Chamlian, "Use of prostheses in lower limb amputee patients due to peripheral arterial disease," *Einstein (São Paulo)*, vol. 12, no. 4, pp. 440–446, 2014.

[15] F. Lachmann, "Design and Evaluation of a Light-Weight Transfemoral Prosthesis with Active Stand-Up Support for Elderly Amputees," Master's thesis, Technische Universitat Hamburg-Harburg, 2016.

[16] S. Van Der Helm, "Designing the Sit-to-Stand and Stand-to-Sit Transition for Transfemoral Amputees with a Passive Prosthesis: A Literature Review," unpublished.

[17] A. Leardini, Z. Sawacha, G. Paolini, S. Ingrosso, R. Nativo, and M. G. Benedetti, "A new anatomically based protocol for gait analysis in children," *Gait and Posture*, vol. 26, no. 4, pp. 560–571, 10 2007.

[18] C. A. M. Doorenbosch, J. Harlaar, M. E. Roebroeck, and G. J. Lankhorst, "Two Strategies of Transferring from Sit-To-Stand; The Activation of Monoarticular and Biarticular Muscles," *Journal of Biomechanics*, vol. 27, no. 11, pp. 1299–1307, 1994.

[19] J. C. Gillette and C. A. Stevermer, "The effects of symmetric and asymmetric foot placements on sit-to-stand joint moments," *Gait and Posture*, 2012.

[20] S. J. Fleckenstein, R. L. Kirby, and D. A. MacLeod, "Effect of limited knee-flexion range on peak hip moments of force while transferring from sitting to standing," *Journal of Biomechanics*, 1988.

[21] D. A. Winter, *Biomechanics and motor control of human movement*. Wiley, 2009.

[22] D. M. Scarborough, C. A. McGibbon, and D. E. Krebs, "Chair rise strategies in older adults with functional limitations," *The Journal of Rehabilitation Research and Development*, 2007.

[23] H. A. Varol, F. Sup, and M. Goldfarb, "Powered Sit-to-Stand and Assistive Stand-to-Sit Framework for a Powered Transfemoral Prosthesis," in *IEEE International Conference on Rehabilitation Robotics*. Kyoto, Japan: IEEE, 2009, pp. 645–651.

[24] K. E. Zelik and P. G. Adamczyk, "A unified perspective on ankle push-off in human walking," pp. 3676–3683, 12 2016.

[25] Ã. Gløersen and P. Federolf, "Predicting missing marker trajectories in human motion data using marker intercorrelations," *PLoS ONE*, vol. 11, no. 3, 3 2016.

[26] V. J. Eberly, S. J. Mulroy, J. K. Gronley, J. Perry, W. J. Yule, and J. M. Burnfield, "Impact of a stance phase microprocessorcontrolled knee prosthesis on level walking in lower functioning individuals with a transfemoral amputation," *Prosthetics and Orthotics International*, vol. 38, no. 6, pp. 447–455, 12 2014.

APPENDIX A
PREVIOUS PROTOTYPE EVALUATION

A. Introduction

This appendix summarizes the evaluation of the first prototype of the Energy-Recovering intelligent Knee (ERiK) with transfemoral amputees. The experiments described in this appendix were conducted prior to the scope of this thesis.

In this document, first the experimental method will be explained, and then the results of the experiments will be shown, followed by a short discussion.

B. Methods

The experiment was approved by the ethical review board of Erasmus MC, Rotterdam. Seven participants with a transfemoral amputation were recruited and randomly assigned to one of two groups: One where the support condition was tested first, and one where the unsupported condition was tested first. This was done to avoid an effect of learning effects on the results.

After participants provided informed consent, the prosthesis was fitted on the residual limb. The pre-pressure was adjusted to each participant according to weight and personal preference during intial familiarization trials.

Participants were then asked to perform Sit-to-Stand (SitTS) and Stand-to-Sit (StandTS) transitions in trials of 1, 3 or 5 repetitions, always as fast as possible. One experimentor remotely enabled and disabled the support function of the prosthesis, depending on the experimental condition.

Three-dimensional kinematic data was acquired by a motion capture system consisting of 4 cameras and markers placed over bony landmarks [17]. Missing marker positions were estimated using a combination of linear interpolation over time and the method introduced by Gloersen and Federolf [25]. Anatomical joint angles were determined based on the three-dimensional position of the markers. Ground reaction forces (GRFs) were captured by force plates under both feet and the chair.

The healthy and prosthetic knee torque were each calculated by taking the respective cross product of the position vector of the knee joint with respect to the Center of Pressure (CoP) and the GRF vector at the foot. This neglects inertial and gravitational effects of the shank, but those effects are considered small with respect to the knee moment generated by the ground reaction force.

The main outcome measure was time taken to complete trials.

Also, a symmetry measure for a trial was calculated by taking the median of the ratio of the vertical GRF on the prosthetic limb and the healthy limb. A value of 1 represents full symmetry and a value of 0 means all weight is placed on the prosthesis.

The start of a transition was marked by a deviation from the quiet sitting or standing trunk angle by more than 2% of the peak flexion angle. The end of a transition was marked by the return of the trunk angle within 2% of the quiet sitting or standing angle. If the knee was flexed more than $45°$, the posture was classified as sitting. If the knee was flexed less than $45°$, the posture was classified as standing.

The StandTS transition was also split into four phases, to compare the time taken to complete each phase. The start of the first phase was marked by the start of the movement. The first phase ends when the healthy knee start flexing. The second phase starts with the flexion of the healthy knee, and ends with flexion of the prosthetic knee. The third phase starts with flexion of the prosthetic knee and ends with seat-on. The final phase starts with seat-on and ends in quiet sitting.

Paired t-tests were conducted to compare supported and unsupported conditions.

C. Results

Four of the seven participants showed no difficulty in neither SitTS nor StandTS with and without support. One participant was unable to perform consistent SitTS transitions without support enabled. A second subject showed difficulties performing StandTS with support enabled. A third subject had difficulties performing SitTS and StandTS with support enabled.

The SitTS movement was characterized by an initial position with the prosthetic foot placed in front of the healthy foot in all subjects. The prosthetic foot was often positioned on the toe to achieve some dorsiflexion. The initial position of a single subject is shown in Figure 14. Subjects flexed their trunk extensively both with support and without support. With support enabled, the prosthesic knee tended to be fully extended before the healthy knee was, and before trunk extension commenced. In some trials, this premature extension resulted in balance issues for the subject, and for one subject in a sitback failure.

The weight distribution of all participants was asymmetric towards the healthy side, with little weight being put on the prosthesis. A box plot of the symmetry measure for six subjects is shown in Figure 15. In one subject, the GRF data was corrupted. The t-test showed that symmetry was significantly higher in trials with support ($p = 0.048$).

The sound-side knee torque of the participants was generally similar or lower in trials where support was enabled. This is shown in Table VII and in Figure 16. The difference in peak healthy knee torque was significant during SitTS ($p = 0.015$).

In contrast, the sound-side hip torque of the participants was generally similar or higher in trials where support was enabled. Only the third participant showed lower sound-side hip torque with support enabled. The fifth participant had more than double the hip torque with support enabled, than with support disabled. This is shown in Table VIII and in Figure 17. The difference did not reach significance during SitTS ($p = 0.45$).

The amputated-side hip torque of the participants was generally similar between support conditions. This is shown in Table IX and in Figure 18. There was no significant difference between support conditions during SitTS ($p = 0.46$).

Subjects took a little longer to perform SitTS with support than without support, but this did not reach significance ($p = 0.11$). There was also a substantial increase in variance of the time taken to perform SitTS with support enabled.

The StandTS motion also started with the prosthetic foot placed in front of the healthy foot. In some trials, both with support and without, subjects had difficulties getting the prosthetic knee to flex from its locked position. In those trials, the subjects started by flexing their healthy knee, with insufficient weight on the prosthesis. This caused the COP to move towards the heel and the GRF vector to point in front of the knee, leading to an extension moment in the knee. This is shown in Figure 19. Prosthetic knee flexion occured in most trials only after the prosthesic foot was placed on the toe, and the residual limb was pressed forward to create a flexing torque. After knee flexion, the StandTS motion is most accurately described as controlled collapse. In some instances, after seat-on, the prosthesis extended, because the force on the foot was too small to prevent it.

The vertical GRF distribution of trials with support was significantly more symmetric than in trials without support ($p = 0.008$). During quiet sitting, the prosthetic foot tended to be loaded more than the healthy foot.

During StandTS, the prosthesis provided a supporting knee torque that lowered the required healthy knee torque in all subjects but one. This is also shown in Table VII and Figure 16. This decrease did not reach significance.

The supporting knee torque provided by the prosthesis during StandTS did not lower the required sound-side hip torque in all subjects. Most subjects even showed slightly higher sound-side hip torque during StandTS. This is also shown in Table VIII and in Figure 17. There is no significant difference between support conditions.

The amputated-side hip torque was higher with support enabled for all participants but the seventh. This is also shown in Table IX and in Figure 18. This increase does not reach significance during StandTS.

StandTS took significantly longer with support than without support ($p = 0.075$). This is also shown in Table X and Figure

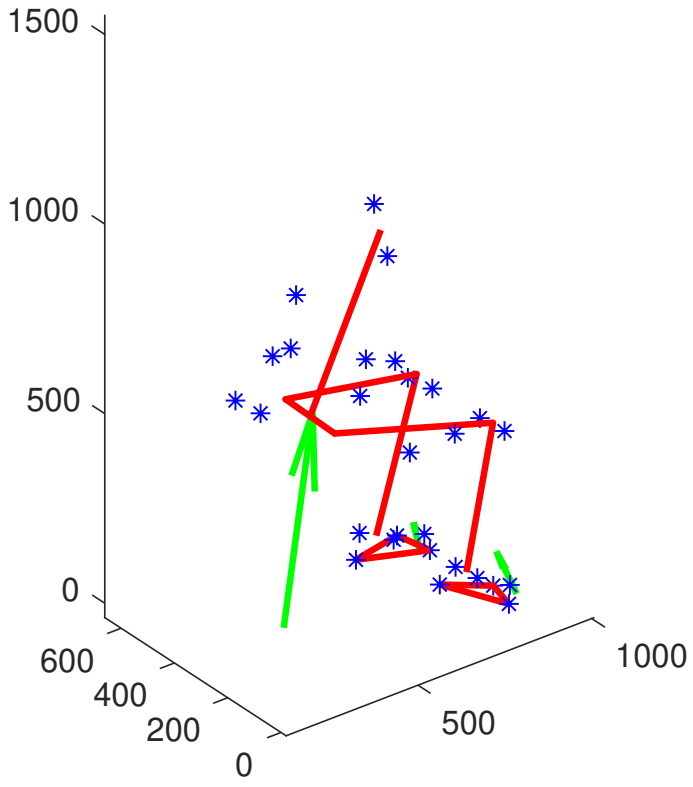

Fig. 14: The initial position of a subject performing SitTS. The prosthetic foot (right) is placed on the toe, as is also visible by the location of the COP at the front of the foot.

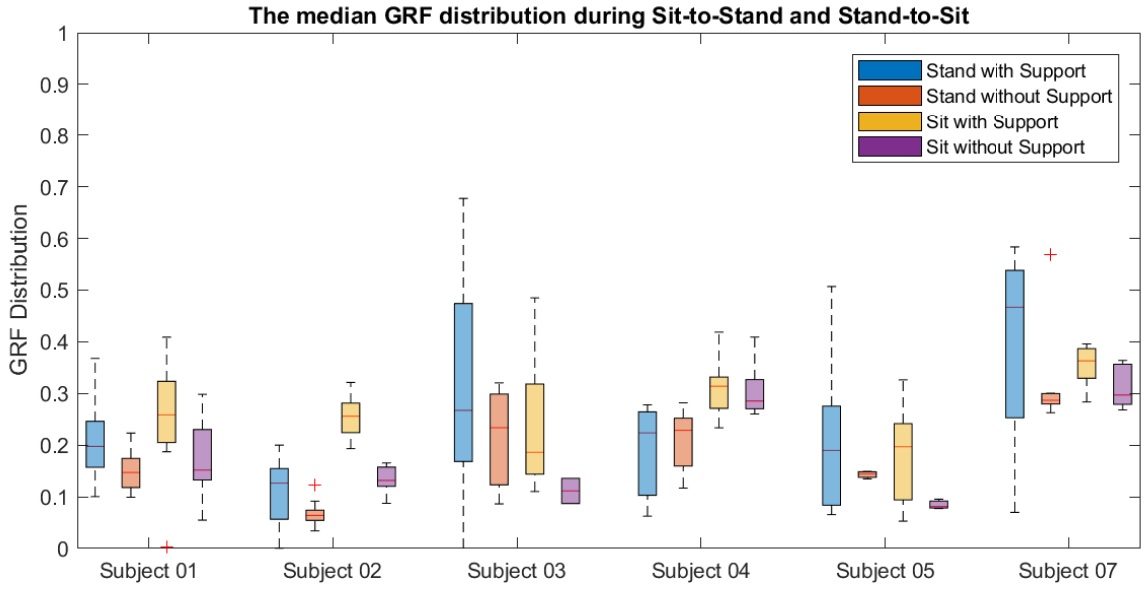

Fig. 15: The median GRF distribution during SitTS (Stand) and StandTS (Sit). Only the standing part of the transition was considered. The red line represents the median, and the box represent the 25th and 75th percentile. A measure of 1 indicates perfect symmetry, a measure of 0 indicates that all weight is on the healthy-side leg.

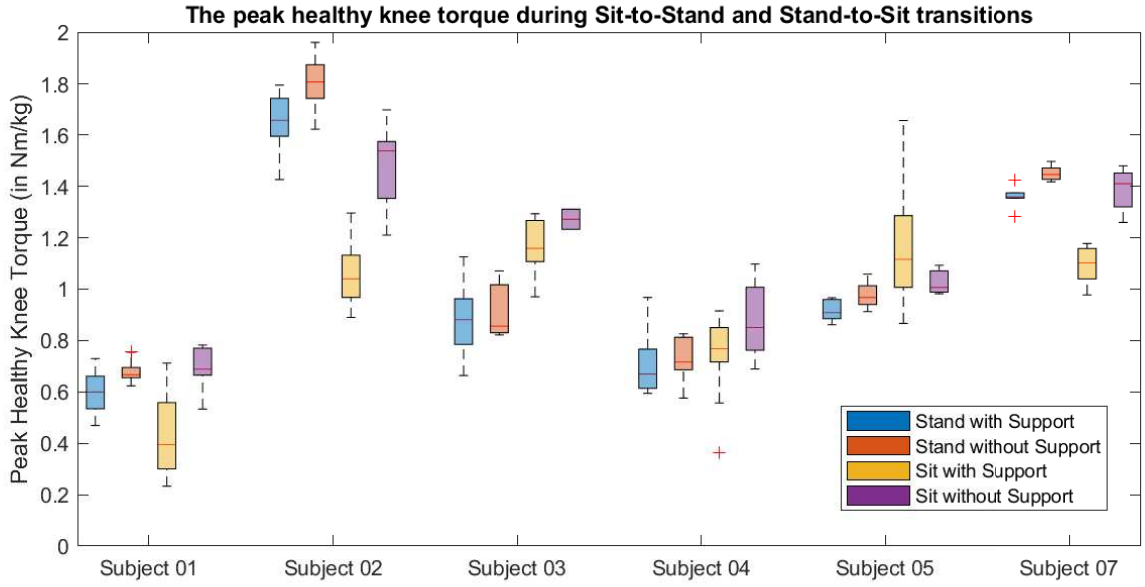

Fig. 16: The peak healthy knee torque during SitTS (Stand) and StandTS (Sit). The knee torque was normalized by the subject's body weight. The red line represents the median, and the box represent the 25th and 75th percentile.

20. In Figure 21, the duration of the four different phases are shown. The length of the individual phases did not significantly change between conditions.

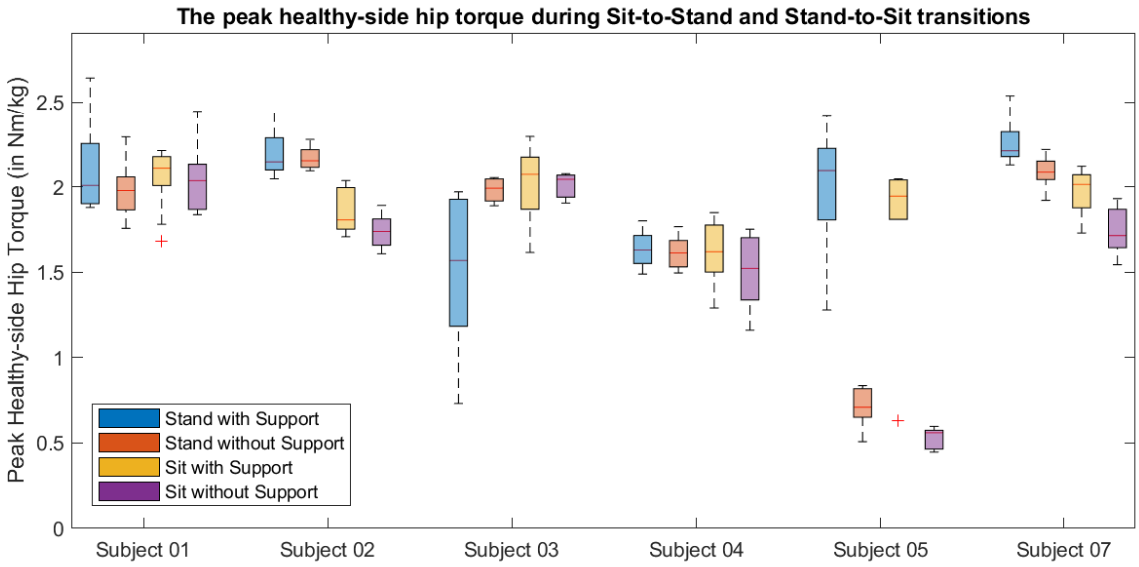

Fig. 17: The peak hip torque during SitTS (Stand) and StandTS (Sit) on the subject's healthy side. The hip torque was normalized by the subject's body weight. The red line represents the median, and the box represent the 25th and 75th percentile.

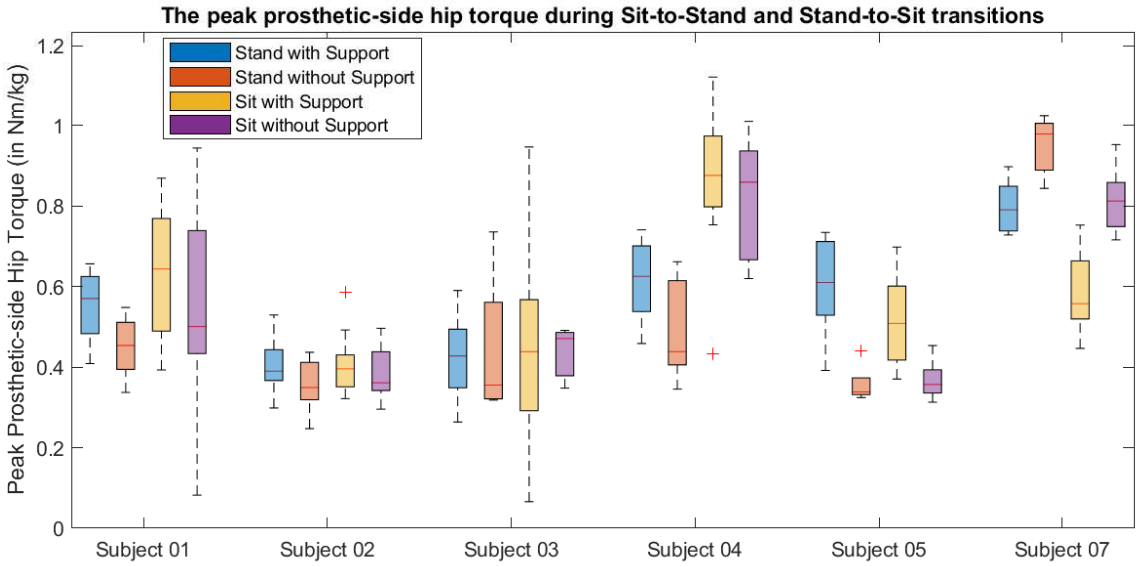

Fig. 18: The peak hip torque during SitTS (Stand) and StandTS (Sit) on the subject's amputated side. The hip torque was normalized by the subject's body weight. The red line represents the median, and the box represent the 25th and 75th percentile.

TABLE VII: The peak healthy knee torque during sit-to-stand and stand-to-sit transitions. The mean (std) values are reported in Nm/kg.

Subject	Sit-to-Stand		Stand-to-Sit	
	Support	No Support	Support	No Support
1	0.60 (0.08)	0.68 (0.05)	0.43 (0.15)	0.70 (0.08)
2	1.65 (0.11)	1.80 (0.10)	1.05 (0.12)	1.48 (0.15)
3	0.88 (0.12)	0.92 (0.13)	1.16 (0.11)	1.27 (0.06)
4	0.71 (0.12)	0.74 (0.08)	0.74 (0.17)	0.88 (0.15)
5	0.92 (0.04)	0.98 (0.06)	1.17 (0.29)	1.03 (0.06)
7	1.36 (0.04)	1.45 (0.03)	1.09 (0.07)	1.39 (0.08)

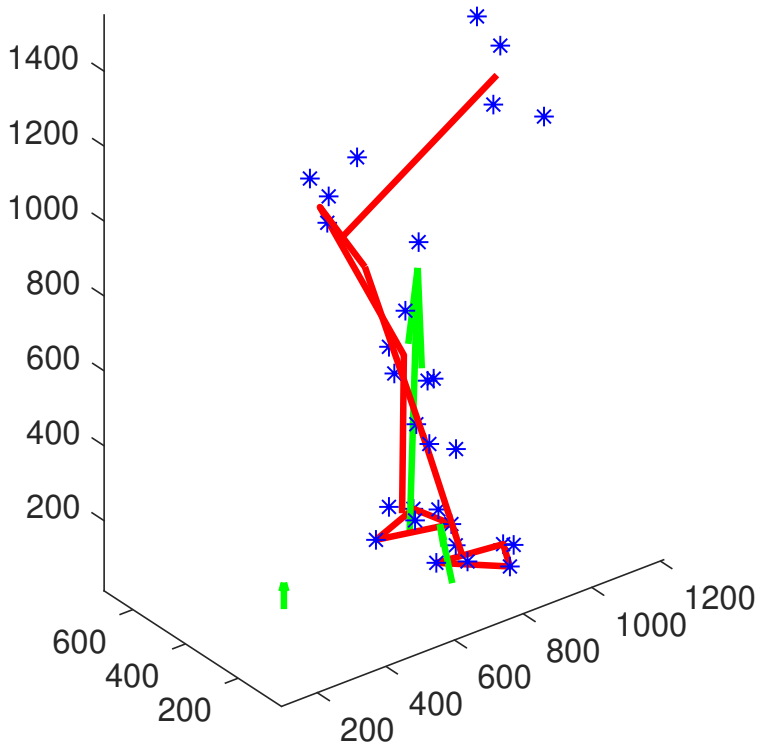

Fig. 19: A subject trying to perform a StandTS transition. The trunk is flexed, as well as the healthy limb. The subject is having trouble flexing the prosthetic limb, because the subject is not able to overcome the pre-tension extension torque generated by the prosthesis.

TABLE VIII: The peak healthy-side hip torque during sit-to-stand and stand-to-sit transitions. The mean (std) values are reported in Nm/kg.

Subject	Sit-to-Stand		Stand-to-Sit	
	Support	No Support	Support	No Support
1	2.11 (0.26)	1.98 (0.16)	2.05 (0.18)	2.04 (0.20)
2	2.20 (0.12)	2.17 (0.07)	1.86 (0.12)	1.74 (0.10)
3	1.51 (0.44)	1.98 (0.08)	2.01 (0.22)	2.01 (0.09)
4	1.64 (0.11)	1.61 (0.10)	1.62 (0.19)	1.50 (0.21)
5	1.99 (0.40)	0.71 (0.13)	1.74 (0.55)	0.53 (0.07)
7	2.26 (0.14)	2.09 (0.09)	1.97 (0.14)	1.74 (0.14)

TABLE IX: The peak prosthetic-side hip torque during sit-to-stand and stand-to-sit transitions. The mean (std) values are reported in Nm/kg.

Subject	Sit-to-Stand		Stand-to-Sit	
	Support	No Support	Support	No Support
1	0.55 (0.09)	0.45 (0.07)	0.63 (0.16)	0.55 (0.26)
2	0.41 (0.07)	0.36 (0.06)	0.41 (0.07)	0.39 (0.06)
3	0.42 (0.10)	0.44 (0.20)	0.49 (0.34)	0.44 (0.08)
4	0.62 (0.10)	0.57 (0.32)	0.86 (0.20)	0.82 (0.15)
5	0.60 (0.13)	0.36 (0.05)	0.52 (0.12)	0.37 (0.05)
7	0.80 (0.06)	0.95 (0.07)	0.59 (0.11)	0.81 (0.08)

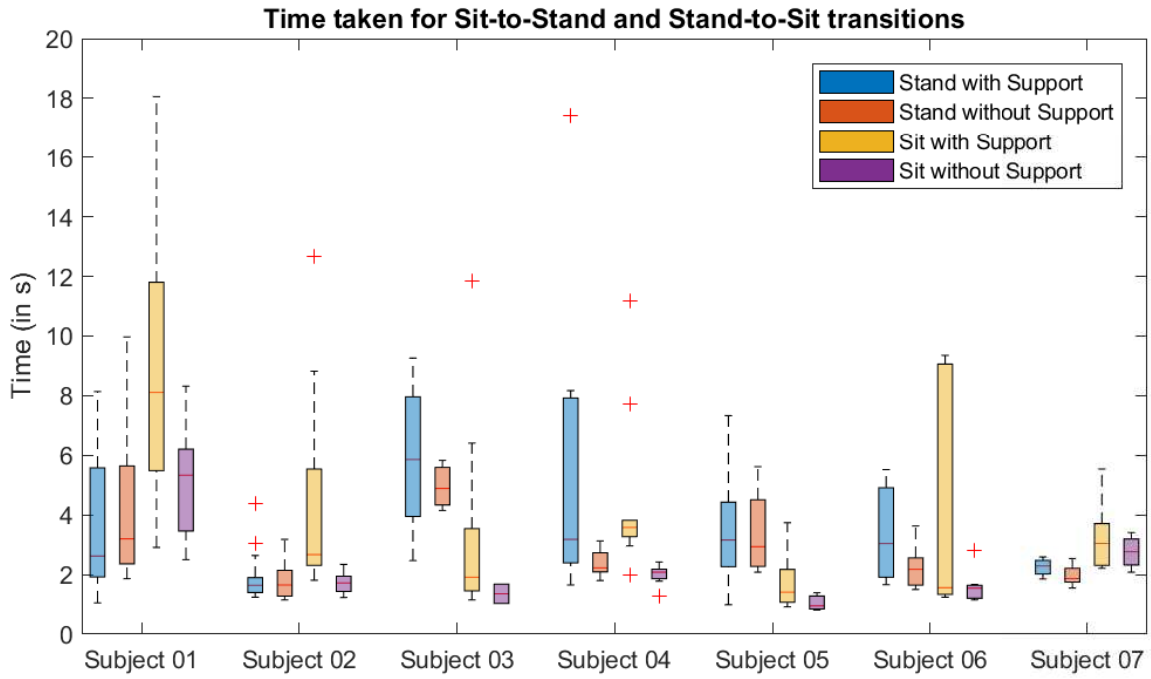

Fig. 20: The time taken by different subjects to perform SitTS and StandTS transitions. The red line represents the median and the box the 25th and 75th percentile. Outliers are marked by a red plus.

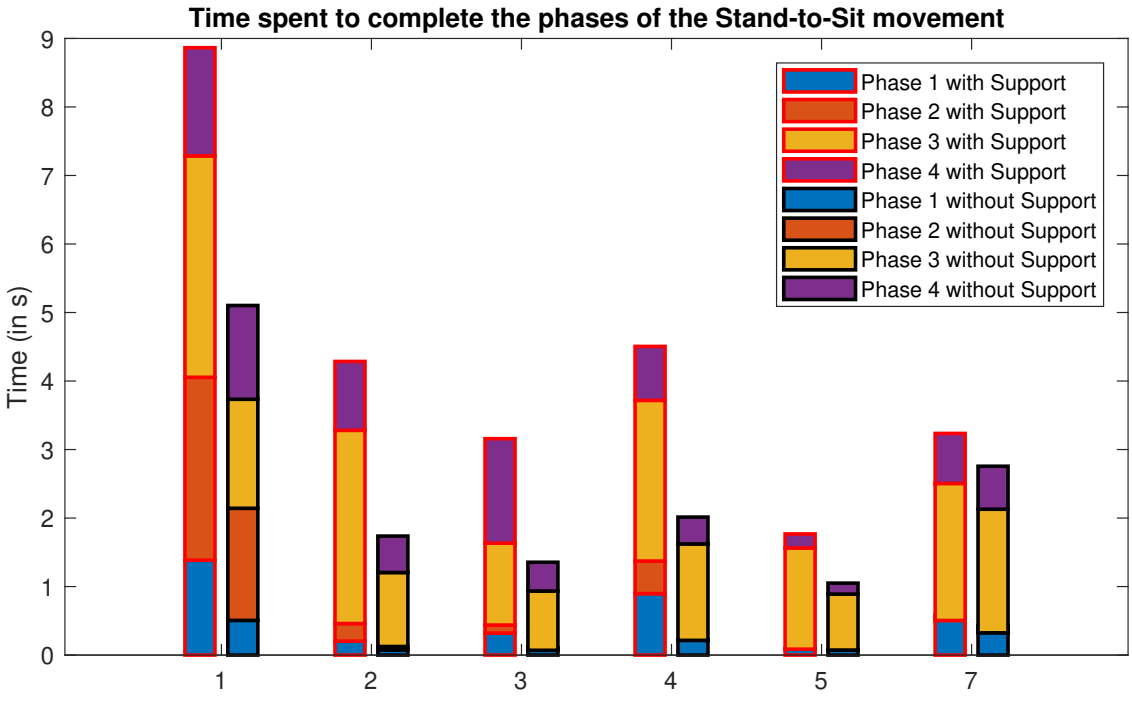

Fig. 21: The time spent in the different phases during Stand-to-Sit. The beginning of the phases are marked by initial trunk flexion, initial healthy knee flexion, initial prosthetic knee flexion and seat-on. The bars with red edges represent transitions with support, the bars with black edges without.

TABLE X: The transition time for sit-to-stand and stand-to-sit transitions with support enabled and disabled. Mean times (std) are given in seconds.

	Sit-to-Stand		Stand-to-Sit	
Subject	**Support**	**No-Support**	**Support**	**No-Support**
1	3.73 (2.53)	4.23 (2.75)	8.87 (4.93)	5.10 (1.91)
2	1.89 (0.80)	1.80 (0.60)	4.29 (3.19)	1.74 (0.35)
3	7.64 (7.54)	4.96 (0.84)	3.16 (2.99)	1.36 (0.46)
4	5.42 (5.11)	2.41 (0.50)	4.51 (2.78)	2.01 (0.37)
5	3.53 (2.33)	3.39 (1.58)	1.77 (1.14)	1.05 (0.30)
6	3.31 (1.60)	2.24 (0.70)	6.57 (9.10)	1.59 (0.53)
7	2.25 (0.27)	1.97 (0.33)	3.24 (1.12)	2.76 (0.51)

D. Discussion

1) Functionality of the Current Prototype: The results from this evaluation study of a passive energy recovering prosthesis indicate that there is some benefit of the support during both SitTS and StandTS.

The subjects showed lower peak healthy knee torque, which reached significance for SitTS. The average peak healthy knee torque found was 1.02 Nm/kg with support and 1.09 Nm/kg without support. To compare these values to the values reported by Highsmith for the Power Knee, the C-Leg and the Mauch SNS, they have to be normalized to the subject height (0.57 and 0.60 N/kg). The first two participants are excluded from this analysis, since their height was not recorded. These values are comparable to the values Highsmith found for the Power Knee and the Mauch SNS (0.57 and 0.59 N/kg), but higher than he found for the C-Leg (0.42 N/kg) [12]. Most of the peak healthy knee torques found in this study, and the average peak healthy knee torque both with and without support, are lower than the ones Burger found for several passive prostheses (1.38, 1.63 and 1.90 Nm/kg for three individual subjects) [11]. During StandTS the average peak healthy knee torque found was 0.94 Nm/kg with support, and 1.13 Nm/kg without support. Normalized for subject height, these values become 0.61 and 0.67 N/kg. That is higher than the peak healthy knee torque Highsmith found for the Power Knee, the C-Leg and the Mauch SNS (0.36, 0.48 and 0.57 N/kg) [12]. However, these values should be seen in context with the corresponding hip torque values. Subjects can distribute the required joint torques over their hips and knees, by means of foot placement and trunk flexion. Burger found higher knee torques, but lower hip torques than Highsmith.

Compared to the reported sound-side hip torque of a single subject by Burger (1.20 Nm/kg) [11], the sound-side hip torques found in this study for SitTS are higher (1.96 Nm/kg with and 1.76 Nm/kg without support). To compare the sound-side hip torque with the data from Highsmith, it again has to be normalized for the subject's length. This results in hip torques of 1.09 N/kg with and 0.93 N/kg without support enabled. These values are similar to the ones Highsmith found for all three prostheses (0.92, 0.91 and 1.02 N/kg for the Power Knee, C-Leg and Mauch SNS) [12].

The amputated-side hip torques in this study are generally a bit higher than the amputated-side hip torque found by Burger (0.56 and 0.52 Nm/kg for with and without support in this study respectively, versus 0.29 Nm/kg in the study by Burger) [11]. Compared to the values found by Highsmith, after normalization for length, the prosthesis in this study (0.36 N/kg with and 0.34 N/kg without support) rates between the Power Knee, and the C-Leg and the Mauch SNS (0.46 N/kg, 0.25 N/kg and 0.26 N/kg respectively) [12].

During StandTS, Highsmith found sound-side hip torques of 0.78, 0.70 and 0.76 N/kg for the Power Knee, C-Leg and Mauch SNS respectively. In this study, we found values of 1.08 N/kg with support and 0.84 N/kg without support. For the amputated side, Highsmith found hip torques of 0.32, 0.12 and 0.28 for the Power Knee, C-Leg and Mauch SNS. We found amputated-side hip torques of 0.36 N/kg both with and without support.

When comparing these joint torques, one has to keep in mind that Highsmith calculated the joint torques using inverse dynamics, while in this study the joint torque was calculated using the cross product of the position vector of the joint with respect to the CoP and the GRF vector, ignoring the inertia of the leg. The resulting errors are bigger for the hip than for the knee, because the ignored leg segment is longer and thus heavier. The calculation method used by Burger is unknown.

The distribution of the subjects' weight over the two limbs was more symmetric with support enabled. This leads to lower loads on the healthy limb, and possibly a prolongation of the time elderly are able to perform SitTS and StandTS transitions. In the initial trials, subjects seemed reluctant to put weight on the prosthesis, possibly due to a lack of confidence in its support. Subsequently, they struggled with flexing the prosthetic knee during StandTS, and with a prematurely extended knee during SitTS. This improved in latter trials. Since this study was performed without initial training, this indicates that some additional training might help to improve the performance further.

The increase in the time to perform the StandTS can have several explanations. One possibility is that the subjects are more in control of their descent, and therefore collapse more slowly into the chair. The initial impact force in the chair however, is not significantly lower. Another explanation is that subjects have more difficulties getting the knee into flexion, and therefore struggle with the transition. The fact that the percentage of the time spent in different phases does not significantly change between conditions indicates that the cause may be a combination of both.

There is a higher variance in the transition times for both transition with support than without support. This might indicate that the subjects are still in a trial-and-error mode with the prosthesis, to determine the best strategy.

Kinematically, the prosthesis shows room for improvement. Most subjects started both transitions on the toe of the prosthesis. This had two benefits for them: First, the positioning on the toe mimics dorsiflexion, which is prevented by the rigid ankle joint of the prosthesis. Dorsiflexion is crucial during SitTS and StandTS to attain the COM over the base of support. Second, positioning the prosthesis on the toe prevents it from slipping forwards, as knee extension presses the toe into the ground. This might originate in a trust issue with the prosthesis. Slipping is enhanced by insufficient weight placed on the prosthesis, which results in unwanted knee extension during the StandTS transition.

2) Future Work: The kinematic issues with the device might be solved by adding a degree of freedom in the ankle, and increasing range of motion in the knee. This would allow subjects to place the prosthetic foot backwards, thereby reducing the distance the COM has to travel during SitTS. Furthermore, it enables subjects to have a more natural and stable descent during StandTS.

Additionally, a larger actuator might help improve the amount of support provided by the prosthesis. This however, also brings the risk of stability and trust issues, if the subjects cannot handle the torque. Therefore, a more gradual control method might have to be added, which allows subjects to control the torque in an intuitive way.

Finally, the transmission of the actuator force could be improved. In the current design, there is a considerable residual force during quiet sitting and quiet standing. During sitting, this might lead to unwanted knee extension, which is inconvenient in situations of daily living. During standing, this leads to trouble with flexing the knee. This should be solved either mechanically, or by using a control method.

E. Conclusion

In conclusion, the energy-recovering prosthesis shows clear potential to help elderly amputees maintain or regain their mobility. The support function reduces the healthy knee torque, and makes for a more symmetric GRF distribution. Some changes, both related to mechanics and control, are required to improve the function as well as usability.

APPENDIX B
CONCEPT OPTIMIZATION

In this appendix the optimization of the final concept, and other potential concepts will be discussed. First, the scripts used for optimization will be described, and the calculations are explained. Then the results of some different concepts are shown, and the decision for the final concept is substantiated.

A. Optimization Script

The optimization of the concepts is performed in Matlab (Matlab 2017b, MathWorks), using some custom scripts and some built-in functions. The used optimization algorithm is the built-in gradient search function *lsqnonlin*. It requires a cost function, an initial state for the parameters and upper and lower bounds as input. This gradient search optimization is repeated multiple times with randomized initial states to diminish the odds of a local minimum as result. The cost function takes the parameter values as input, as well as the reference torque and angle profiles of the knee and ankle and a structure array, that describes the elements in the specific concept. The parameter values are supplied in a $6xN$-matrix, where N is the total number of elements in the concept. The reference data is supplied in four $1x51$-arrays, that describe the torque or position of a joint at timestamps ranging from 0 to 100% completion, with 2% intervals.
The structure array describing the elements has one structure for each element, which contains some crucial information. The fields of the structure are defined by the type of the element. In table XI an overview is published of all possible entries. A new design is constructed by entering a structure for each of the elements in the Elements array. Elements that share the same value in the 'Pressure Tank' field share the same pressure tank, which should always contain exactly one pressure tank. The values in the 'Valves' field correspond with parameter indices in the column of the parameter matrix that represents the element. Therefore the values should be in the range $3-6$.
In table XII the layout of the column in the parameter matrix is shown for each corresponding element array entry. The coordinates of the attachment points $x_{Segment}$ and $y_{Segment}$ are defined in a coordinate system with the origin at the joint axis. The y-axis points in the direction of the primary axis of the proximal segment of the joint. For distal segments the coordinate system is constructed with the joint in a neutral position. The x-axis is directed perpendicular in the anterior direction of the limb. The length of the connection rod l_{Rod} is calculated in terms of the minimal length, i.e. the length of the rod for which the joint would be in a singular position somewhere in the range of motion. A value of 1.1 would mean the rod is 1.1 times as long as the minimal length. d_{Att} represents the attachment point of the cylinder along the main axis of the shank. This value only influences the result if the value for α is non-zero, since the cylinder acts along the main axis of the shank otherwise. The diameter of the cylinder is represented by D_{Act}. For a spring, the spring constant and resting length are given by k and l_0. For each pressure tank, the pressure in the most expanded state of the system p_0 and the maximum pressure p_1 are given. Note that these pressures are hypothetical values, that might not actually be encountered during the reference cycle. The other parameters of a pressure tank are set by the matrix in the Valves field of that element. The first row of the matrix represents the data point from 1 to 51 at which a valve closes between a piston and the pressure tank, breaking the connection. The second row of the matrix represents the fraction of the volume of the pressure tank that is left on the piston side of the valve after closing, i.e. the dead volume.
In Table XIII the initial constraints for the optimization are shown. During the optimization of the prototype, some of these constraints were changed for practical reasons. Furthermore in latter optimizations some parameter values were fixed, to optimize others.

B. Joint Moment Calculations

Joint moment calculations start with the calculation of the position of the joints during the cycle. The ankle joint is used as the origin of the global coordinate system. The position of the knee joint is calculated using a lower leg length of 0.430 m, which corresponds to a user height of about 1.75 m [21]. This value is arbitrary, as it does not influence the further calculations. The positive direction of the global x-axis is anterior and parallel to the ground. The global y-axis is directed upwards and perpendicular. All rotations are defined as counterclockwise positive, which means that ankle plantarflexion and knee flexion increases the angle. The neutral position for the ankle is defined as a 90° angle. The neutral position for the knee is fully extended. The calculations are performed in 2D.
The second step is calculating the position of the attachment points at every step of the cycle, using trigonometry. As the positions of the attachment points are defined in terms of the local coordinate systems, they have to be transformed to the global coordinate system. For attachment points defined in the foot coordinate this step is not necessary, as the local coordinate system coincides with the global coordinate system. For attachment points defined in the ankle-shank coordinate system this step is given by equation 3. For attachment points defined in the knee-shank coordinate system this step is given by equation 4 and for points defined in the knee-thigh coordinate system it is given by equation 5. In these equations α is the ankle angle and

TABLE XI: The possible fields of the Elements structure array and the type or options of the entries

Field				
Type	**Push Actuator**	**Pull Actuator**	**Spring**	**Pressure Tank**
Name	[string]	[string]	[string]	[string]
Pressure Tank	[integer]	[integer]	-	[integer]
Joint	{Ankle **OR** Knee}	{Ankle **OR** Knee}	{Ankle **OR** Knee}	-
Transmission	{Direct **OR** Single-rod}	{Direct **OR** Single-rod}	{Direct}	-
Pistons	-	-	-	[1xN string array]
Valves	-	-	-	[2xN integer matrix]

TABLE XII: The parameter indices defined for each type of Elements array entry

Parameter Index	**Push/Pull Actuator**				**Spring**		
	Ankle		**Knee**		**Ankle**	**Knee**	
	Direct	**Single Rod**	**Direct**	**Single Rod**	**Direct**	**Direct**	**Pressure Tank**
1	x_{Shank}	x_{Foot}	x_{Thigh}	x_{Thigh}	x_{Shank}	x_{Thigh}	p_0
2	y_{Shank}	y_{Foot}	y_{Thigh}	y_{Thigh}	y_{Shank}	y_{Thigh}	p_1
3	x_{Foot}	L_{Rod}	x_{Shank}	L_{Rod}	x_{Foot}	x_{Shank}	According to entries in Valves field
4	y_{Foot}	d_{Att}	y_{Shank}	d_{Att}	y_{Foot}	y_{Shank}	
5	D_{Act}	D_{Act}	D_{Act}	D_{Act}	k	k	
6	-	α	-	α	L_0	L_0	

TABLE XIII: The initial constraints of the optimization parameters.

Push/Pull Actuator				**Spring**				**Pressure Tank**	
Ankle		**Knee**		**Ankle**		**Knee**			
Parameter	**Range**	**Parameter**	**Range**	**Parameter**	**Range**	**Parameter**	**Range**	**Parameter**	**Range**
x_{Shank}	−50-50 mm	x_{Thigh}	−50-50 mm	x_{Shank}	−50-50 mm	x_{Thigh}	−50-50 mm	p_0	0-5 bar
y_{Shank}	−50-200 mm	y_{Thigh}	−50-50 mm	y_{Shank}	−50-200 mm	y_{Thigh}	−50-50 mm	p_1	3-10 bar
x_{Foot}	−50-50 mm	x_{Shank}	−50-50 mm	x_{Foot}	−50-50 mm	x_{Shank}	−50-50 mm	t_c	1-51
y_{Foot}	−50-0 mm	y_{Shank}	−200-0 mm	y_{Foot}	−50-0 mm	y_{Shank}	−200-0 mm	V_d	0.02-0.2
D_{Act}	1-63 mm	D_{Act}	1-63 mm	k	100-10000 Nm^{-1}	k	100-10000 Nm^{-1}		
L_{Rod}	1.1-1.5	L_{Rod}	1.1-1.5	L_0	0-500 mm	L_0	0-500 mm		
d_{att}	25-250 mm	d_{att}	25-250 mm						
α	−10°-10°	α	−10°-10°						

β is the knee angle. Note that these calculations will result in a $2x51$ matrix with an x- and a y-coordinate for every timestamp.

$$\boldsymbol{x}_{\text{global}} = \begin{bmatrix} \cos\alpha & -\sin\alpha \\ \sin\alpha & \cos\alpha \end{bmatrix} \cdot \boldsymbol{x}_{\text{local}} \tag{3}$$

$$\boldsymbol{x}_{\text{global}} = \boldsymbol{x}_{\text{Knee}} + \begin{bmatrix} \cos\alpha & -\sin\alpha \\ \sin\alpha & \cos\alpha \end{bmatrix} \cdot \boldsymbol{x}_{\text{local}} \tag{4}$$

$$\boldsymbol{x}_{\text{global}} = \boldsymbol{x}_{\text{Knee}} + \begin{bmatrix} \cos\alpha+\beta & -\sin\alpha+\beta \\ \sin\alpha+\beta & \cos\alpha+\beta \end{bmatrix} \cdot \boldsymbol{x}_{\text{local}} \tag{5}$$

The next step is to find the working line of the force and the length of the actuators or springs. For a direct transmission the working line is given by a unit vector, pointing from the attachment point on the distal segment to the attachment point on the proximal segment. The length of the element is calculated by using Pythagoras' theorem.
For a single rod transmission this step is more difficult, as the attachment point of the connection rod to the piston rod is unknown. However, the length of the connection rod and the position of its attachment point, and the working line of the actuator are known. The position of the unknown point can be found by taking the intersection of the working line of the actuator and a circle with a radius of the connection rod length around the attachment point. The equation of the line and the circle are given in equations 6 and 7. Here x_A and y_A represent the coordinates of the attachment point. r is the length of the connection rod and l is the distance from the joint to the virtual attachment point, i.e. the point where the working line of the actuator crosses the main axis of the shank. The angle between the main axis of the shank and the working line of the actuator is given by θ.

$$ax + by + c = 0 \tag{6}$$

With $a = 1$, $b = \tan\alpha + \theta$ and $c = \sin\alpha \cdot l - \cos\alpha \cdot \tan(\alpha+\theta) \cdot l$.

$$(x - x_A)^2 + (y - y_A)^2 - r^2 = 0 \tag{7}$$

After filling in $x = -\frac{by+c}{a}$ in equation 7 and some simplification equation 8 remains.

$$A \cdot y^2 + B \cdot y + C = 0 \tag{8}$$

Where:

$$A = b^2 + a^2 \tag{9}$$
$$B = 2bc + 2ab \cdot x_A - 2a^2 \cdot y_A \tag{10}$$
$$C = c^2 + 2ac \cdot x_A - a^2 \cdot (r^2 - x_A^2 - y_A^2) \tag{11}$$

This equation can be solved using the quadratic formula to find two y-coordinates. For the ankle the highest value is chosen, and for the knee the lowest value is chosen, as these represent the most logical configurations. The according x-coordinate can be found by filling in the y-coordinate in $x = -\frac{by+c}{a}$. Again the working line is represented by a unit vector pointing from the attachment point on the distal segment to the attachment point on the proximal segment. The length of the element is taken from the virtual attachment point to the new attachment point. Note here that the length can also be negative if the new attachment point transfers to the other side of the shank.
The lengths can be used to calculate the volume of the pressure systems at each instance, and thus the pressure in the system. The volume ratio RV between the uncompressed and compressed states of a pressure system is calculated by entering the pre-pressure p_0 and compressed pressure p_1 in equation 12.

$$RV = \left(\frac{p_1}{p_0}\right)^{\frac{1}{\kappa}} \tag{12}$$

Where κ is the ratio between specific heats, which is about 1.4 for air. Equation 12 is derived from the formula of isentropic expansion, which is given in equation 13.

$$\frac{p_1}{p_0} = \left(\frac{V_0}{V_1}\right)^{\kappa} \tag{13}$$

The difference between the uncompressed volume V_0 and the compressed volume V_1 is the volume of the cylinders connected to the pressure system. To calculate the volume of the cylinders the difference between the maximum and minimum length L, as calculated in the previous step, is multiplied with the area of the piston, as shown in equation 14.

$$V_{\text{cylinder}} = (\max(L) - \min(L)) \cdot \frac{D^2}{4} \cdot \pi \tag{14}$$

Where D is the diameter of the cylinder, as defined in the parameters. The cylinder volume is used to calculate the compressed and uncompressed volumes. If the pressure tank has one or more valves that close during the cycle, one of the parameters describes the percentage of the total volume that is left as dead volume attached to a cylinder. After subtracting these dead volumes from the compressed volume the volume of the pressure tank is left.
At each instance a compression rate is calculated for all cylinders connected to the pressure system. For push cylinders the compression rate is given by equation 15, and for pull cylinders it is given by equation 16. A compression rate of 0 means the cylinder is not compressed, while a compression rate of 1 means the cylinder is fully compressed. These compression rates are later used to calculate the pressure in the pressure tank, and in each individual cylinder with a closed valve.

$$c_i = \frac{\max(L) - L_i}{\max(L) - \min(L)} \tag{15}$$

$$c_i = \frac{L_i - \min(L)}{\max(L) - \min(L)} \tag{16}$$

The pressure in the system is calculated using the formula of isentropic expansion. The volume of the system is calculated by multiplying the compression rate for each cylinder with its volume, and subtracting it from the uncompressed volume.

$$p_{1,i} = p_{base} \cdot \left(\frac{V_{base}}{V_0 - \sum_{j=1}^{n} c_j, i \cdot V_{\text{cylinder},j,i}}\right)^{\kappa} \tag{17}$$

Here $p_{1,i}$ is the pressure in the system at a time instance. V_{base} and p_{base} are the base volume and pressure. If there are no closing valves, or the valves have not closed yet, these are the uncompressed pressure and volume. When a valve closes, the volume and pressure at the instance of closing become the base pressure and volume for the subsequent pressure calculations. The volume of the closed-off cylinder, and the corresponding dead volume, are subtracted from the uncompressed volume V_0 for subsequent calculations. The pressure in the closed-off valve are calculated in the same way, with the sum of the cylinder volume and the dead volume serving as uncompressed volume.

The next step is calculating the magnitude of the force of each element in the system at all time instants. For spring elements the force is calculated by subtracting the resting length from the current length of the spring, and multiplying it with its stiffness. For pressure cylinders the force is calculated by multiplying the area of the piston with the pressure in the cylinder. Multiplying this magnitude with the unit vector that describes the direction of the force gives a force vector. For push actuators the direction is flipped. The joint moment that results from the elements is calculated by taking the cross product of the vector from the joint to the attachment point on the distal segment and the force vector. These joint moments can be summed to find the joint moments in the knee and ankle.

C. Evaluated Concepts

In the previous two sections an optimization strategy and moment calculations are described. In this section these will be used to optimize and evaluate a number of different concepts, to find an optimal concept for the prosthesis.
The first evaluated concept is a simple design with cylinders at the knee and ankle, both using a direct transmission. It is based on the design of the ERiK prosthesis [15], but expanded with an extra cylinder at the ankle to accommodate for the extra range of motion. Both cylinders have their own pressure tank. The calculated joint torques of this prosthesis, and a schematic representation are shown in figure 22. The cost function returns a fitness value of 4010.8 Nm^2.

From figure 22 it becomes clear that this configuration does not fit the ankle torque very well. The reason for this is that the ankle does not behave as a linear spring, as it requires different torques for the same angle during the movement. The knee torque does get close to the required knee torque.
A second concept is coupling the cylinders, and let them share a pressure tank. This could resolve the non-linearity issue, as the knee and ankle angle combined do not reach the same configuration twice during the movement. However, when looking at the results in figure 23, the ankle torque is not resolved. The reason for this is that since the two cylinders share a pressure system, they always have the same pressure, and therefore exert force at the same time. The ankle requires a small plantarflexing torque at the start of the movement, that rises until maximum dorsiflexion, and then stays constant until the end. The knee on the contrary, requires a torque peak right after seat-off near maximum dorsiflexion, that diminishes towards the end of the movement. The fitness of this design is 8631.9 Nm^2.

A third concept adds a separate actuator to the design, with a separate pressure tank, that counteracts the first ankle actuator. It is close to the final design, but all actuators still have direct transmission. One of the biggest problems this configuration

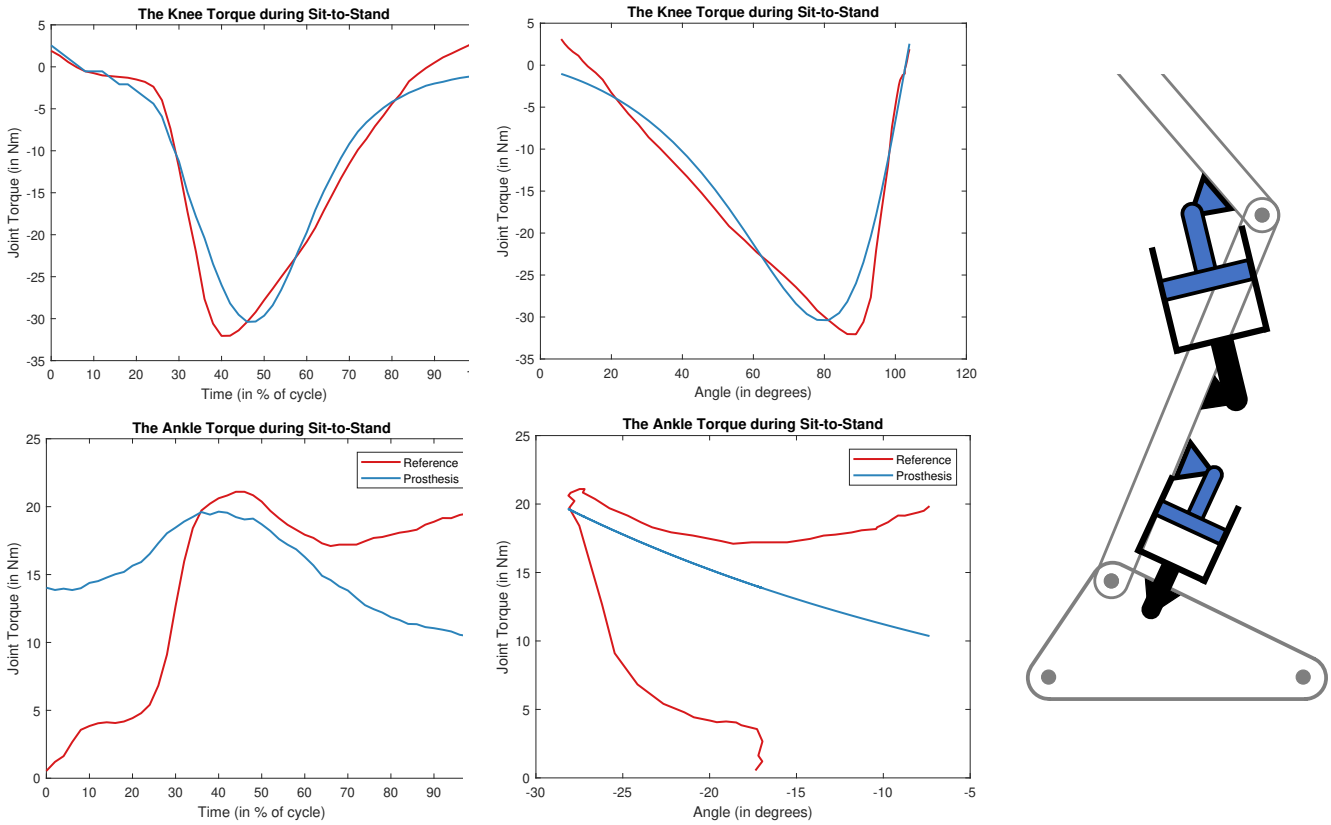

Fig. 22: The schematic design and results of a prosthesis with independent knee and ankle cylinders with direct transmission.

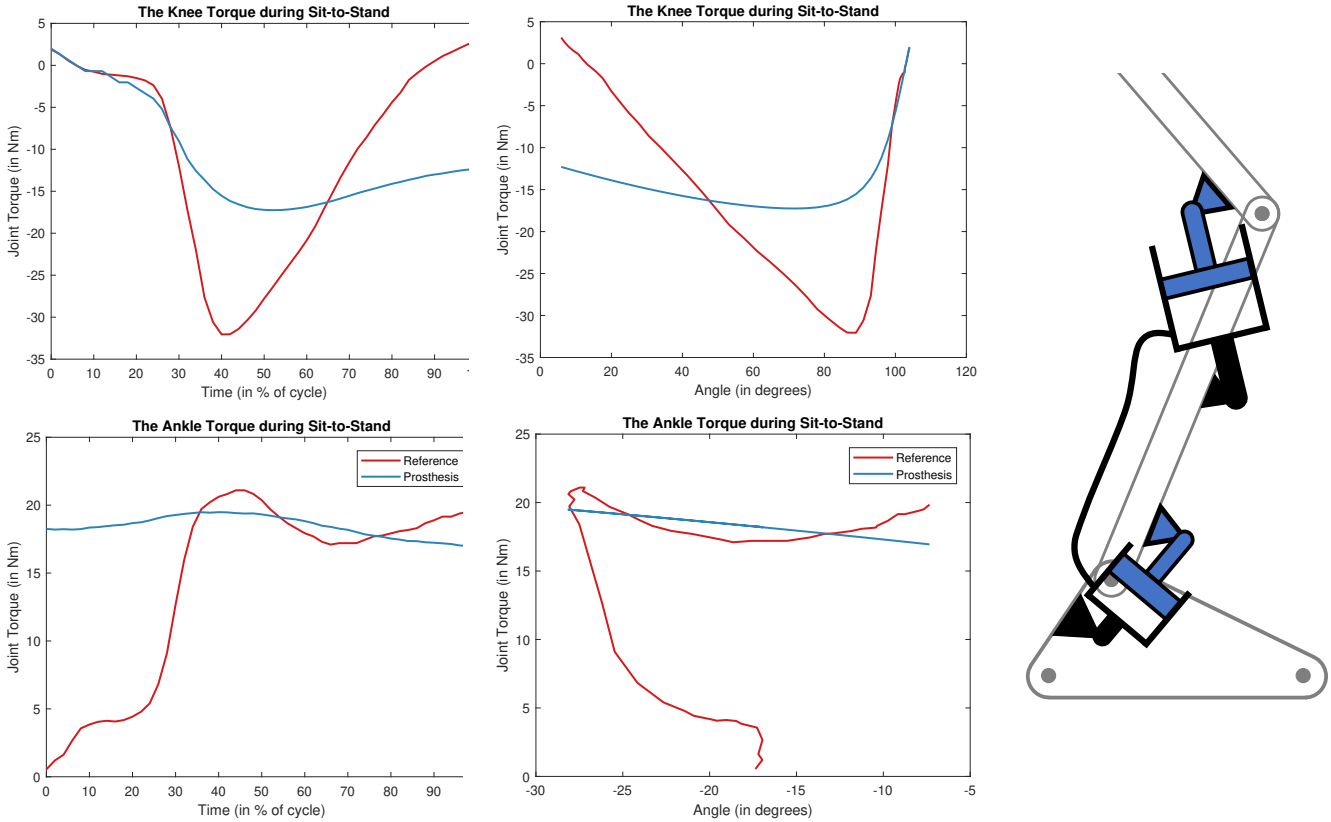

Fig. 23: The schematic design and results of a prosthesis with connected knee and ankle cylinders with direct transmission.

encounters is placement of all the actuators. In addition, since there is three of them and they are bigger than the actuator in the previous design, the weight of the actuators becomes an issue. In figure 24 the performance of this design, and the placement problems in the schematic design are shown. This configuration performs similar to the final design, but the weight and placement issues make it less attractive. The overall fitness of the design is 758.0 Nm^2.

The fourth concept fixes the primary knee and ankle cylinder in the shank, while the force is transmitted through a transmission rod. The primary cylinders are still linked, and a separate ankle cylinder is added. The performance of this concept is shown in figure 25. The benefits of this design are the reduced weight, since the cylinders are used as structure elements, and the decent performance. On the downside, multiple cylinders are required for the ankle torque. The overall fitness of the design is 1862.2 Nm^2.

A design similar to this concept is one where the secondary ankle cylinder is replaced by a spring. The performance of this concept is shown in figure 26. It performs a little better than the previous design, with a fitness of 750.3 Nm^2. The addition of the spring might reduce some weight, but since the required force is quite large it will not be by much. The risk of malfunction due to leakages is reduced by the use of a spring. However, the force of pneumatic cylinder can be adjusted more easily by adjusting the pre-pressure and pressure tank volume, to adjust for the user's body weight and support requirements. At least for the proof-of-concept phase, that is a big downside.

In a final design the non-linearity of the ankle cylinder is handled, by opening a valve half-way through the cycle, at maximum dorsiflexion. During the first part of the movement, from the start to maximum dorsiflexion, the pressure in a cylinder declines as the ankle dorsiflexes, to reduce the dorsiflexing torque of the cylinder. Similar to the previous design, this dorsiflexing torque is countered by a plantarflexing torque, exerted by a spring. At maximum dorsiflexion, a valve to the outside atmosphere opens, to ensure that the pressure in the cylinder does not rise during the second part of the movement, when the ankle plantarflexes again. During the StandTS movement, the valve closes at maximum dorsiflexion, to start building the pressure in the cylinder, which results in an equilibrium point for the ankle angle that is close to the starting angle of the SitTS movement. The performance of this design is shown in figure 27. The overall fitness of the design is 539.4 Nm^2. Although this design has a better knee performance than the other designs, it has some downsides. The main downside is the switching behaviour that might occur, and that might be hard for the users to deal with. Although the switching would be

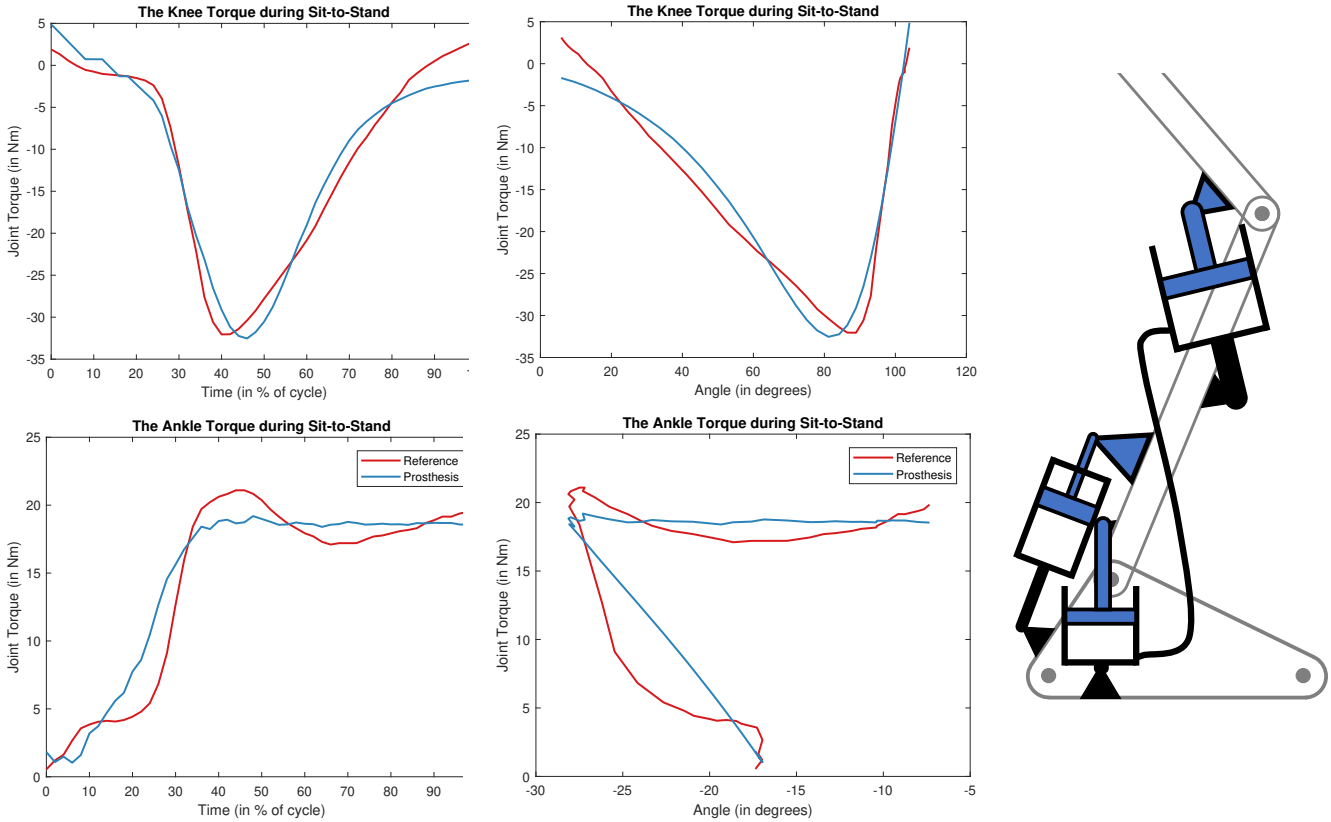

Fig. 24: The schematic design and results of a prosthesis with connected knee and ankle cylinders with direct transmission. A third, independent, cylinder with direct transmission is added to the ankle.

smooth for the reference trajectory, it is hard to predict how individuals will use the prosthesis. This might lead to unexpected forces for the users, which can result in loss of balance and a lack of trust in the prosthesis.

D. Concept Selection

The selection of the final concept is not only based on the overall fitness of a concept. In terms of fitness, the concept with the switching valve performs best. However, as stated previous, the switching behavior of this concept poses a serious downside. Additionally it is more complicated than other concept, due to the necessity for a valve in the foot, that has to be precisely controlled.

The next best performing concepts are the concept with cylinders integrated in the shank and an additional spring, and the concept with three direct transmission cylinders. The both have their downsides however. The first is less easy to adjust, due to the spring characteristics. This is specifically unfit for a proof of concept prototype.

The second concept is hard to realize due to placement issues of three cylinders. In addition, this adds significant weight to the prosthesis.

A fourth concept that scored sufficiently is a concept with cylinders integrated in the shank and an additional cylinder at the ankle. This concept scored a little worse than the others, mostly due to the poorer fit of the ankle torque near full extension. However, the benefit of this concept is the weight reduction due to the use of cylinders as structural elements.

The fourth concept was selected, because it is craftable, and more lightweight than the other concepts. The overall fitness of the concept might be improved by stretching the limits of the actuator placement during the design phase.

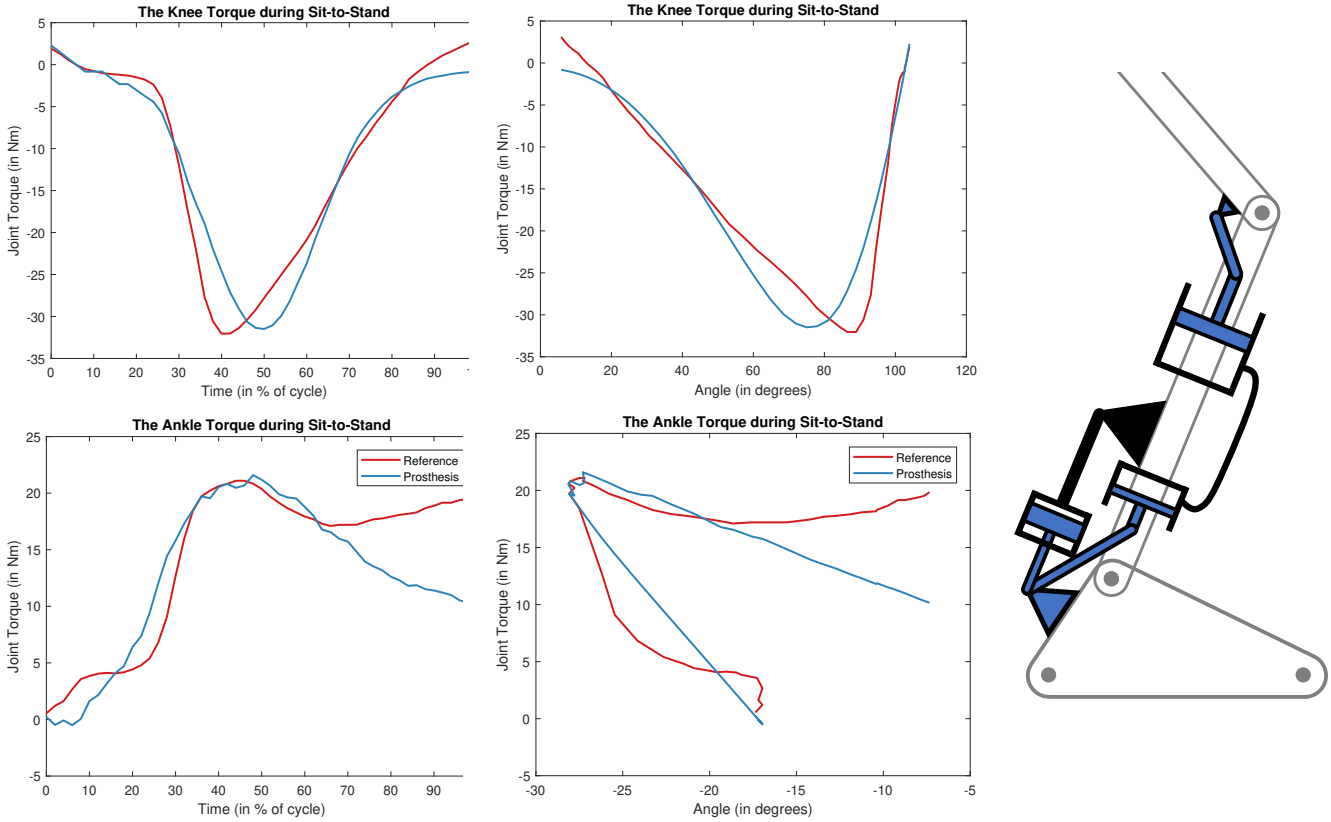

Fig. 25: The schematic design and results of a prosthesis with connected knee and ankle cylinders with connection rod transmission. A third, independent, cylinder with direct transmission is added to the ankle.

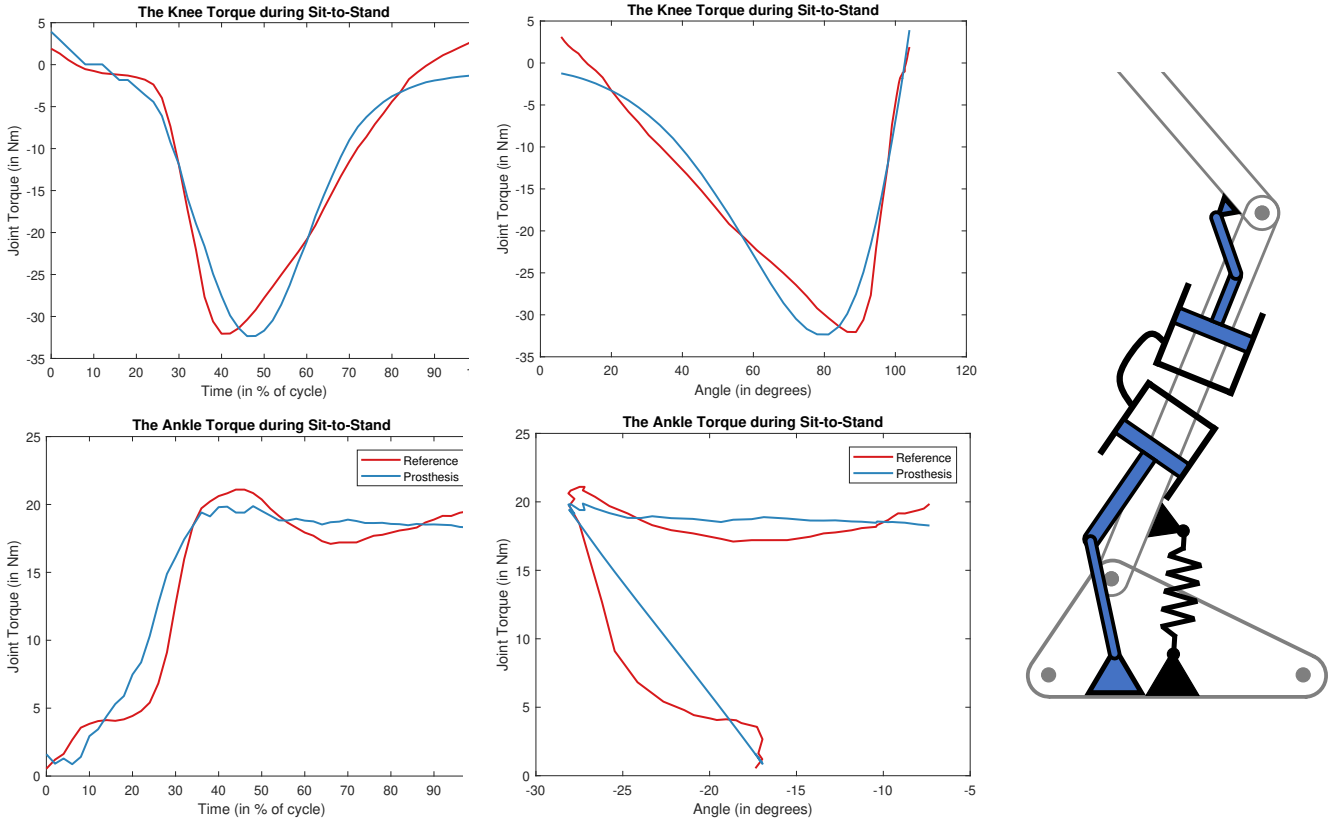

Fig. 26: The schematic design and results of a prosthesis with connected knee and ankle cylinders with direct transmission. An additional spring is added to the ankle.

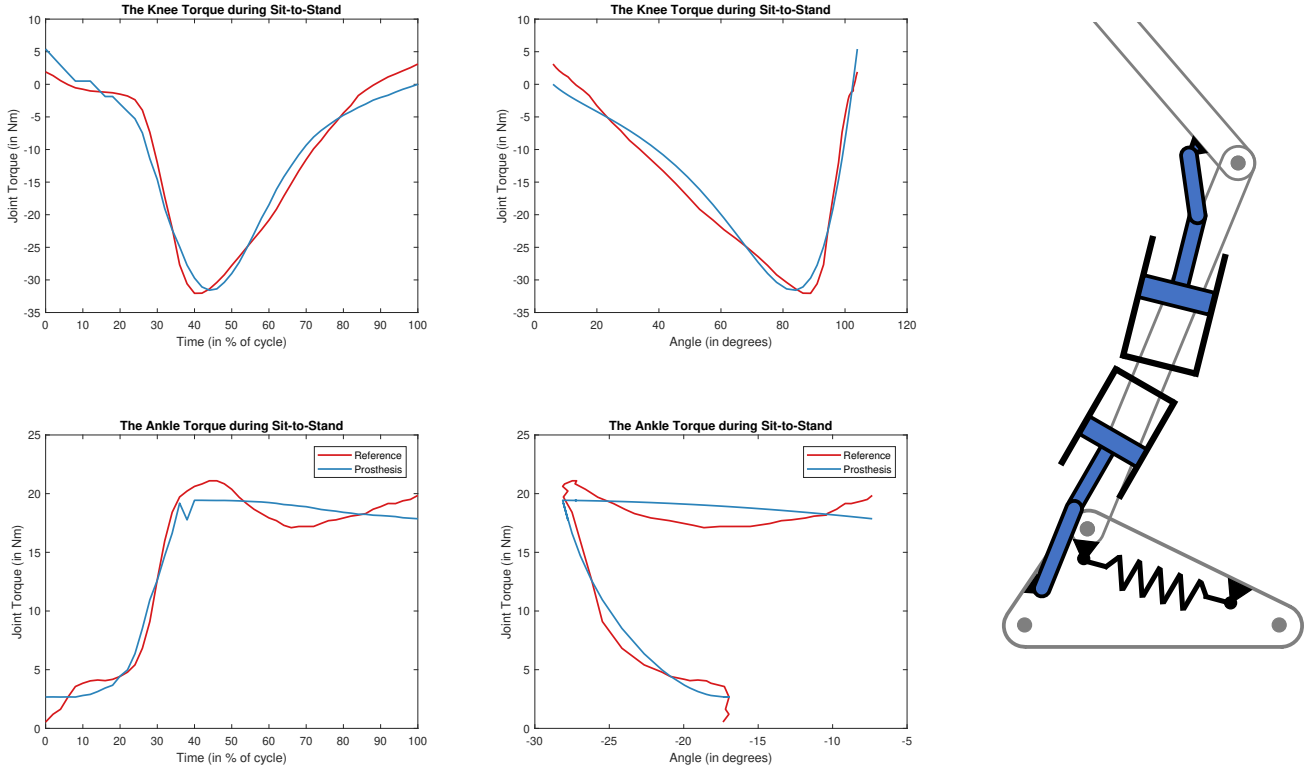

Fig. 27: The schematic design and results of a prosthesis with independent knee and ankle cylinders with connection rod transmission. The ankle cylinder has a valve to the atmosphere, that opens at maximum dorsiflexion. A spring is added to the ankle.

APPENDIX C
DETAILED PROTOTYPE DESIGN

In this appendix a more detailed description is given of the prototype design. First the design choices and components will be elaborated. Then the finite element analysis of some key components is shown. And finally the calculation of buckling, shear stress and flow rates is elaborated.

A. *Design Choices*

In this subsection the design choices will be elaborated. These choices will be grouped based on location and function. Multiple uses of identical or similar components will be discussed together. In figure 28 the overview of the prosthesis is shown.

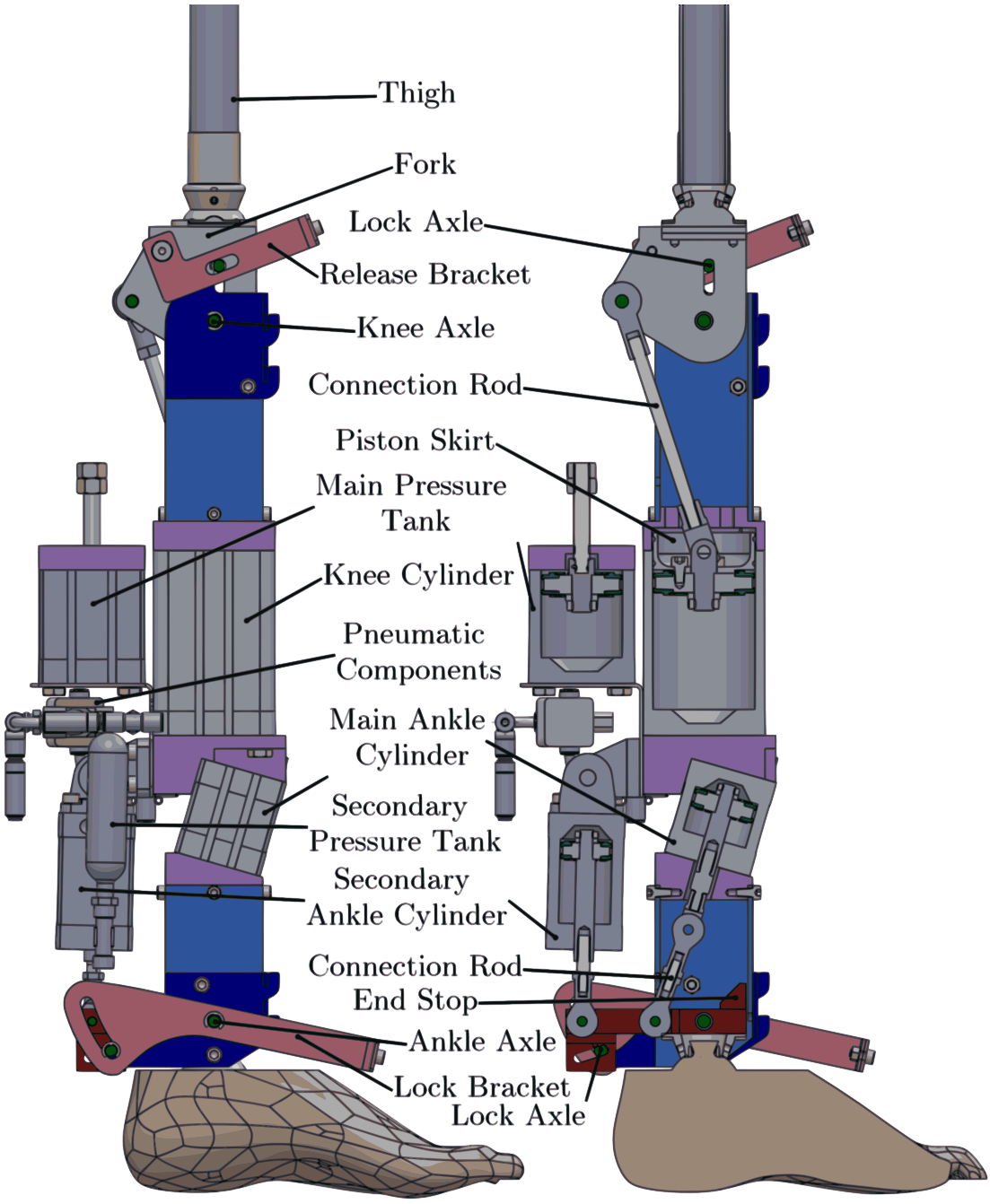

Fig. 28: Outside and sectional overview of the prototype design

1) Pneumatic Cylinders: The base of the prosthesis is formed by the pneumatic cylinders, which are all mounted in the shank assembly. For the cylinders the standard compact cylinders from Festo were selected (ADN series, Festo, Esslingen, Germany). These cylinders were selected because they are cheap and available. The cylinders are designed for industrial use, which is evident from the heavy build quality, with thick walls and heavy piston rods. These pistons are longer than necessary for the length of the stroke.
The benefit of the design of the pistons is the attachment method, and the availability of connection pieces. All pistons have four threaded holes in a square pattern, which directions are aligned with the direction of the piston. These threaded holes make the integration of the cylinders in the shank as structure elements easy.
The attachment of the secondary ankle cylinder is realised using a clevis foot and a swivel flange (SNCS/LBG, Festo, Esslingen, Germany). The swivel flange has a spherical bearing, which allows some misalignment. However, since the rod-eye at the foot connection has a similar spherical bearing, this results in some unwanted motion of the secondary cylinder. Therefore, in a future improvement, a swivel flange should be selected without spherical bearing.
The fourth cylinder, the main pressure tank, is bolted to a folded stainless steel plate, using the threaded holes in the cylinder. Since this cylinder does not contains a piston that exerts force on any other components, a more rigid connection is not required.

2) Connection Pieces: Besides the pneumatic cylinders, the shank consists of aluminium connection pieces (Aluminium 7075-T6) and aluminium square tube (Aluminium 5050). The connection piece in the center of the shank has a complicated shape, to allow the rotated placement of the main ankle cylinder. The piece is shown in figure 29. The main ankle cylinder is connected using three standard Allen screws (DIN912), which are counterbored. The knee cylinder is connected using two hex bolts (DIN931), which can be tightened with all cylinders in place. The clevis foot is connected to the side of the connection piece, using Allen screws and three threaded holes.
A second connection piece connects the main ankle cylinder to an aluminium square tube. This piece is shown in figure 30.

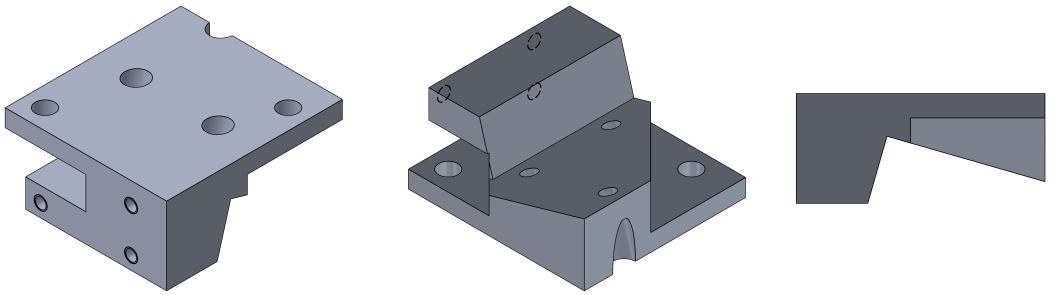

Fig. 29: The connection piece that holds the main knee and ankle cylinders together

This connection piece has an angled side. It is connected to the cylinder using counterbored inbus screws. The square tube slides over part of the connection piece, until it is flushed with a ridge. It is kept in place by four inbus screws, which are screwed into threaded holes in the side of the connection piece.
A similar connection is used between a third connection piece and the upper aluminium square tube. This connection piece

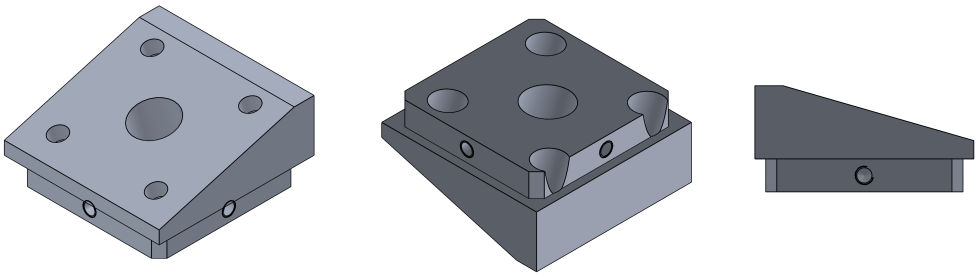

Fig. 30: The lower connection piece that connects the main ankle cylinder to the lower square tube.

replaces the cap of the cylinder, and is shown in figure 31. The connection piece has a slot hole to allow the connection rod to rotate inside the cylinder. On the bottom of the cylinder a round recess is included for the piston skirt.

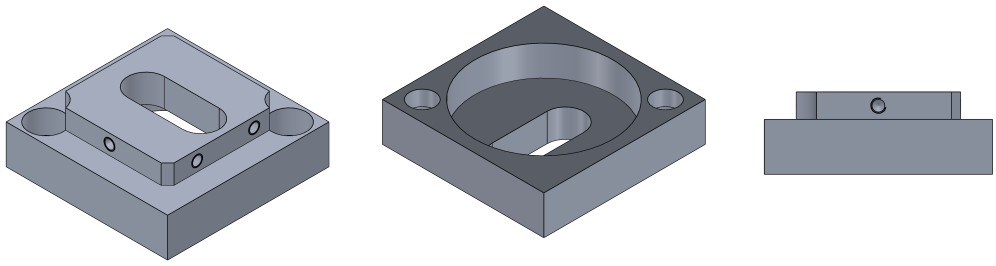

Fig. 31: The upper connection piece that connects the main knee cylinder to the upper square tube

3) Square Tubes: Two pieces of aluminium square tube are used to connect the pneumatic cylinders to the joint axles. Square tube was selected because it can be connected to the cylinders easily. Additionally, it allows movement and rotation of connection rods. The downside of the square tube is that it is only available in an inferior quality of aluminium (Aluminium 5050).
The square tubes at the top and bottom are shaped to not interfere with the rotation of components. In the posterior part of the tubes, slot holes are milled for the rotation of the connection rods.
The upper square tube is shown in Fig. 32. The top of the tube is milled at an angle to not interfere with the curved shape of the reinforcement plate. The posterior wall of the tube is removed at the top to allow the rotation of the fork piece. The lower square tube is shown in Fig. 33. The bottom of the tube is milled at an angle to not interfere with the foot at full dorsiflexion. A small part of the posterior wall is removed to make space for the foot connection piece.

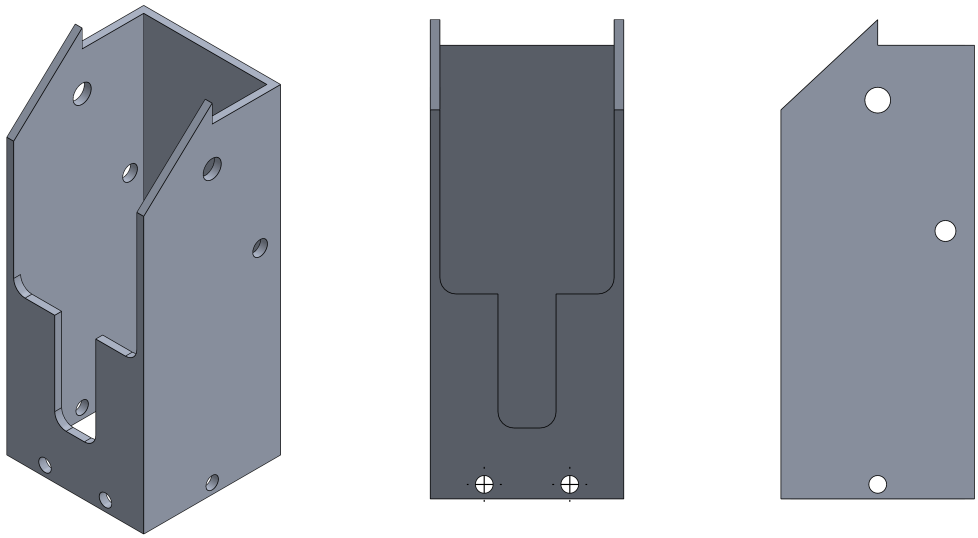

Fig. 32: The upper square tube that is used to bridge the gap between the cylinders and the knee axle.

4) Connection Rods: The force of the main pneumatic cylinders was transmitted to the thigh and foot subassemblies through connection rods. The upper connection rod consists of a piece of steel threaded rod (M8 8.8), a clevis (Similar to DIN 71752, Mädler, Stuttgart, Germany) and a rod eye (DIN 12240-4, Mädler, Stuttgart, Germany). The clevis joint was selected for an easy connection to the piston rod. The rod eye was selected for an easy, off-the-shelf solution for a low friction connection to the fork piece. The buckling calculation of this connection rod is shown in subsection C-C2.
The lower connection rod consists of a small piece of steel threaded rod (M6 8.8) and two rod-eyes (DIN 12240-4, Mädler, Stuttgart, Germany). The threaded rod has one two flattened sides for a wrench. The rod-eyes are selected for the same reason as the rod-eyes in the upper connection rod. Since this connection rod is shorter, and the force of the cylinder is smaller, a

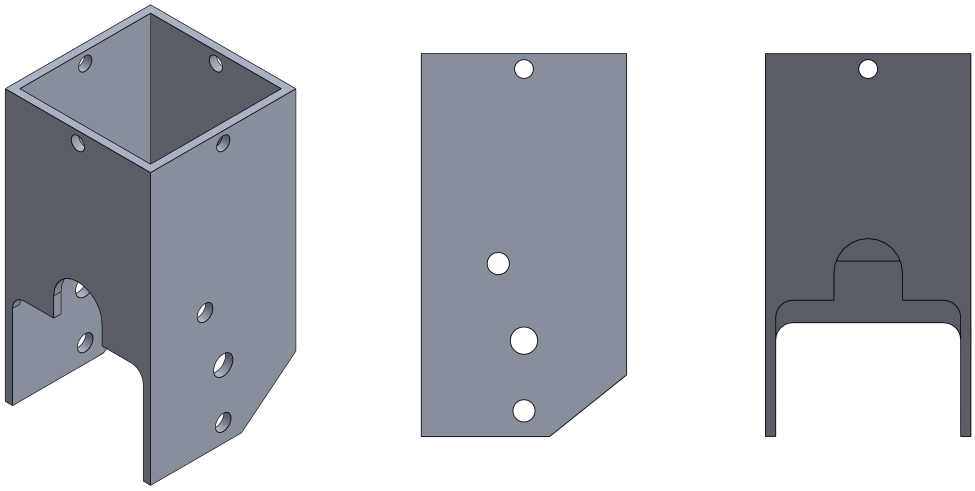

Fig. 33: The lower square tube that is used to bridge the gap between the cylinders and the ankle axle.

smaller thread and smaller rod-eyes were selected. The buckling calculation was only performed for the upper connection rod, since the thread length of the lower connection rod is negligible.

5) Thigh Fork: The main part of the thigh subassembly is the thigh fork. It consists of two separate parts, which are shown in Fig. 34. The two halves of the fork are held together by a male pyramid adapter (Type 4R54, Otto Bock). The male pyramid adapter is also used to connect the prosthesis to the socket of the user. The fork is split in two separate parts to ease the production of the part. The placement of the main axle and the connection rod axle are forced by the optimization parameters. The bottom of the fork was designed to be round to have a smooth top surface when the knee is bent.
Anterior and above the main axle a slot is milled in the fork to house the lock axle. The lock axle can move in this slot to lock and unlock movement of the knee. The axle is pressed against the side of the slot when the knee is locked.

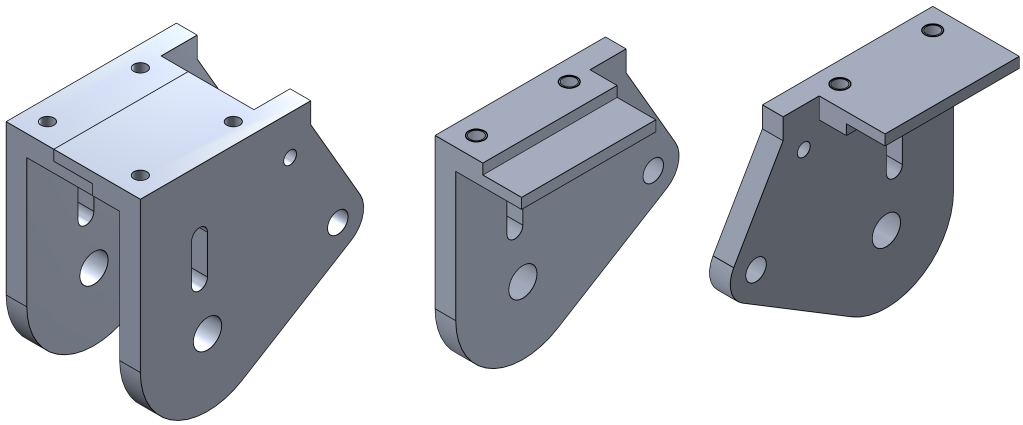

Fig. 34: The thigh fork, with holes for the knee axle and the connection rod axle. The fork is split in two parts, which are held together by a pyramid adapter.

6) Knee Lock: The knee lock design is based on the knee lock in the previous ERiK prosthesis [15], which in turn is based on the Otto Bock 3R33 prosthetic knee. The knee lock consists of a flattened axle, which can move up and down in the slot in the thigh fork. A spring pulls the lock axle to the main knee axle, and thus the bottom of the slot. The knee lock is shown while opened and closed in Fig. 35.
In the locked position the lock axle is compressed between the inner surface of the slot and the surface of the reinforcement plate on the shank, thus preventing rotation. The lock can be released by manually pulling the release bracket. This pulls the

lock axle upwards in the slot, and over the top of the reinforcement plate. Since the lock axle is no longer compressed between the surfaces, knee rotation is unlocked.
The designs of the lock axle and release bracket were dominated by the estimated compression force in the lock axle and release force in the release bracket. The compression force, and corresponding surface pressure, forced a flattened axle design, to reduce the surface pressure. The result of this is an increased friction between the lock axle, and the reinforcement plate and slot surfaces, which increases the required unlock force in the release bracket. Calculations of these forces are shown in section C-D.

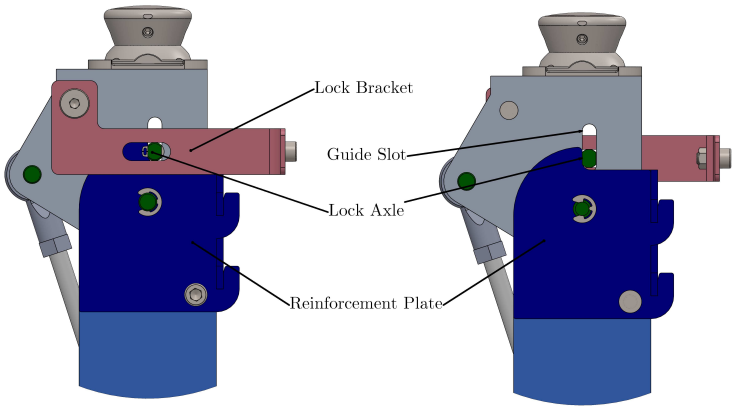

(a) The knee lock while closed

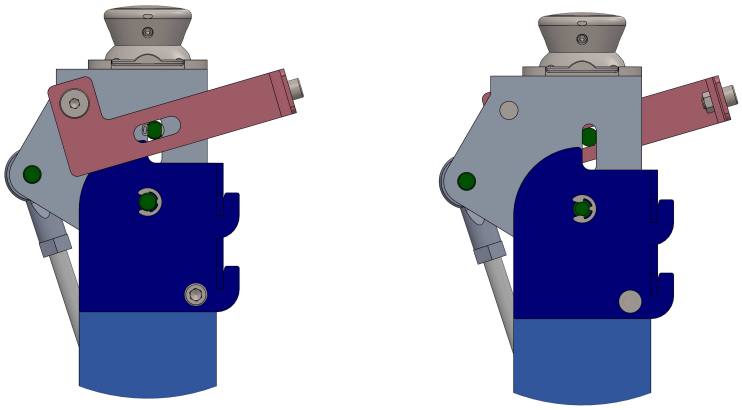

(b) The knee lock while opened

Fig. 35: The knee lock while closed and opened. By rotating the lock bracket the lock axle is moved along the guide piece. When the lock bracket is fully rotated, the lock axle can move along the reinforcement plate, and the knee can flex.

7) Ankle Lock: The ankle lock design is very similar to the knee lock design. In figure 36 the ankle lock is shown in an opened and in a closed configuration. The lock consists of a lock axle moving in a slot, which is pressed onto the reinforcement plate surface. The placement of the ankle lock however, is complicated by a lack of space around the ankle joint. Furthermore, the load on the ankle lock is much higher than the load on the knee lock, due to the higher ankle torque during gait. To diminish the effects of the higher load, the lock axle is placed down and more posterior. The surfaces of the slots and reinforcement plates are angled to allow this placement to increase the moment arm.
As in the design of the knee lock, the lock axle is flattened to reduce the surface pressure. The release force however, is reduced further by curving the slot in the release bracket. The release force is exerted by the side of the slot, which has a consistently small moment arm around the main axle. Through the leverage effect, this small moment arm leads to a large unlock force on the lock axle through the entire unlock motion.

8) Foot: For the foot of the prosthesis a low profile prosthetic foot is selected, such as the Otto Bock G6 Pedilan. An off-the-shelf prosthetic foot is used to make the prototype more convenient for walking, as it has an intrinsic stiffness suitable for walking. The use of an off-the-shelf foot however, also introduces some design issues. Even low profile feet have a build

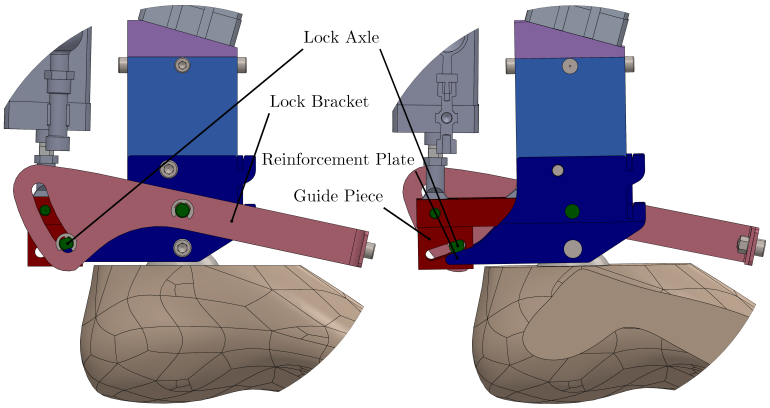

(a) The ankle lock while closed

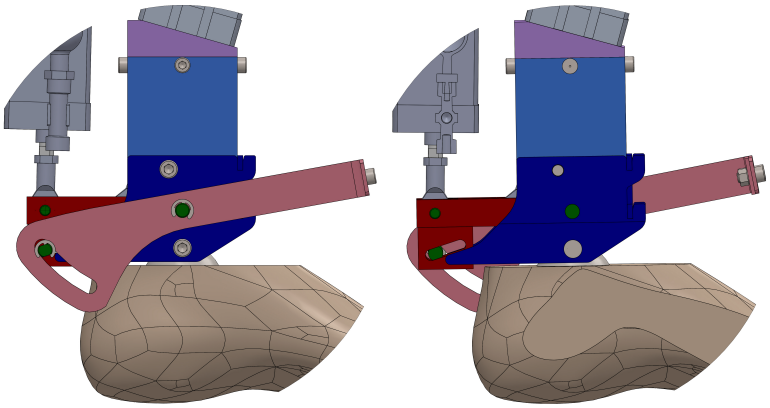

(b) The ankle lock while opened

Fig. 36: The ankle lock while closed and opened. By rotating the lock bracket the lock axle is moved along the guide piece. When the lock bracket is fully rotated, the reinforcement plate can move past the lock axle, and the ankle can dorsiflex.

height that is higher than a normal ankle joint. This means the ankle joint of the prosthesis is shifted upwards, which might impede the performance of the prosthesis during StandTS or SitTS.
To place the ankle joint as low as possible, a female pyramid adapter (4R55, Otto Bock) is used to connect the prosthetic foot to the foot connection piece, which is shown in Fig. 37. This foot connection piece consists of a thick plate in which the main ankle axle and the support axles are housed. The placement of all axles at the same height makes this part more simple and lightweight. Friction is reduced at the main axle through the use of bronze bushings, pressed into the foot connection piece.

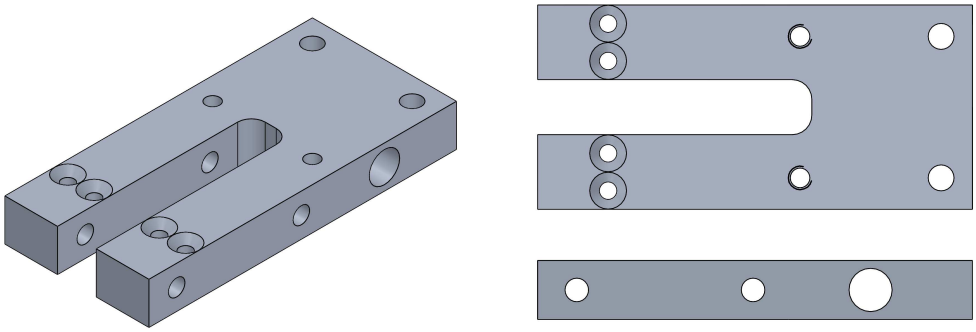

Fig. 37: The foot connection piece that connects the prosthetic foot to the ankle and the ankle pistons.

9) Endstops: Joint limits are enforced through the use of mechanical endstops. For the ankle, plantarflexion is limited to $0°$ by means of an aluminium triangular bar, placed on top of the foot connection piece, inside the square tube. A thin strip of rubber is glued to the surface. Dorsiflexion at the ankle is limited by the range of motion of the actuators.
At the knee, extension is limited to $0°$ by the shape of the thigh fork. The round shape of the bottom can rotate freely inside the square tube, but the straight part at the top can not. When the knee is overextended the rotation is stopped by the straight part of the thigh fork pressing against a thin rubber strip on the inside o the square tube. Flexion of the knee is limited to $106°$ by the bolts holding the release bracket of the knee lock touching the side of the reinforcement plate.

B. Finite Element Analysis

In this subsection the finite element calculations of the prosthesis are evaluated. First the shank body will be tested for load cases during stance. Then the foot piece and endstop are tested, and finally the lock axle.

1) Shank: The shank is loaded in three conditions. In all conditions a human user with a bodyweight of 100 kg places all his bodyweight on the prosthetic leg. In the first condition the limb is vertical, and the load of the bodyweight presses down on the shank along the main axis. The limb is fixed in the ankle joint. Since the moment around this joint is small, a fixation suffices.
The results of this condition are shown in Fig. 38. The stresses occuring in this load condition in the weak aluminium of the square tubes amount to a safety factor of 9.2. This means the yield strength of the material is 9.2 times larger than the highest stress concentration. Because the reinforcement plate material has a higher yield strength than the aluminium, the safety factor is even higher in the reinforcement plates. The safety factor of 9.2 should be high enough to accomodate the impact loads during walking. The maximum displacement of 0.02 mm should not be an issue.
In the second condition the load on the limb is rotated counter clockwise $8.6°$ to represent the maximum ankle dorsiflexion

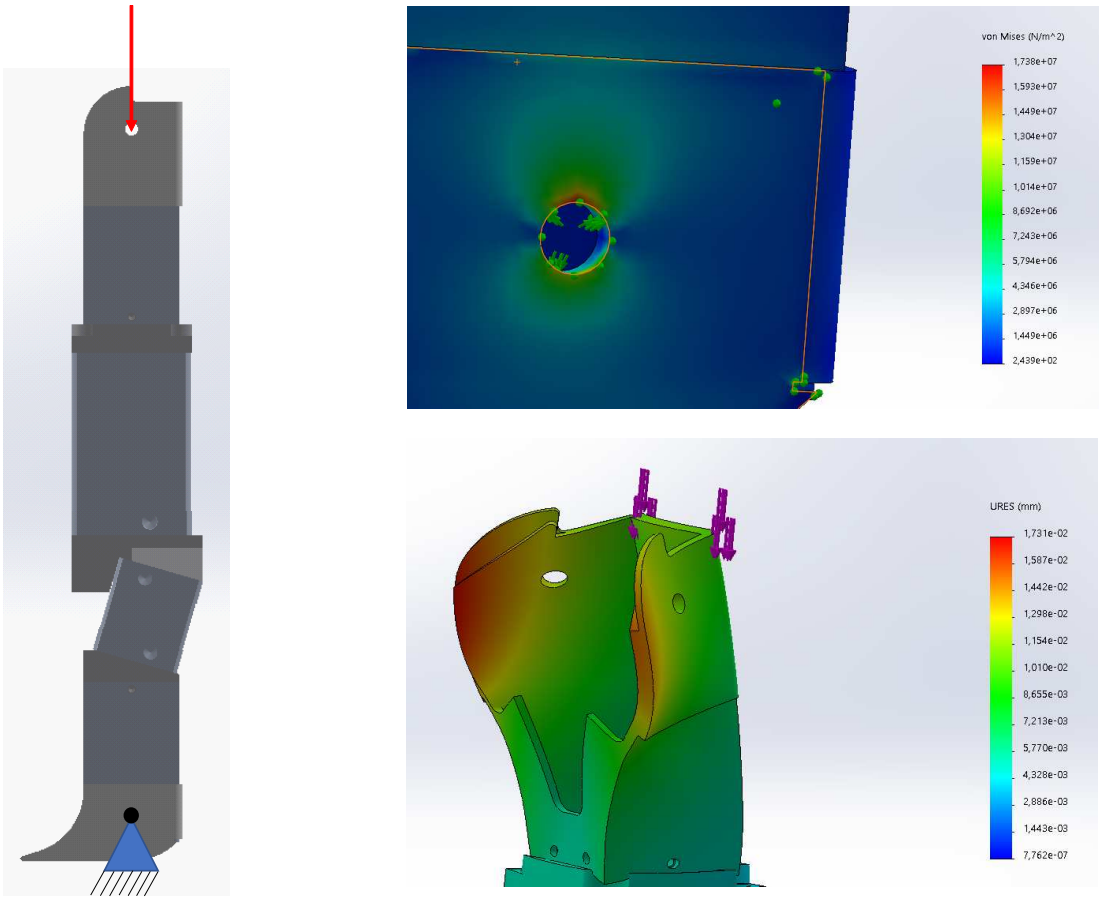

Fig. 38: On the left the first load condition of the shank is shown. On the top right the stress concentration in the hole for the ankle axis is shown. On the bottom right the displacements are shown. The stress concentration is 9.2 times smaller than the yield strength. The maximum displacement is about 0.02 mm.

torque that occurs during gait [26]. The shank is fixed with a fixed rotation in the ankle axis, and a surface fixation at the tip of the reinforcement plate to represent the ankle lock.

The results of the second condition are shown in Fig. 39. This load condition amounts to a safety factor of 1.55 in the reinforcement plates. The stress is concentrated at the location where the reinforcement plates interact with the lock axle. The failure mode of this load is probably a plastic deformation of the reinforcement plate. This is inconvenient, since it will make unlocking the ankle lock harder, but it does not endanger the user. Since this load condition occurs near the end of the stance phase during gait, impact loads are not expected. Therefore the stresses in this load condition are acceptable. A deformation distance of less than half a millimeter over the entire length of the prosthesis is acceptable as well.

In the third condition the load on the limb is rotated 1.9° clockwise to represent the maximum ankle plantarflexion torque that occurs during gait [21]. The shank is fixed with a fixed rotation in the ankle axis, and a surface fixation on the inside of the bottom square tube to represent the ankle end stop.

The results of the third load condition are shown in Fig. 40. The safety factor in this load condition is 5.5, in the aluminium square tube. Since this load condition occurs in early stance phase, impact loads are expected in this load condition. However, this load condition is based on healthy gait, and not on prosthetic gait. Prosthetic gait tends to be smaller, and thus less stressful. Combined, the safety factor and the overestimated load make this load condition acceptable.

2) Foot Connection Piece: The foot connection piece was evaluated in two load conditions, corresponding to maximum forces in the two ankle cylinders. In the first condition, the main actuator is at maximum force, corresponding to 1082 N. The secondary actuator has an actuator force of 388 N. The magnitude and direction of these forces are calculated using Matlab. Finally there is a resultant force caused by half of the maximum bodyweight, that acts at the main ankle axis. The bottom of the connection piece is fixed, where the connection piece is connected to the female pyramid adapter.

The results of this load condition are shown in Fig. 41. The safety factor for the aluminium block is 72. This means that this block is very unlikely to fail due to these loads.

The second condition corresponds to maximum actuator force in the secondary actuator. The force in the secondary actuator is 709 N in this condition. The force in the primary actuator is 735 N. These loads are again calculated using Matlab. The same resultant force is applied to the main ankle axis to represent half of the maximum bodyweight. The fixation is also the same as the first condition.

The results of this load condition are shown in Fig. 42. The safety factor for the aluminium block in this condition is 36. This means that this block is very unlikely to fail due to these loads as well.

3) Ankle Endstop: The ankle endstop was tested for the third shank load condition, which represents the maximum ankle plantarflexing torque during gait. This corresponds to a force of 880 N. The force was applied to the front surface of the part. The bottom surface of the part was constrained, as well as the threaded holes in the bottom of the part.

The results of the load condition are shown in Fig. 43. This load condition has a safety factor of 39 for the stress concentrations in the part near the threaded holes. These stress concentrations are not reliable, because the thread is not modeled in detail. However, a safety factor of 39 should be enough for this part to sustain this load.

4) Ankle Lock Axle: The ankle lock axle was tested for the second shank load condition, which represents the maximum ankle dorsiflexing torque during gait. This corresponds to a force of 990 N. The force was applied to the parts of the surface on the lock axle that is in contact with the reinforcement plates. The other side of the axle was constrained using fixed geometry on the part of the surface that is in contact with the slots on the foot connection piece.

The results of the load condition are shown in Fig. 44. This load condition has a safety factor of 3.1. The highest stresses occur near the fixed geometry constraint. These stresses are due to shear stress in the axle. The safety factor of 3.1 is high enough that the axle will probably outlast the reinforcement plate.

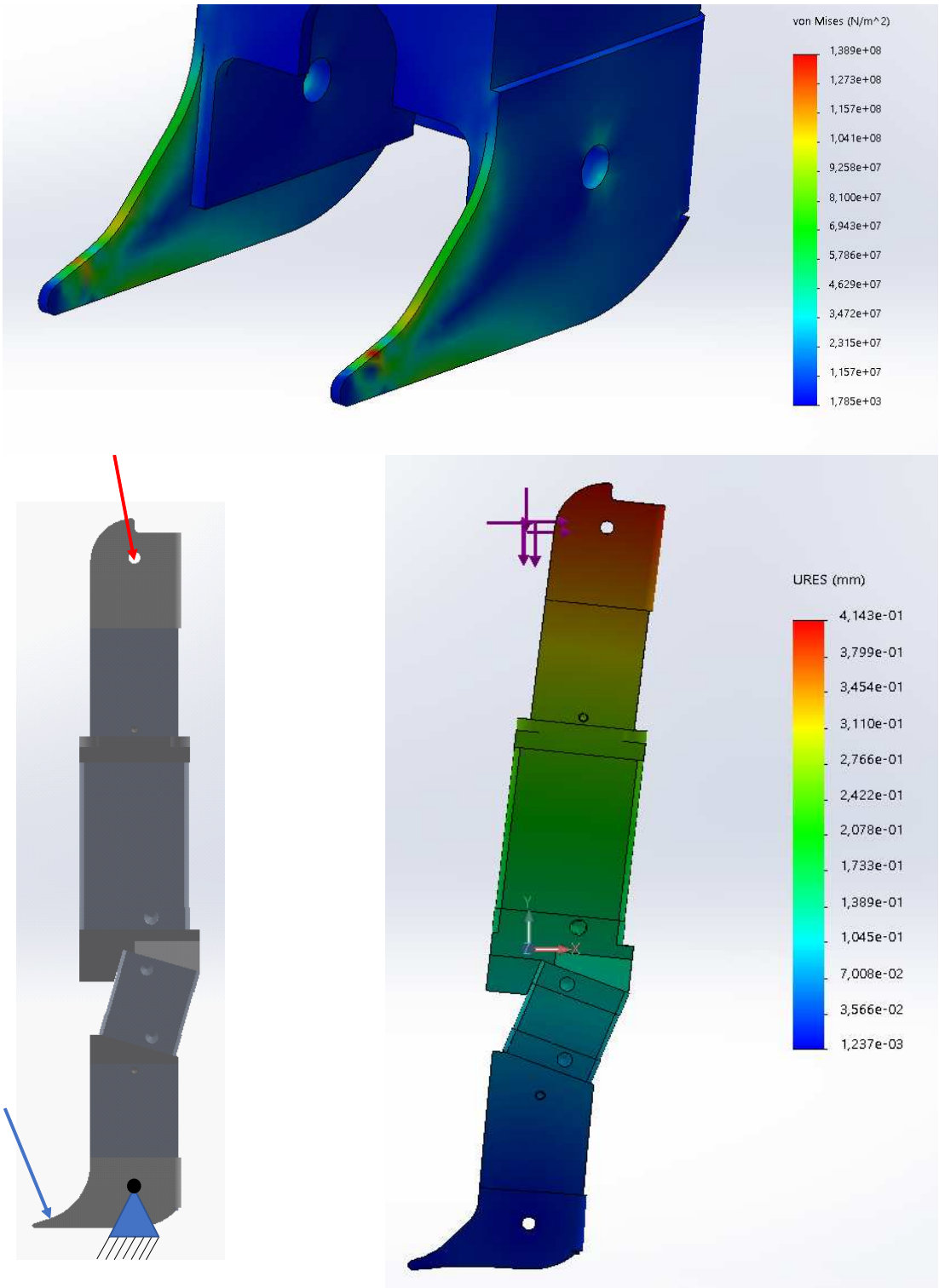

Fig. 39: On the bottom left the second load condition of the shank is shown. On top the stress concentration in the reinforcement plate is shown. On the bottom right the displacements are shown. The stress concentration is 1.55 times smaller than the yield strength. The maximum displacement is about 0.5 mm.

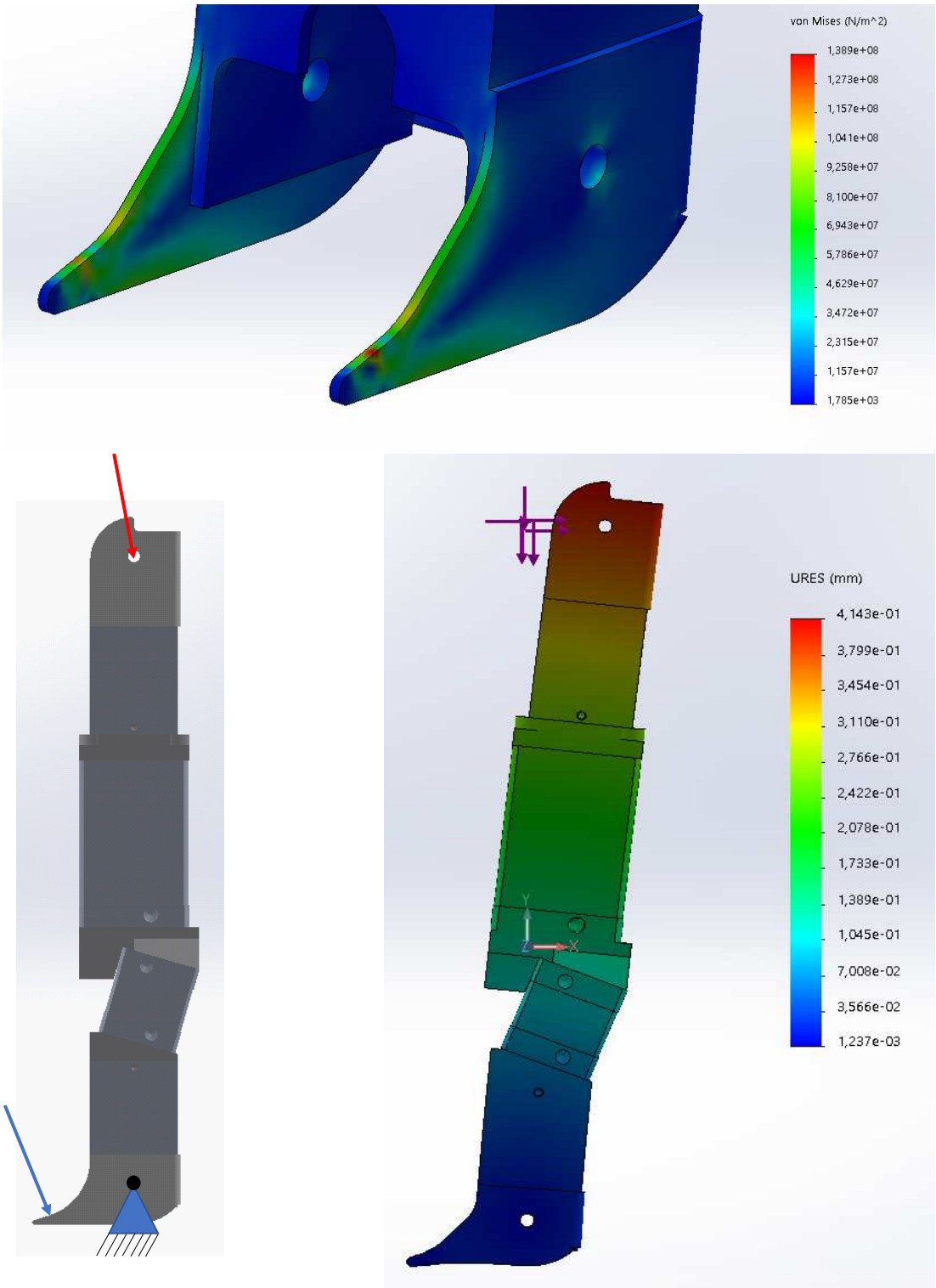

Fig. 40: On the bottom left the third load condition of the shank is shown. On top the stress concentration in the hole for the ankle axis is shown. On the bottom right the displacements are shown. The stress concentration is 5.5 times smaller than the yield strength. The maximum displacement is about 0.1 mm.

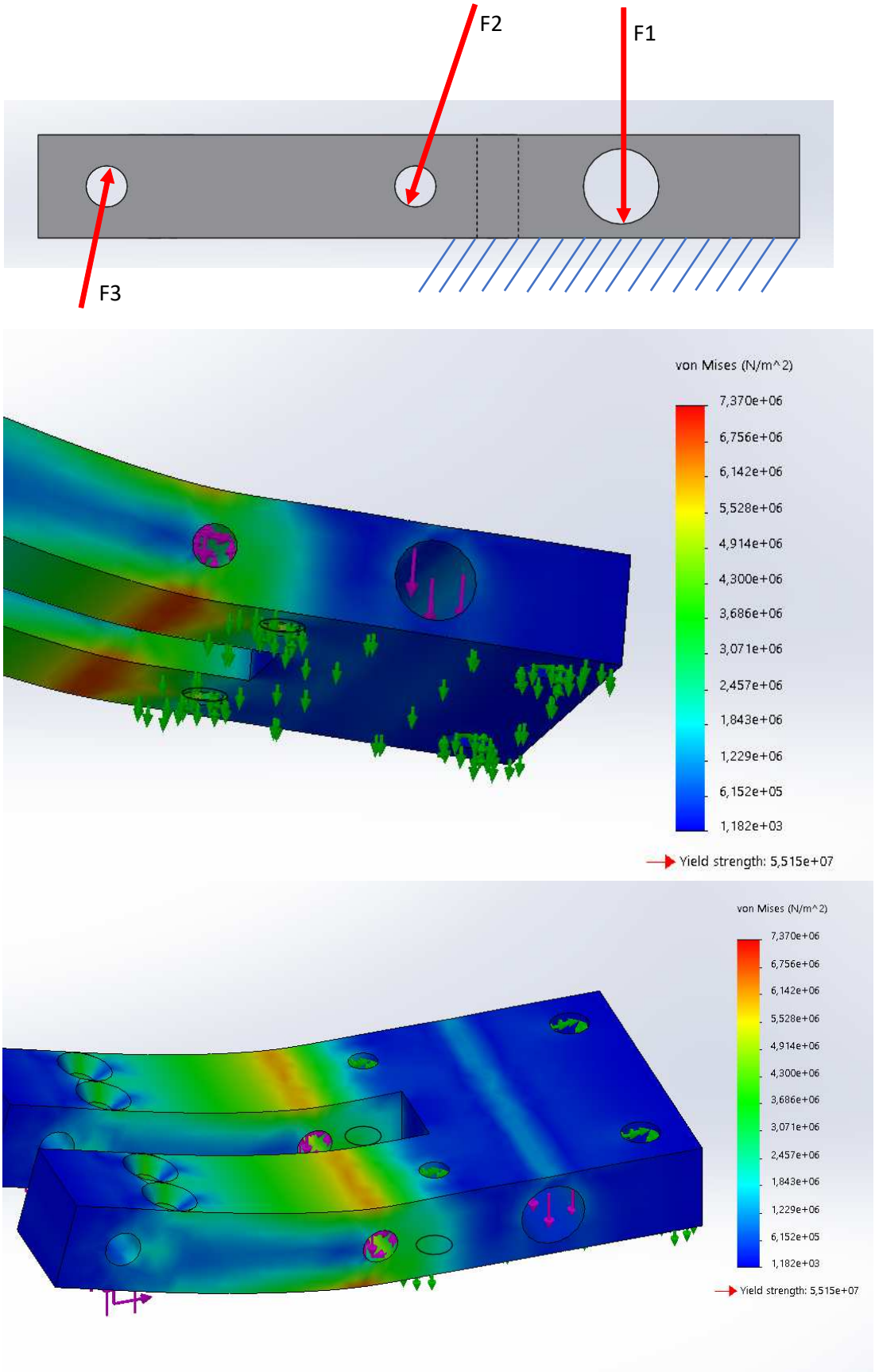

Fig. 41: On the top left the first load condition of the foot connection piece is shown. In the middle the stress concentration on the bottom of the connection piece is shown. On the bottom the stress concentration at the top of the connection piece is shown. The stress concentration is 72 times smaller than the yield strength.

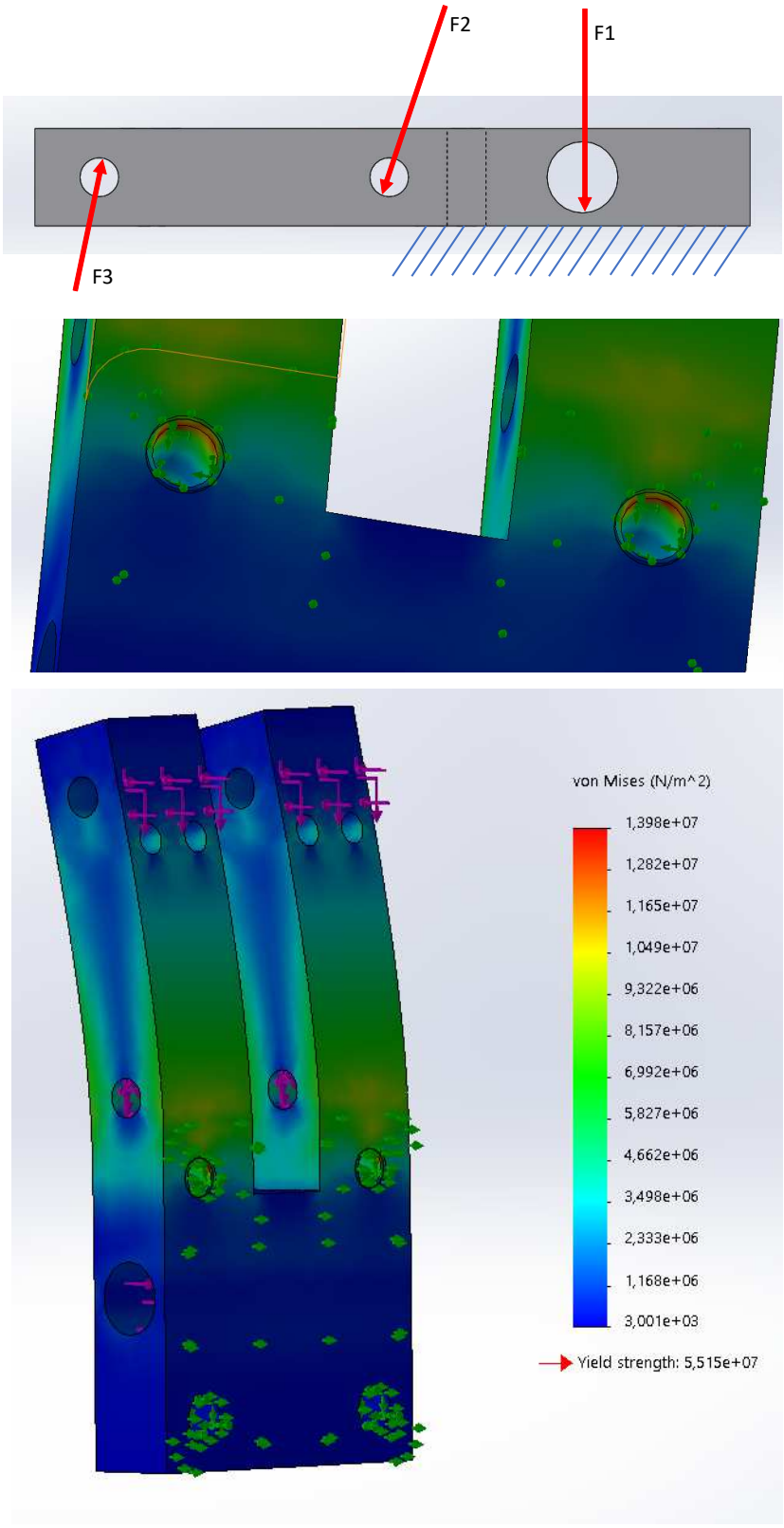

Fig. 42: On the top left the second load condition of the foot connection piece is shown. In the middle the stress concentrations in the connection holes are shown. On the bottom the stress concentration at the bottom of the connection piece is shown. The stress concentration is 36 times smaller than the yield strength.

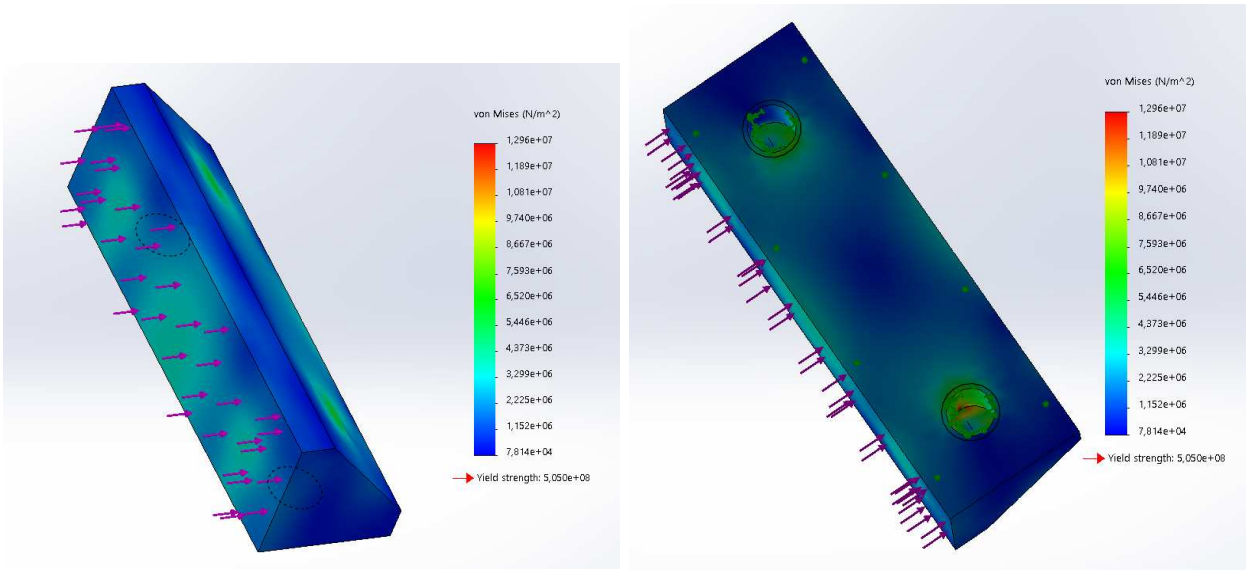

Fig. 43: On the left the stress in the contact surface of the endstop is shown. On the right the stress in the bottom of the endstop and in the holes is shown. The maximum stress concentration is 39 times smaller than the yield strength.

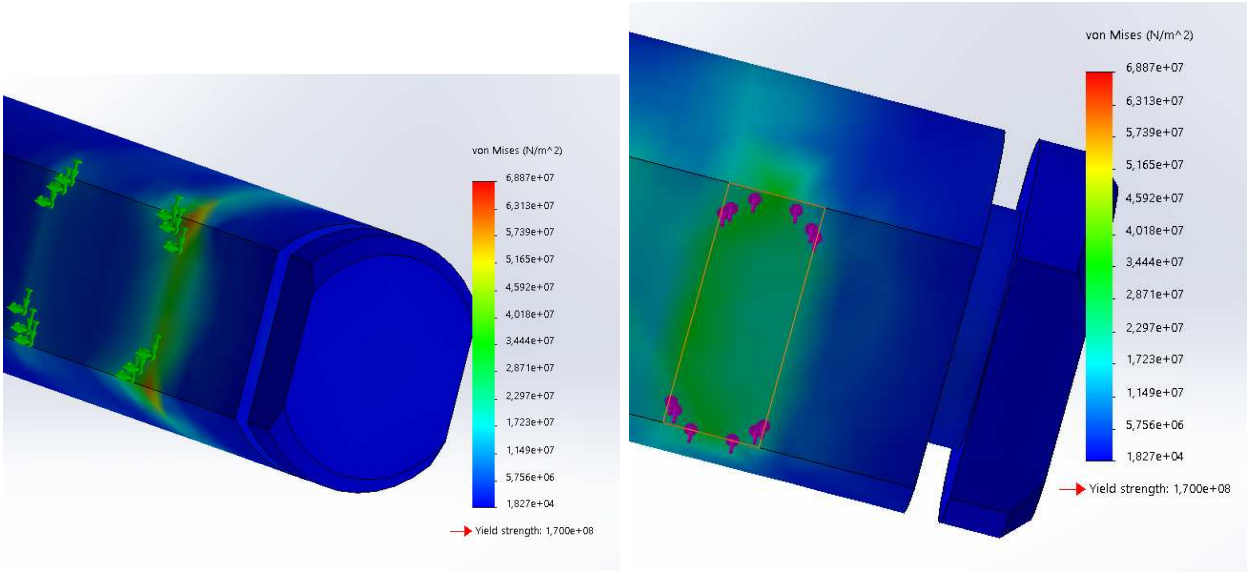

Fig. 44: The stress on both sides of the ankle lock axle. On the left the stress concentration is shown near the contact with the guide slot. On the right the stress concentration is shown near the contact with the reinforcement plate. The maximum stress concentration is 3.1 times smaller than the yield strength.

C. Additional Calculations

In this section the additional calculations on the prosthesis are shown. First, the shear stress in the main joint axles is calculated. Then the buckling of the connection rods is shown. Finally, some calculations are made about flow rates and pressure drop in the pneumatic elements.

1) Shear Stress: The main joint axles can be loaded during gait with the full bodyweight of the user. The maximum supported bodyweight of the prosthesis is 100 kg, thus the maximum load on the axles is 981 N. The load is divided over 2 contact points, which equates to 490.5 N per contact point. The axles have a diameter of 8 mm. The shear stress is calculated using equation (18).

$$\tau = \frac{4P}{\pi d^2} \tag{18}$$

If we fill in the loads and diameters, the shear stress is equal to 9.76 MPa. The maximum shear stress is equal to half of the yield stress of the material. That comes to 107.5 MPa for the stainless steel axles. That gives the shear stress in the axles a safety factor of 11. That safety factor is high enough for the shear stresses in the axles not to be a problem. The surfaces in the aluminium square tubes and reinforcement plates are more likely to wear out due to surface stress before the shear stress becomes an issue.

2) Buckling: The connection rods are used to transfer the force from the actuators to the limbs. Since the connection rod length and the force in the knee actuator is higher than in the ankle, it is most prone to buckling. The critical buckling load can be calculated using equation (19).

$$P_{crit} = \frac{\pi^2 EI}{(kL)^2} \tag{19}$$

Here E is the modulus of elasticity of the material, and I is the minimum area moment of inertia. L is the unsupported length of the beam and k is the beam effective length factor. The beam effective length factor is determined by the type of connection on both sides of the beam. Since rotation is free on both sides of the connection rod, the beam effective length factor is 1. The unsupported length is 160 mm. The modulus of elasticity of the 8.8 thread steel is 190 GPa. The thread used for the connection rod is M8, which has a core diameter of 6.5 mm. The area moment of inertia is calculated using equation (20).

$$I = \frac{\pi}{4} r^4 \tag{20}$$

In this equation r is equal to the core radius of the connection rod. Filling everything in gives a critical buckling load of 6418.6 N, which is higher than the maximum actuator load of 2650 N. This gives a safety factor of 2.4 for buckling in the connection rod. Since no impacts are expected in the connection rod, the rod is not expected to buckle.

D. Flow Rate and Pressure Drop

One of the losses in a system like this prosthesis is the pressure drop between the pneumatic actuators and the tank. This pressure drop is most prevalent in the main knee actuator, since the flow rate is the largest and the airflow is constricted by a solenoid valve. Therefore in this subsection we will calculate the pressure drop associated with the main knee actuator.

The flow rate is determined by the rate of chance of the length of the actuator and the actuator diameter. The highest flow rate occurs at around 70 % of the transition, at an angle of $41°$. The maximum flow rate is $2.49 \cdot 10^{-}4$ m^3s^{-1}. In the previous prototype weight was saved by using a miniature pneumatic valve (IEP Valve, The Lee Company, Westbrook, Connecticut). The flow rate of this valve is expressed in a unit called Lohm (Lee Ohm). The pressure drop for subsonic flow can then be calculated using equation (21).

$$\Delta p = \frac{\left(\frac{Q \cdot L}{2 K f_t}\right)}{p_2} \tag{21}$$

Here Δp is the pressure drop and Q is the flow rate. L is the Lohm rating of the valve. K is the gas unit constant, which is 3930 Lohm L bar^{-1} min^{-1}. The temperature correction factor f_t is 1 for room temperature. Finally, p_2 is the downstream pressure.

When the pressure and flow rate of the main knee actuator are used in equation (21), the maximum pressure drop is 20.6 bar. This does not comply with the prerequisites for subsonic flow. The conclusion is that the valve does not have the flow capacity for the application. To get the pressure drop below 1 bar, 5 valves would be required.

Another, heavier and bigger valve is selected for this application. The flow rate of the selected valve (VX210, SMC Corporation, Tokyo, Japan) is expressed in a critical pressure ratio b and a sonic conductance C. To find the pressure drop we can use equation (22).

$$\Delta p = \left(1 - (1-b)\sqrt{1 - \left(\frac{Q}{C p_1}\right)^2} + b\right) \cdot p_1 \tag{22}$$

Here, Δp again is the pressure drop. b is the critical pressure ratio, which is 0.63 for the selected valve. C is the sonic conductance, which is $0.63 \cdot 10^{-3}$ m^3 s^{-1} bar^{-1}. Q is the flow rate and p_1 is the upstream pressure.

With the pressure and flow rate of the prosthesis, the maximum pressure drop across this valve becomes $9.8 \cdot 10^{-3}$ bar. That is not significant, and thus the valve suffices.
Another source of pressure drop is the tubing. The used tubing has an inside diameter of 4 mm. The pressure drop across tubing is given by equation (23).

$$\frac{\Delta p}{L} = \frac{128}{\pi} \cdot \frac{\mu Q}{D^4} \tag{23}$$

Here Δp is the pressure drop and L is the length of the tube. μ is the dynamic viscosity of the fluid, which is $18 \cdot 10^{-11}$ bar s. Q is the flow rate and D is the tube diameter.
With the flow rate of the prosthesis the maximum pressure drop per meter becomes $7.1 \cdot 10^{-3}$ bar m^{-1}. With a total tube length of less than 1 meter, this is not a significant pressure drop in this application.

Release Force

In this subsection the required pulling force to unlock the joint locks is calculated. For the knee lock, this is relatively easy, since the design of the release bracket is easy. To start, an assumption is made about the joint torque that is exerted on the lock. Assuming that the user places half of his 100 kg bodyweight on the prosthesis, 5 cm in front of the joint, the joint torque is 24.5 Nm.
In Fig. 45 the knee lock is shown. Force F_A can be calculated by dividing the joint torque by the height of the lock axle in reference to the joint axle. This is given in equation (24).

$$F_A = \frac{M}{h} \tag{24}$$

Here F_A is the force on the axle, M is the joint torque and h is the height of the axle. The friction force that has to be overcome is calculated by multiplying the force by the coefficient of friction and by 2, since the force is acting on both sides of the axle. A coefficient of friction of 0.4 was assumed.
Next, the angle of the bracket is required. The equation for this is given in (25).

$$\theta = \tan^{-1}\left(\frac{b}{a-h}\right) - \tan^{-1}\left(\frac{x}{y}\right) \tag{25}$$

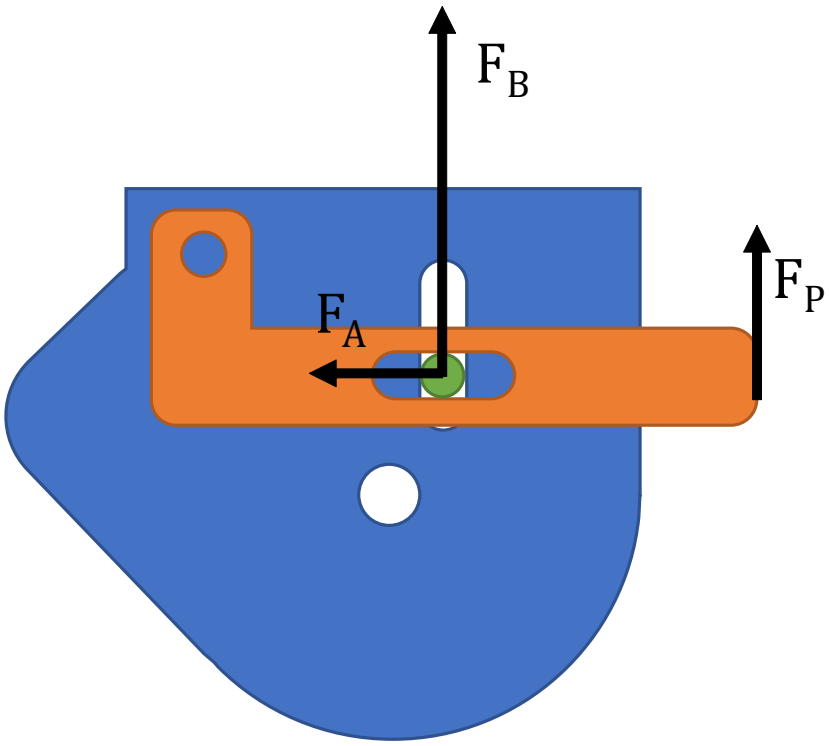

Fig. 45: The knee lock with the release bracket, the guide slot and the lock axle. F_A is caused by the joint torque. F_P is the pull force, which leads to unlock force F_B.

Here θ is the bracket angle. b is the horizontal distance from the bracket attachment to the slot. a is the vertical distance from the bracket attachment to the knee axle. h is the height of the lock axle. x and y are the distances from the bracket attachment to the lock axle along the bracket. x is calculated using equation (26).

$$x = \sqrt{b^2 + (a-h)^2 - y^2} \tag{26}$$

The values of the constants are presented in Table XIV.

TABLE XIV: The dimensions of the knee and the ankle lock.

Knee		Ankle	
a	43 mm	L_1	79.19 mm
b	32 mm	L_2	65.46 mm
y	21 mm	L_3	13 mm
L	90 mm	L_4	100 mm
μ	0.4	L_5	1.71 mm
		α	25°
		β	16°
		μ	0.4

Now the angle is known, the unlock force can be calculated. First the friction force is divided by the cosine of the bracket angle. Then this force is multiplied by the horizontal distance x to find the unlock moment. This is divided by the horizontal distance to the rope attachment point to find the unlock force. This is shown in equation (27).

$$F_P = \frac{\frac{F_f \cdot x}{\cos\theta}}{\sin\theta \cdot y + \cos\theta \cdot L} \tag{27}$$

The final forces for the trajectory are shown in Fig. 46.

For the ankle the calculations are more complicated, because of the curved shape of the slot. In Fig. 47 the outline of the foot connection piece and the unlock bracket are shown. F_A is the load force on the ankle axle due to the joint torque, and F_B is the unlock force caused by the bracket. Moment arms r_A and r_B are required to calculate the moments.
In Fig. 48 the dimensions of the release bracket are shown. Lengths L_1 and L_2 arise from the design of the foot connection piece and the guide slots. The values of all dimensions are presented in Table XIV.
To find the moment arms, first the radius of curvature of the slot is required. To find it, the width of the slot h is calculated using the cosine formula, as shown in equation (28). In Fig. 49 the triangle used for the cosine formula is shown in blue.

$$h = L_1^2 + L_2^2 - 2 \cdot L_1 \cdot L_2 \cdot \cos\alpha \tag{28}$$

By using h in the green triangle in Fig. 49, the angle δ can be calculated using equation (29).

$$\delta = \cos^{-1}\left(\frac{\sin\alpha \cdot L_2}{2h}\right) \tag{29}$$

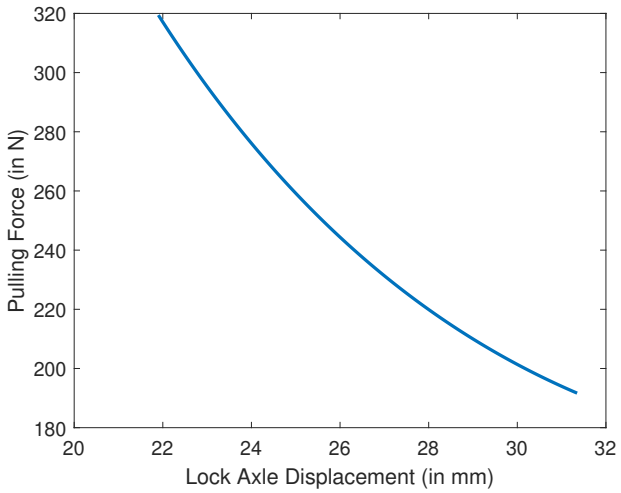

Fig. 46: The pulling force required to unlock the knee lock. The pulling force is plotted over the vertical position of the lock axle in the slot, compared to the knee axle.

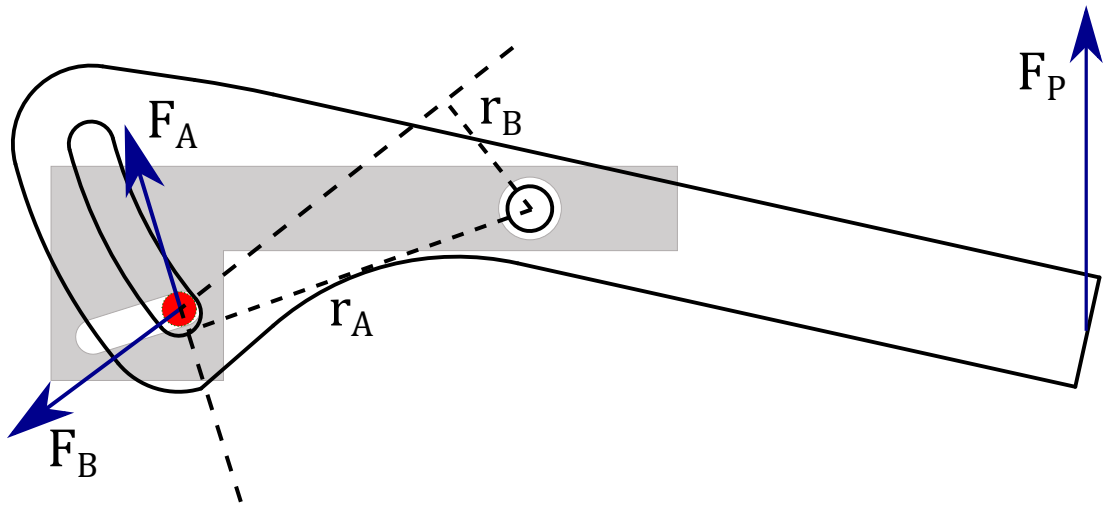

Fig. 47: The ankle lock with the release bracket, the guide piece and the lock axle. F_A is caused by the joint torque. F_P is the pull force, which leads to unlock force F_B. r_A and r_B are the moment arms of the corresponding forces.

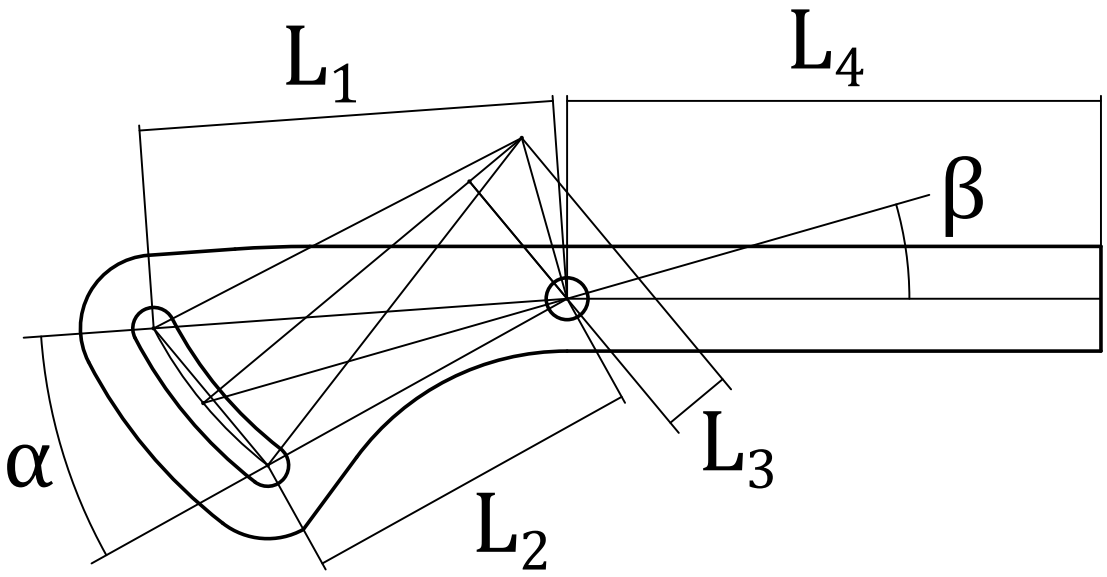

Fig. 48: The dimensions of the release bracket of the ankle lock. The values for the dimensions are given in Table XIV.

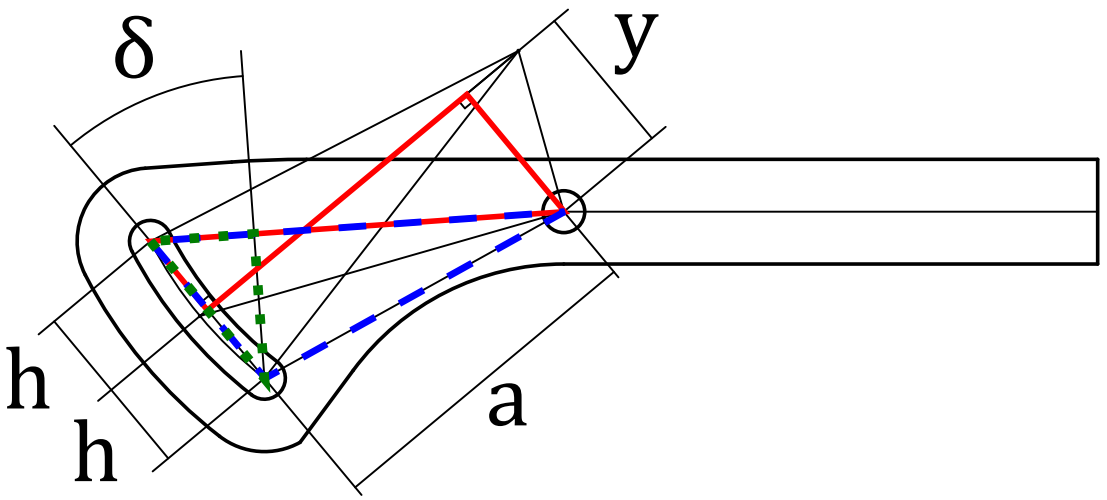

Fig. 49: The unlock bracket geometry used to calculate slot width h, radius of curvature r, angle δ and distance a.

Now the two red triangles are used to find the distance a. Equation (30) is used for this.

$$a = \sin(\frac{\pi}{2} - \delta) \cdot L_1 \tag{30}$$

This distance a is used to calculate the radius of curvature r using Pythagoras' theorem, as shown in equation (31).

$$r = \sqrt{(a + L_3)^2 + h^2} \tag{31}$$

The perpendicular distance y can also be calculated now. This is done using equation (32).

$$y = \cos(\frac{\pi}{2} - \delta) \cdot L_1 \tag{32}$$

Now the angle ϕ is defined, as the clockwise angle from the line that connects the center of the slot curvature and the midpoint of the slot to the line that connects the center of the slot curvature and an arbitrary point on the slot. It is shown in Fig. 50. For all ϕ the distance between the joint axle and the lock axle d can be calculated using Pythagoras' theorem, as shown in equation (33).

$$d = \sqrt{(\cos\phi \cdot r - L_3)^2 + (\sin\phi \cdot r - y)^2} \tag{33}$$

The next step is to find a couple of angles, which are shown in Fig. 51. The angle κ is the angle between the line from the center of the slot curvature and the slot midpoint and the line from the ankle axis to the slot midpoint. It is calculated using equation (34).

$$\kappa = \tan^{-1}\left(\frac{y}{r - L_3}\right) \tag{34}$$

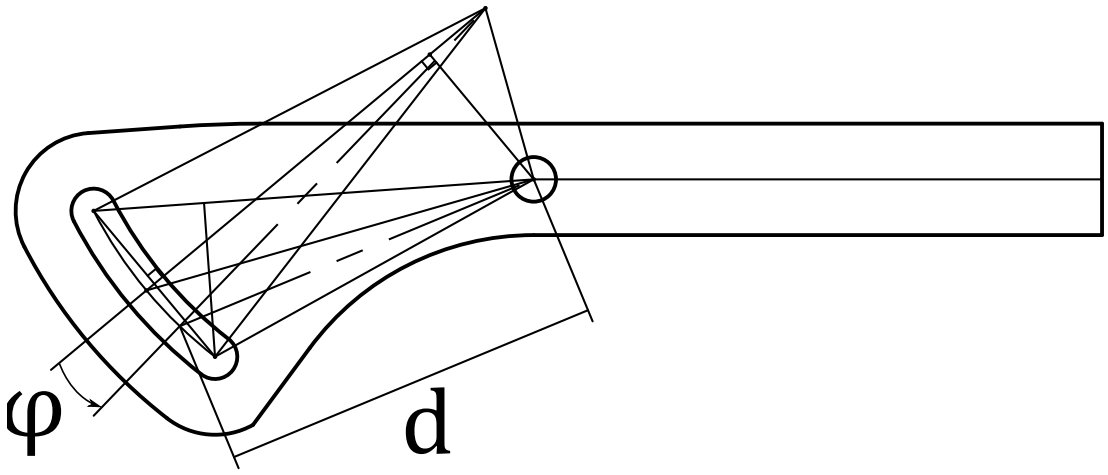

Fig. 50: The geometry used to calculate distance d. The angle phi is applicable for all angles within the limits of the slot.

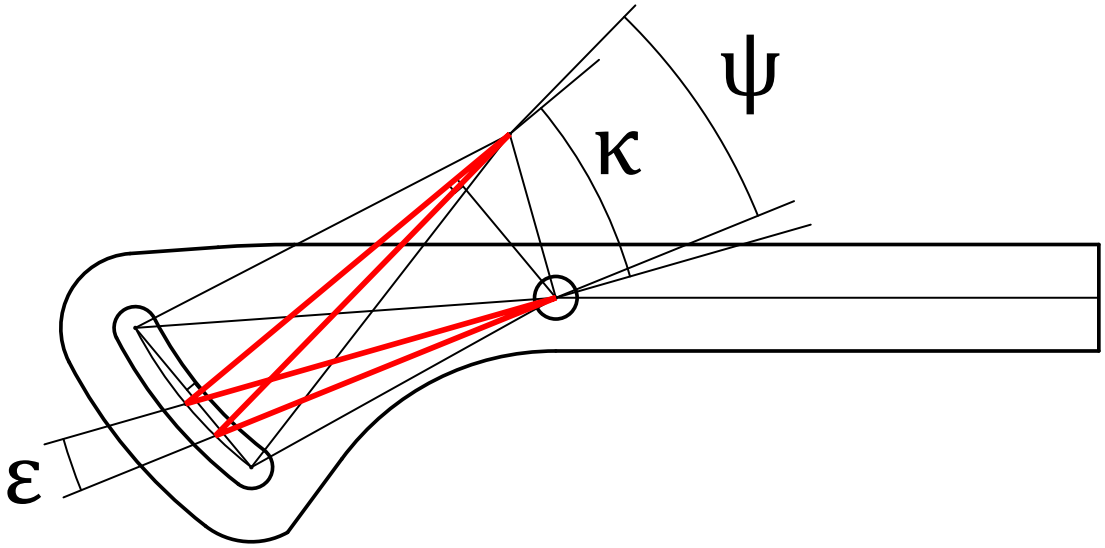

Fig. 51: The geometry used to calculate angles κ, ψ and ϵ. The two red triangles are used to calculate ϵ, using κ and ψ.

The angle ψ is the angle between the line from the center of the slot curvature to the arbitrary point on the slot and the line from the ankle axis to the arbitrary point. It is calculated using the cosine formula, as shown in equation (35).

$$\psi = \cos^{-1}\left(\frac{r^2 + d^2 - y^2 - L_3^2}{2rd}\right) \tag{35}$$

Now the two red triangles in Fig. 51 are used to show that the angle between the line from the ankle axis to the midpoint of the slot to the line from the ankle axis to the arbitrary point on the slot can be found using equation (36).

$$\epsilon = \phi + \kappa - \psi \tag{36}$$

The angle ψ can also be used to find the moment arm r_B, with the help of equation (37).

$$r_B = \sin\psi \cdot d \tag{37}$$

To find the other moment arm r_A, the distance between the working line of the guide slot and the ankle axis L_5 is required. This distance is used in equation (38), to find the moment arm.

$$r_A = \sqrt{d^2 - L_5^2} \tag{38}$$

Now that we have both moment arms, the required forces can be calculated. First the load on the lock axle is calculated by dividing the joint torque by r_A. This load is multiplied by the coeffiecent of friction of 0.4 and by 2 to find the friction force. Now the angle between the friction force vector and the unlock force vector is required to calculate the unlock force magnitude. The friction force acts along the slot, which means it acts at an angle of $17.5°$ to the horizontal. The unlock force acts perpendicular to the slot edges, which means it acts along the line from the slot curvature center to the axle. Here, the angle γ between the line from the lock axle and the ankle axle and the horizontal is required. It is used in equation 39 to calculate the unlock force.

$$F_B = \frac{F_f}{\cos(\psi + \gamma - 17.5)} \tag{39}$$

Multiplying the unlock force F_B with the moment arm r_B, the unlock torque can be found. The final step is to calculate the pull force F_P that is required to unlock the joint. Here we require the angle β between the line from the slot midpoint to the ankle axle and the line from the ankle axle to the rope attachment point. ϵ and β are summed, and substracted from γ to find the angle between the line from the ankle axle to the rope attachment point and the horizontal. This angle is used in equation (40) to calculate the pull force.

$$F_P = \frac{M_U}{\cos\left(\gamma - \epsilon - \beta\right) \cdot L_4} \tag{40}$$

The resulting pull force for the entire range of motions is shown in figure 52.

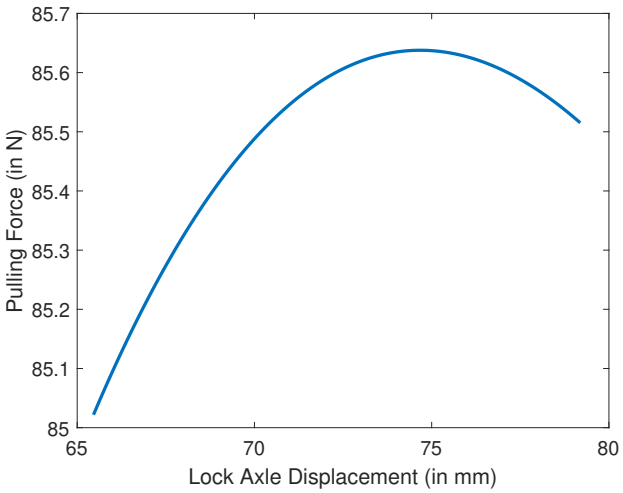

Fig. 52: The pulling force required to unlock the ankle lock. The pulling force is plotted over the distance from the lock axle to the knee axle.